Louisiana Transportation Research Center

Technical Assistance Report 16-03TA-C

Evaluation of Cores from Jefferson Highway Near Airline Highway

by

Tyson Rupnow, Ph.D., P.E.
Amar Raghavendra, P.E.
Zachary Collier, E.I.

LTRC

4101 Gourrier Avenue | Baton Rouge, Louisiana 70808
(225) 767-9131 | (225) 767-9108 fax | www.ltrc.lsu.edu

1. Report No. **FHWA/LA.16/16-03TA-C**	2. Government Accession No.	3. Recipient's Catalog No.
4. Title and Subtitle **Evaluation of Cores from Jefferson Highway Near Airline Highway**	5. Report Date September 2016 6. Performing Organization Code LTRC Project Number: 16-03TA-C SIO Number: DOTLT1000106	
7. Author(s) Tyson Rupnow, Ph.D., P.E., Zachary Collier, E.I., and Amar Raghavendra, P.E.	8. Performing Organization Report No.	
9. Performing Organization Name and Address Louisiana Transportation Research Center 4101 Gourrier Avenue Baton Rouge, LA 70808	10. Work Unit No. 11. Contract or Grant No.	
12. Sponsoring Agency Name and Address Louisiana Department of Transportation and Development P.O. Box 94245 Baton Rouge, LA 70804-9245	13. Type of Report and Period Covered **Technical Assistance** **May 2016** 14. Sponsoring Agency Code	

15. Supplementary Notes
Conducted in Cooperation with the U.S. Department of Transportation, Federal Highway Administration

16. Abstract
This technical assistance report documents the investigation conducted by the Louisiana Transportation Research Center (LTRC) of the cored concrete from Westbound Jefferson Highway near Airline Highway in Baton Rouge, LA. The petrographic analysis showed that the cause of cracking was primarily due to Alkali-Carbonate Reaction (ACR). Possible remedies for this section include continued patching efforts and full-depth replacement of the section since ACR cannot be mitigated with an overlay.

17. Key Words		18. Distribution Statement **Unrestricted. This document is available through the National Technical Information Service, Springfield, VA 21161.**	
19. Security Classif. (of this report)	20. Security Classif. (of this page)	21	22

Evaluation of Cores from Jefferson Highway Near Airline Highway

by

Tyson Rupnow, Ph.D., P.E.
Amar Raghavendra, P.E.
Zachary Collier, E.I.

Louisiana Transportation Research Center
4101 Gourrier Avenue
Baton Rouge, LA 70808

LTRC Project No. 16-03TA-C
SIO Number: DOTLT1000106

conducted for

Louisiana Department of Transportation and Development
Louisiana Transportation Research Center

September 2016

ABSTRACT

This technical assistance report documents the investigation conducted by the Louisiana Transportation Research Center (LTRC) of the cored concrete from Westbound Jefferson Highway near Airline Highway in Baton Rouge, LA. The petrographic analysis showed that the cause of cracking was primarily due to Alkali-Carbonate Reaction (ACR). Possible remedies for this section include continued patching efforts and a full-depth replacement of the section since ACR cannot be mitigated with an overlay.

TABLE OF CONTENTS

ABSTRACT iii
TABLE OF CONTENTS v
INTRODUCTION 1
OBJECTIVE AND SCOPE 3
METHODOLOGY 5
DISCUSSION OF RESULTS 7
Core Conditions 7
Petrographic Results 7
CONCLUSIONS 11
APPENDIX 13

INTRODUCTION

This report will detail the condition of cores taken from Westbound Jefferson Highway near Airline Highway. The cores were investigated due to visible surface cracking and spalling in select areas and the cracking is thought to be due to Alkali-Aggregate Reaction (AAR). AAR can manifest itself in two forms, Alkali-Silica Reaction (ASR) and Alkali-Carbonate Reaction (ACR). ASR can be mitigated through the use of overlays and other surface treatments. ACR cannot be mitigated through the use of any known surface treatments. At this time, the only known remedy for ACR-affected pavements is full removal and replacement.

OBJECTIVE AND SCOPE

The objective of the study was to determine and document the extent and cause of cracking and spalling noted in a section of Jefferson Highway generally located between I-12 and Airline Highway. To meet the objective, three cores were obtained for petrographic analysis on Westbound Jefferson Highway near Airline Highway.

METHODOLOGY

LTRC Concrete Research Laboratory personnel obtained three cores (see Figure 1) with assistance of District personnel in March 2016. The cores were photographed and sent to the petrographer for analysis. A petrographic analysis was conducted according to ASTM C856 and ASTM C1723. The full report from the petrographer can be found in the Appendix.

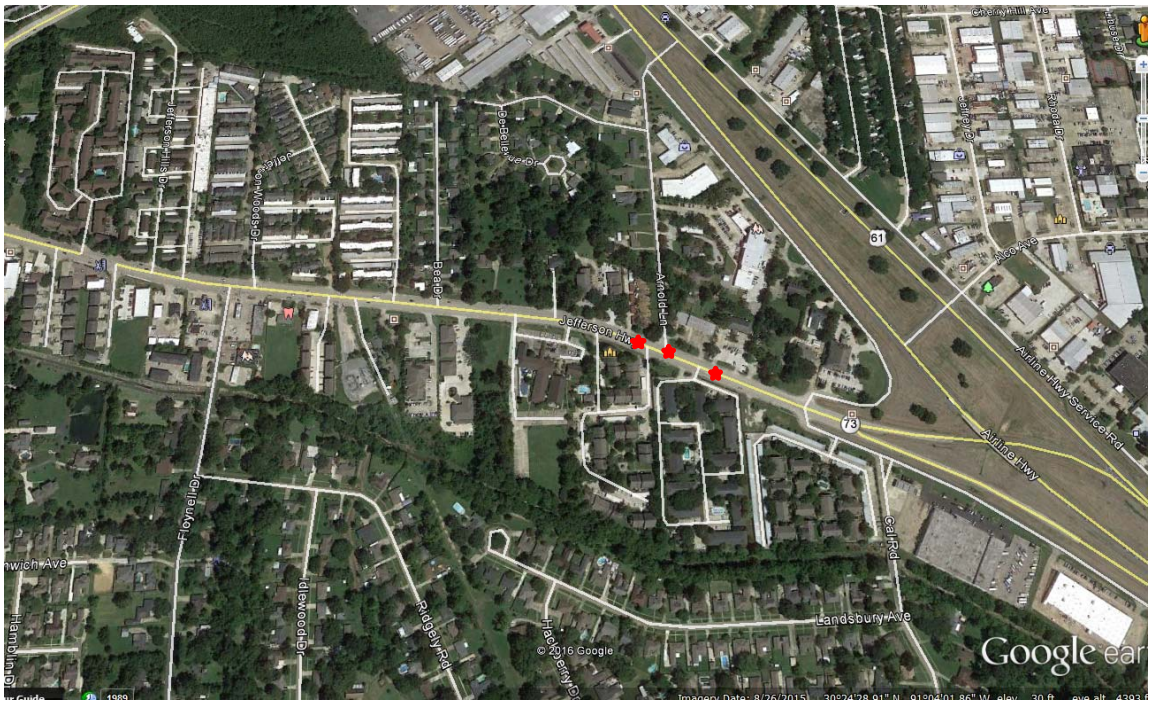

Figure 1
Core locations

DISCUSSION OF RESULTS

This section will provide a brief overview of the petrographic analysis results.

Core Conditions

The cores were retrieved to about a 9-inch depth. In general, the cores showed extensive cracking and microcracking over the full depth.

Petrographic Results

The results from the petrographic analysis showed that there is AAR occurring in the samples. Extensive cracking and microcracking typical of AAR was observed in all three cores, but more prevalent in Cores 1 and 3. Brown dolomitic limestone particles observed in the coarse aggregate are associated with ACR where extensive peripheral micro cracks are present in the aggregate and cut from these particles into the paste.

All three cores showed evidence of ACR, but the most advanced evidence was exhibited in Core 3. Numerous limestone particles show microcracking around the perimeter of the aggregate particle (See Figure 2). Yellow and green arrows indicate the microcracking around the perimeter of the aggregate with the red arrows showing cracks cutting from the aggregate into the paste. Figure 3 shows another image of Core 3 with the microcracking and cracking occurring in the paste. Note that the purple arrows show the thickness of the reaction rim of an ACR aggregate.

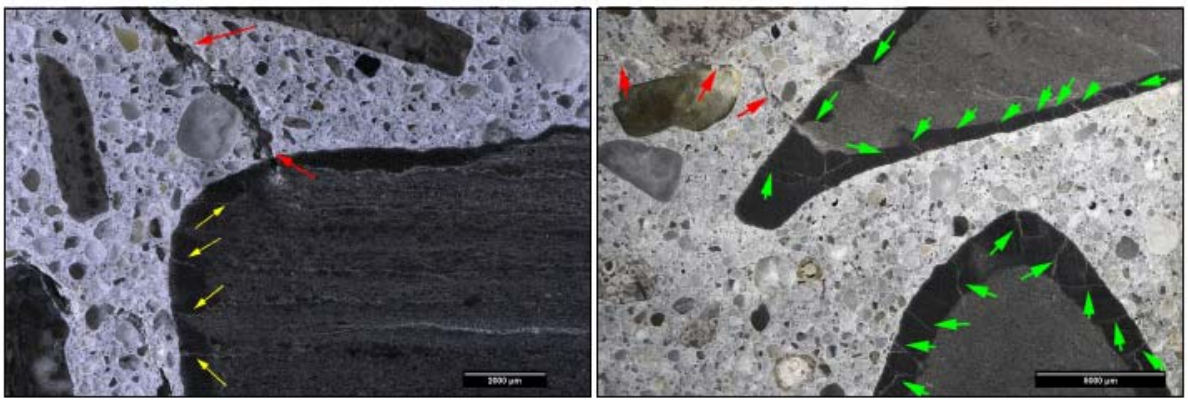

Figure 2
Images of Core 3 showing perimeter microcracking and cracks cutting into the paste

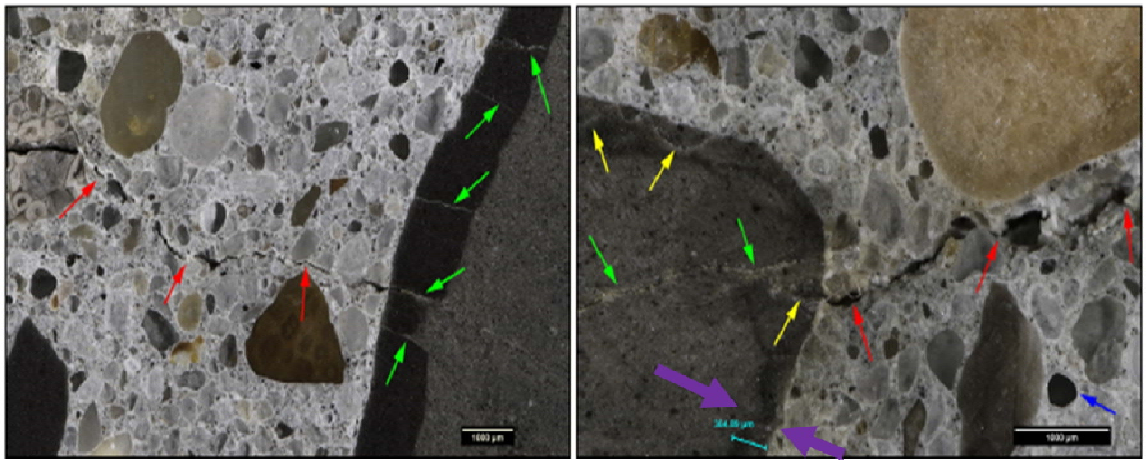

Figure 3
Core 3 showing perimeter cracking and reaction rim

Core 2 showed ACR cracking as evidenced in Figure 4. Note the yellow arrow shows the crack originating in the dolomitic limestone particle and extending outward throughout the core structure with the red arrows. The scale at the left is in mm.

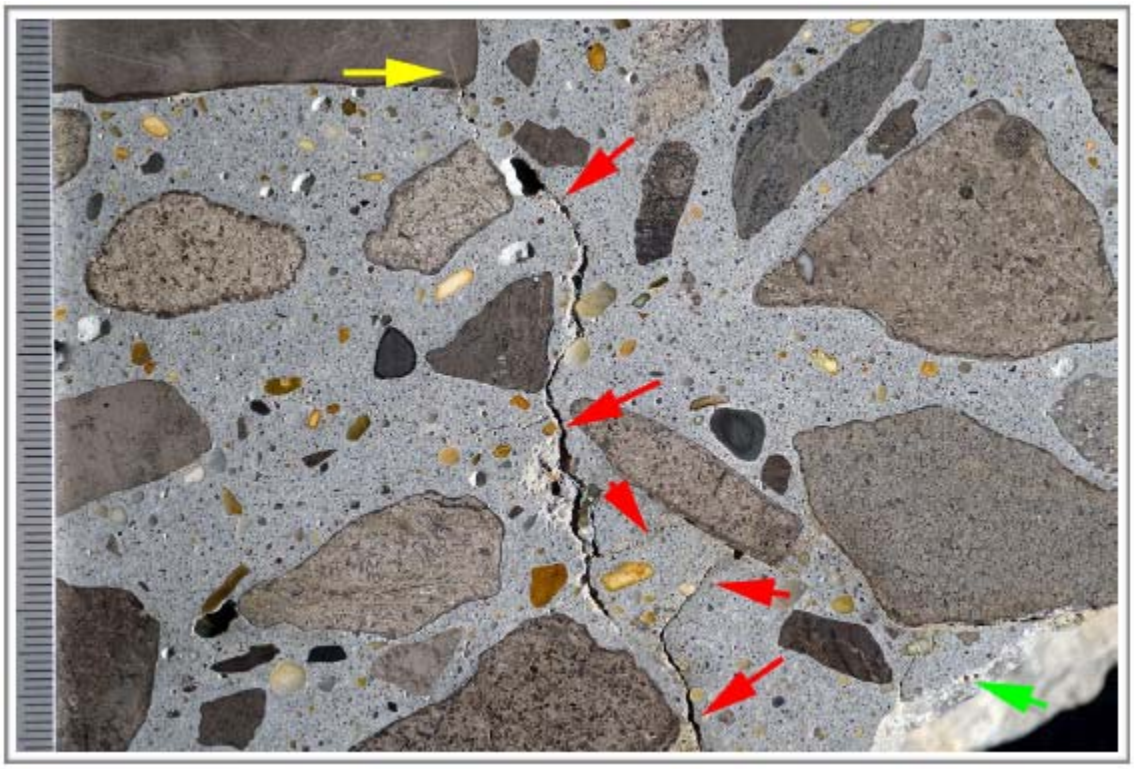

Figure 4
Section of Core 2 showing ACR cracking originating at a dolomitic limestone particle and extending outward in the paste and concrete structure

Being that the evidence strongly indicates that this pavement section is affected by ACR, possible remedies include continued patching efforts and a full-depth replacement of the affected section since ACR cannot be mitigated with an overlay.

CONCLUSIONS

The petrographic analysis of the cores showed that the distress is due to ACR. ACR was prevalent in all three cores and most extensive in Core 3. Possible remedies for this section include continued patching efforts and a full-depth replacement since ACR cannot be mitigated with an overlay.

APPENDIX

Petrographic Investigation of Concrete Cores Extracted from Cracked Pavement Slabs on Jefferson Highway in Baton Rouge, Louisiana

(RE: LTRC Project 16-1TA-C)

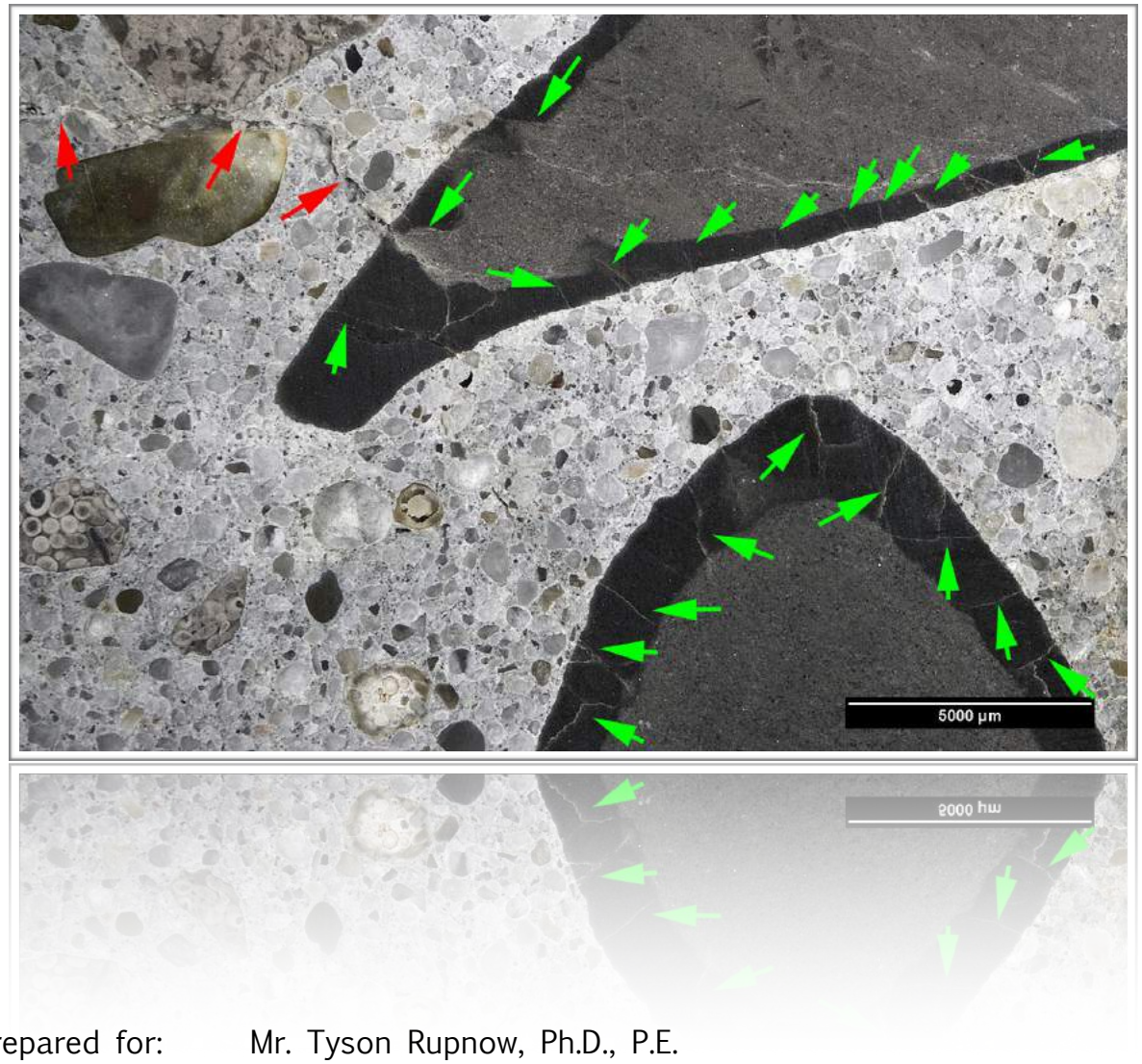

Prepared for: Mr. Tyson Rupnow, Ph.D., P.E.
Louisiana Transportation Research Center
Baton Rouge, Louisiana

Prepared by: David Rothstein, Ph.D., P.G., FACI
Report No.: DRP16.1410

12 April 2016

DRP Consulting, Inc. 3200 Carbon Place #104 Boulder, CO 80301
www.drpcinc.com

EXECUTIVE SUMMARY

Petrographic analysis following ASTM C856 supplemented with scanning electron microscopy and energy-dispersive x-ray spectrometry as described in ASTM C1723 was done on three cores extracted from cracked pavement slabs on Jefferson Highway in Baton Rouge, Louisiana for the Louisiana Transportation Research Center project 16-1TA-C. Extensive cracking and microcracking was observed over the full thickness of all three cores. The mechanisms associated with the cracking involve drying shrinkage and AAR. The shrinkage cracks and microcracks are typical of concrete with significant gap grading. Extensive sub-horizontal cracking and microcracking typical of AAR was observed in all three cores but is most prevalent in Core 1 and Core 3. These cores also show the most extensive ettringite mineralization, which is consistent with higher internal relative humidity.

The reactive components for AAR were observed primarily in the coarse aggregate. Rocks that show evidence of ASR include fossiliferous and oolitic limestone particles that contain interstitial quartz and chert. Minor ASR was also observed in association with some of the chert particles observed in the fine aggregate. Brown dolomitic limestones observed in the coarse aggregate are associated with ACR where extensive peripheral microcracks are present and cracks cut from these particles into the paste.

The concrete represented by the cores is made from similar components. The paste consists of hydrated portland cement with fly ash; no slag cement or other supplemental cementitious materials observed. The physical and optical properties of the paste observed in all the cores indicate broad consistency in the proportioning of water and cementitious materials. The cores are not purposefully air entrained but Core 1 and Core 3 contain 3-4% air whereas Core 4 contains less than 2% air as estimated from visual and microscopical observations (not measured per ASTM C457). The coarse aggregate is a limestone gravel with a 38 mm (1 ½ in.) nominal top size and the fine aggregate is a natural siliceous sand. All three cores show significant gap grading in the coarse aggregate.

1.0 INTRODUCTION

Mr. Tyson Rupnow, Ph.D. P.E. of the Louisiana Transportation Research Center (**LTRC**) located in Baton Rouge, Louisiana requested DRP Consulting, Inc. (**DRP**) to perform petrographic analyses on concrete cores extracted from cracked pavement slabs on Jefferson Highway in Baton Rouge, Louisiana for **LTRC** project 16-1TA-C. The objective of the work was to determine mechanisms associated with the cracking. On 1 March 2016 **DRP** received three cores from **LTRC**. The cores were designated No. 1-3 and were assigned **DRP** sample numbers 20YD8002-20YD8004, respectively.

No information was provided regarding the age of the concrete represented by the cores, the concrete mix design, the project specifications for concrete materials, or the results of testing done during or after construction.

2.0 SCOPE OF WORK

The testing involved petrographic analysis according to ASTM C856 [**1**] supplemented with scanning electron microscopy (SEM) and energy-dispersive x-ray spectrometry (EDS) as described in ASTM C1723 [**2**]. This report summarizes the findings of this scope of work. *Appendices A-C* contain the notes, photographs and micrographs from the petrographic examinations and *Appendix D* describes the procedures used to perform this scope of work.

1 *Standard Practice for Petrographic Examination of Hardened Concrete.* Annual Book of ASTM Standards, Vol. 4.02., ASTM C856-14.

2 *Standard Guide for Examination of Hardened Concrete Using Scanning Electron Microscopy,* Annual Book of ASTM Standards, Vol. 4.02, ASTM C1723-10.

3.0 FINDINGS

The following findings are relevant to the concrete represented by the cores.

3.1 ***Orientation, Dimensions & As-Received Condition*** The cores are vertical in orientation and span from textured surfaces on top to surfaces that are cast against an asphalt sub-base on the bottom. The cores measure 150 mm (6 in.) in diameter and range in length from 220-225 mm (~ 8 ⅝-9 in.; (**Figure 1-Figure 3**).

The cores are hard and compact. None of the cores contains steel reinforcement or other embedded objects. In Core 1 and Core 3 the texture (tines) are intact whereas Core 2 shows significant wear that exposes polished coarse aggregate particles and no tines or other evidence of the original texture was observed. Core 1 showed a spall on one edge that reached a depth of ~ 55 mm (2 ⅛ in.). In Core 3 a large pit measuring 19 x 35 mm (¾ x 1 ⅜ in.) across was observed on the top surface. All three cores showed extensive cracking, as discussed in detail below.

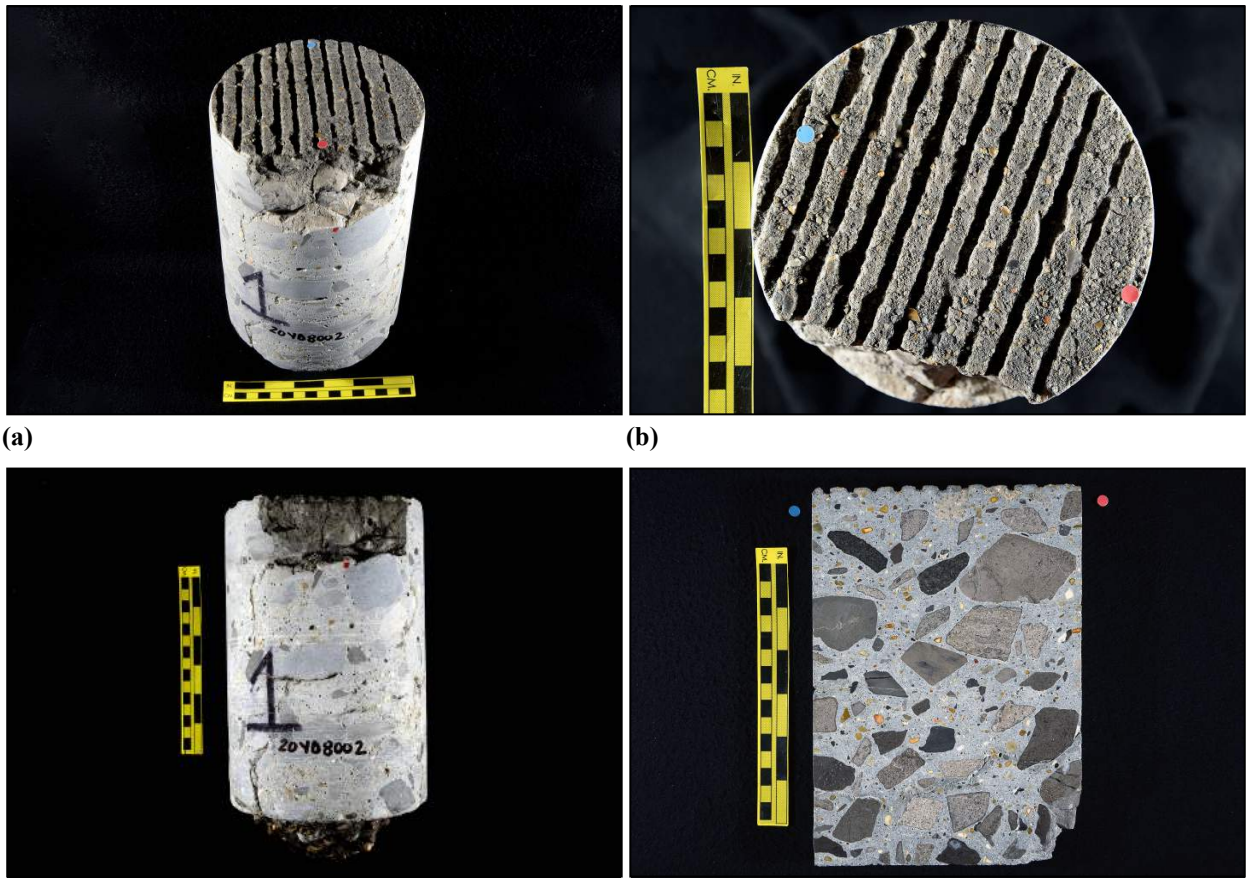

(a) **(b)**

(c) **(d)**

Figure 1. Photographs of Core 1. (a) Oblique view of the top and side of the core. (b) View of the top surface of the core. (c) View of the side of the core; note spalled area. (d) View of the polished surface of the core. Note that both sides of the core were polished. The yellow scale bar is ~ 150 mm (6 in.) long.

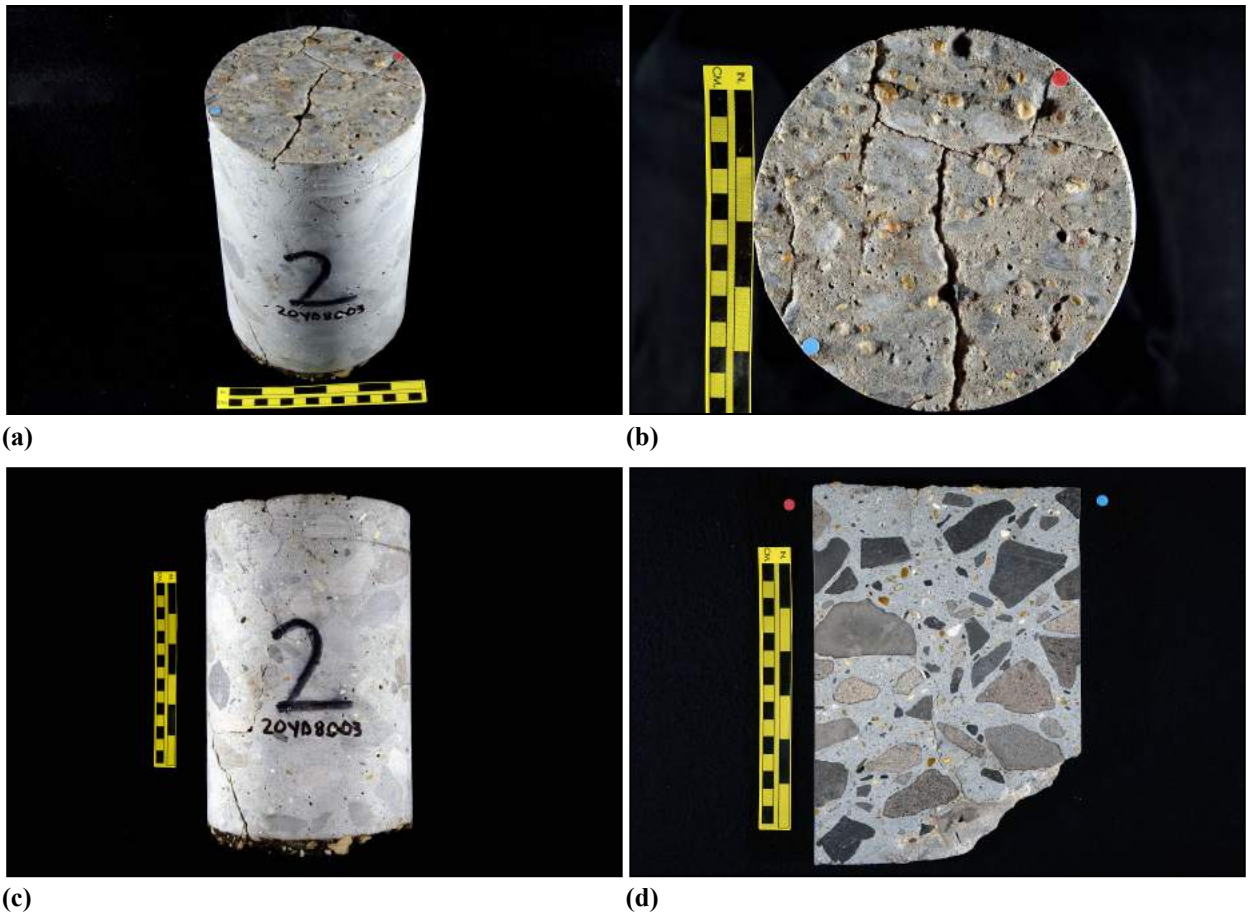

Figure 2. Photographs of Core 2. (a) Oblique view of the top and side of the core. (b) View of the top surface of the core. (c) View of the side of the core. (d) View of the polished surface of the core. Note that both sides of the core were polished. The yellow scale bar is ~ 150 mm (6 in.) long.

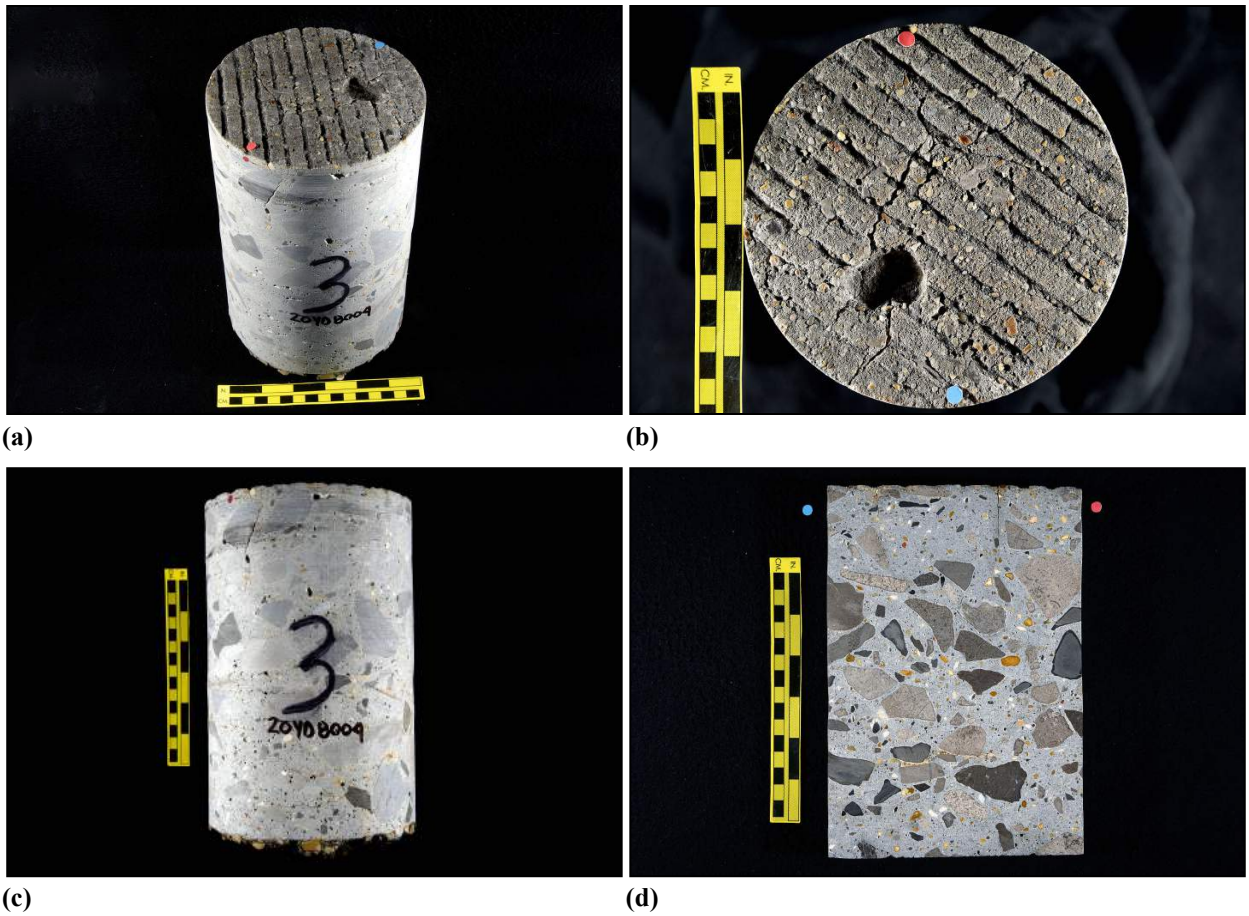

(a) (b)

(c) (d)

Figure 3. Photographs of Core 3. (a) Oblique view of the top and side of the core. (b) View of the top surface of the core. Note large pit. (c) View of the side of the core. (d) View of the polished surface of the core. Note that both sides of the core were polished. The yellow scale bar is ~ 150 mm (6 in.) long.

3.2 ***Components: Paste*** The paste fraction of all the cores consists of hydrated cement with fly ash; no slag cement or other supplemental cementitious materials were observed (**Figure 4, Figure 5)**. The hydration is normal with relict and residual cement grains that consist primarily of belite rimmed by interstitial aluminate and ferrite observed most commonly. Calcium hydroxide is fine to medium-grained and distributed fairly evenly throughout the paste. Very fine fragments of calcite were observed in the paste, suggesting that limestone was blended with the cement. EDS analysis of fly ash particles in all of the cores showed relatively high calcium peaks, which is typical of Class C fly ash (**Figure 5c**). The physical and optical properties of the paste observed in all the cores indicate broad consistency in the proportioning of water and cementitious materials. The cores show layers at the top of the cores that are 1-2 mm (40-80 mil) where the paste is slightly darker than in the rest of the core below.

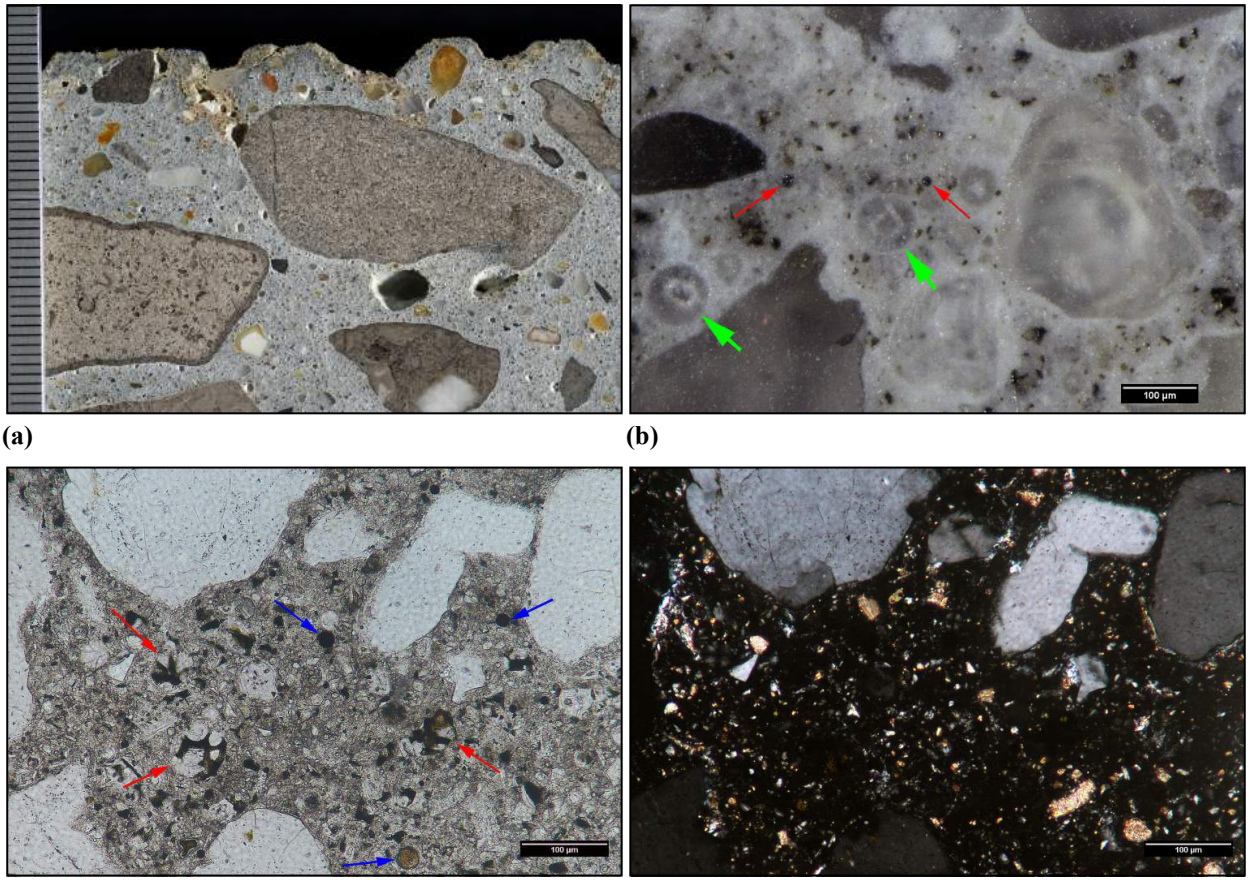

(a) (b)

(c) (d)

Figure 4. Examples of paste properties in Core 1. (a) Photograph of the polished surface showing overview of paste at the top of the core; the scale is in millimeters. (b) Reflected light photomicrograph of polished surface showing paste texture and luster in the middle of the core. The red arrows indicate grains of fly ash and the green arrows indicate deposits of ettringite in voids. Transmitted light photomicrographs of thin section showing detail of paste in (c) plane-polarized and (d) cross-polarized light. The red and blue arrows in (c) indicate relict and residual cement grains and fly ash, respectively.

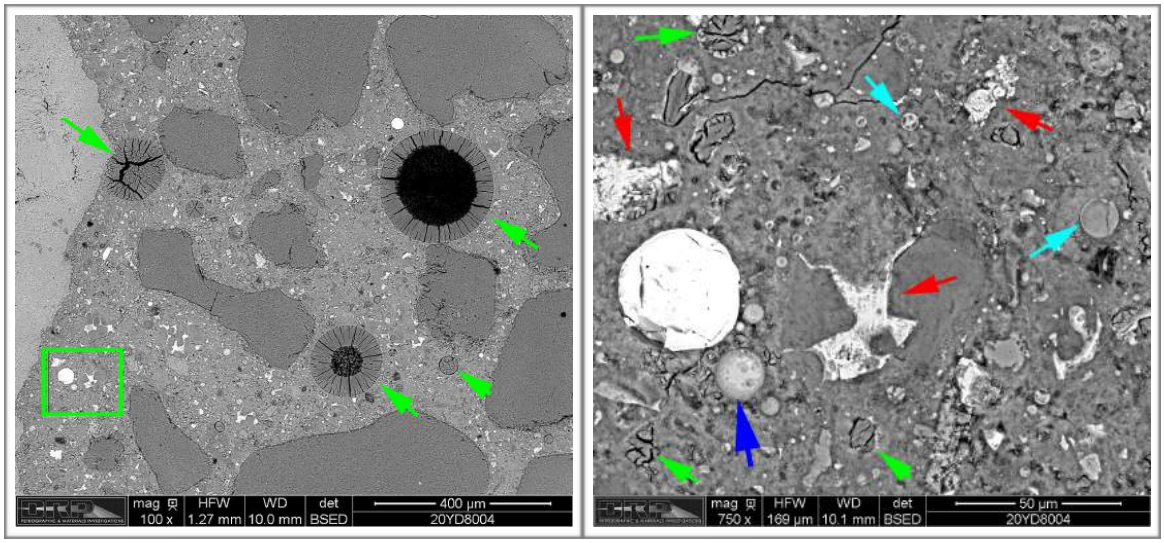

(a) (b)

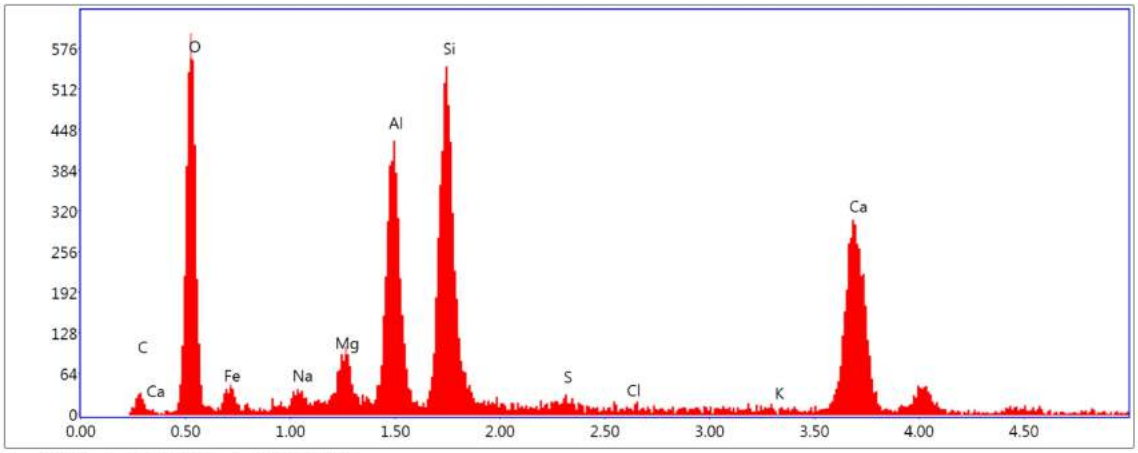

(c)

Figure 5. Backscatter electron (BSE) micrographs of paste from Core 3. The green box in (a) shows the area of (b). The green arrows indicate deposits of ettringite in both micrographs and the red and blue arrows in (b) indicate relict and residual cement grains and fly ash, respectively. (c) EDS spectrum obtained from fly ash particle indicated by the darker blue arrow in (b). Note the high peak for calcium (Ca), which is typical of Class C fly ash.

3.3 ***Components: Air*** Core 1 and Core 3 show marginal entrainment of air voids where most voids are spherical in shape and less than 1 mm (40 mil) across (**Figure 6**). However, the total air contents, which were estimated at 3-4% from visual and microscopical observations, are well below those typically observed in purposefully air-entrained concrete. Core 2 showed markedly lower air content estimated at less than 2%. However, none of the cores are subjects of a quantitative measurement of hardened air per ASTM C457 [**3**]. All three cores were well consolidated with no major entrapped air voids, water voids or consolidation voids observed.

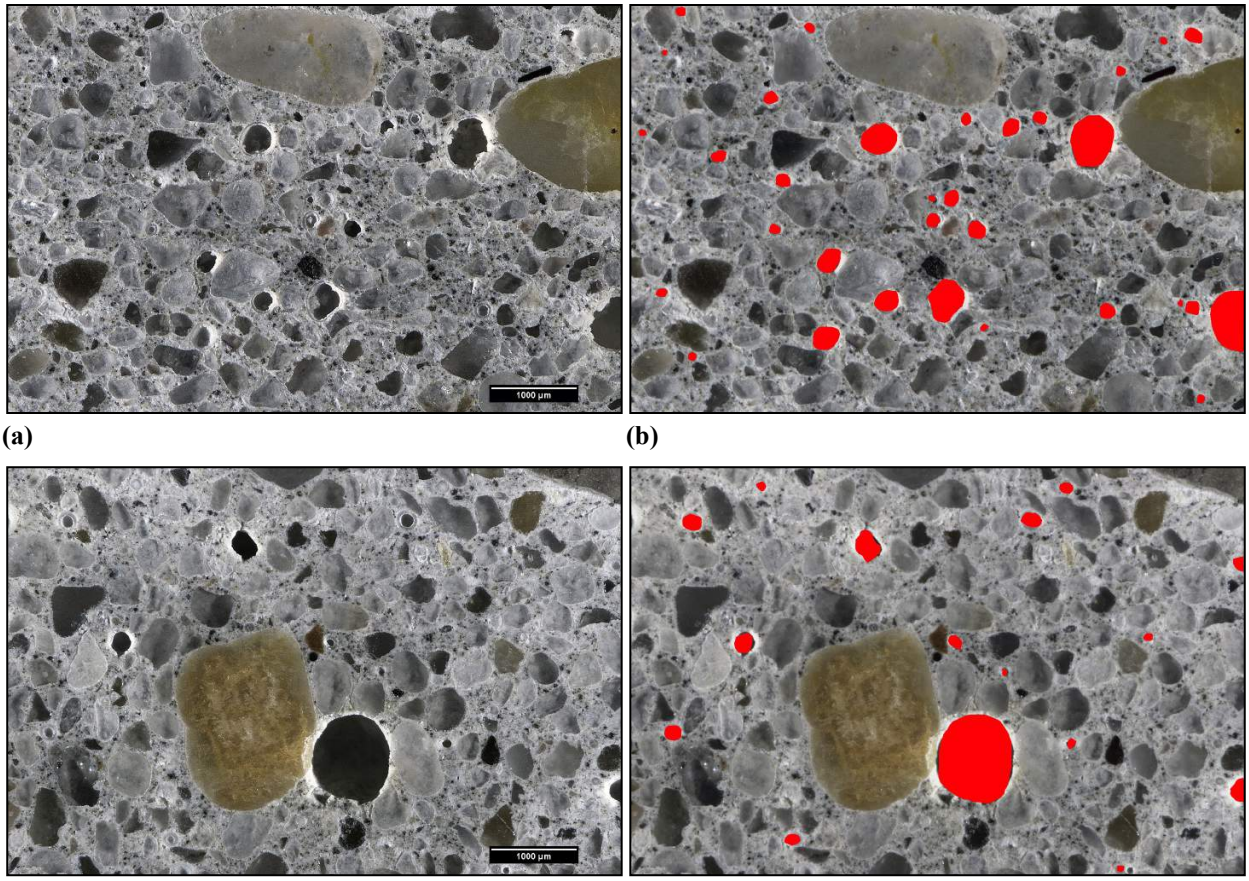

Figure 6. Air voids. (a) and (b) are reflected light photomicrographs of the same are of the polished surface of Core 1 showing air voids, which appear as black areas in (a), were filled in with a red marker as shown in (b). The image in (b) was then subjected to image analysis and the red areas make up ~ 4% of the area. (c) and (d) are reflected light photomicrographs of the same are of the polished surface of Core 3. The air voids, which appear as black areas in (c), were filled in with a red marker as shown in (d). The image in (d) was then subjected to image analysis and the red areas make up ~ 3% of the area.

3 *Standard Test Method for Microscopical Determination of Parameters of the Air-Void System in Hardened Concrete*, Annual Book of ASTM Standards, Vol. 4.02, ASTM C457-12.

3.4 ***Components: Aggregates*** The cores contains similar aggregates. The coarse aggregate is a limestone gravel with a 38 mm (1 ½ in.) nominal top size and the fine aggregate is a natural sand that consists primarily of siliceous rocks with minor amounts of carbonate rocks (limestone) similar to those observed in the coarse aggregate (**Figure 7**). The coarse aggregate shows significant gap grading in all three cores, with a paucity of particles below 25 mm (1 in.) observed such that the sand content of the concrete is high and the distribution of coarse aggregate is somewhat uneven. The coarse aggregate consists of a variety of different limestones that range from dark brown micritic (very fine-grained lime mud) rocks to pale tan oolitic limestones to brown fossiliferous jackstones to brown dolomitic limestones. Many of these particles show well-developed reaction rims, particularly the oolitic limestones and the dolomitic limestones. Examination of the oolitic and fossiliferous limestones in thin section revealed the presence of interstitial quartz and chert, which was commonly chalcedonic. Such rocks are potentially susceptible to alkali-silica reaction (ASR). As discussed below, some of the dolomitic limestones showed evidence of alkali-carbonate reaction (ACR). The natural sand consists primarily of quartz and quartzite with minor amounts of chert and traces of feldspar. Chert is potentially susceptible to ASR and particles of chert commonly showed well-developed reaction rims and occasional microcracks with gel that cut into the paste. Alkali-aggregate reactions (AAR) in the cores is discussed in detail below. The aggregates did not show deleterious coatings or incrustations. Occasional low w/cm mortar coatings were observed on coarse aggregate particles.

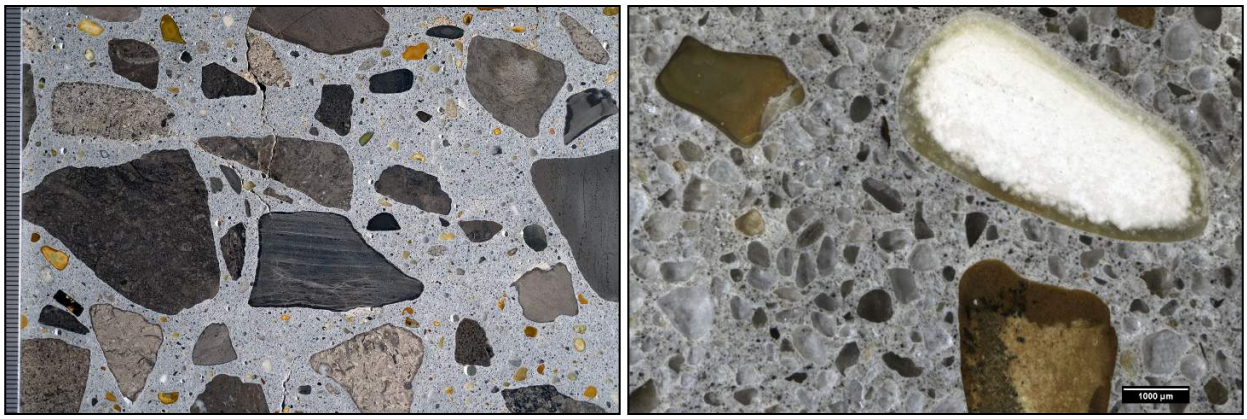

(a) **(b)**

Figure 7. (a) Photograph and (b) reflected light photomicrograph of polished surface of Core 2 showing coarse and fine aggregate, respectively. The scale is in millimeters in (a).

3.5 ***Cracking*** All three cores showed extensive cracking. Triple-point crack systems were observed on the top surfaces of each core and sub-vertical and sub-horizontal cracks were observed within the cores. **Figure 8-Figure 10** show examples of cracking in Cores 1-3 respectively. The main cracking mechanisms observed in the cores are consistent with a combination of shrinkage cracking and cracking due to AAR.

Core 1 Core 1 shows cracks up to 250 µm (10 mil) wide that cut across the the top surface and cracks up to 1.5 mm (60 mil) wide and 70-200 mm (2 ¾ - 8 in.) long on the side of the core. On the polished surface major sub-horizontal cracks up to 2 mm (80 mil) wide that cut across the full width of the core were observed at 75 mm (3 in.), 110 mm (4 ⅜ in.) and 145 mm (5 ¾ in.) below the top surface. Some of the cracks contain deposits of ASR gel and ettringite was observed along segments of the cracks. Microcracking was relatively minor in the core. Several microcracks cut sub-vertically from the top surface to 6 mm (¼ in.). Minor microcracking was observed in reaction rims in some coarse aggregate particles. Occasional microcracks filled with gel cut from limestone particles into the paste (see section on AAR below for more detail).

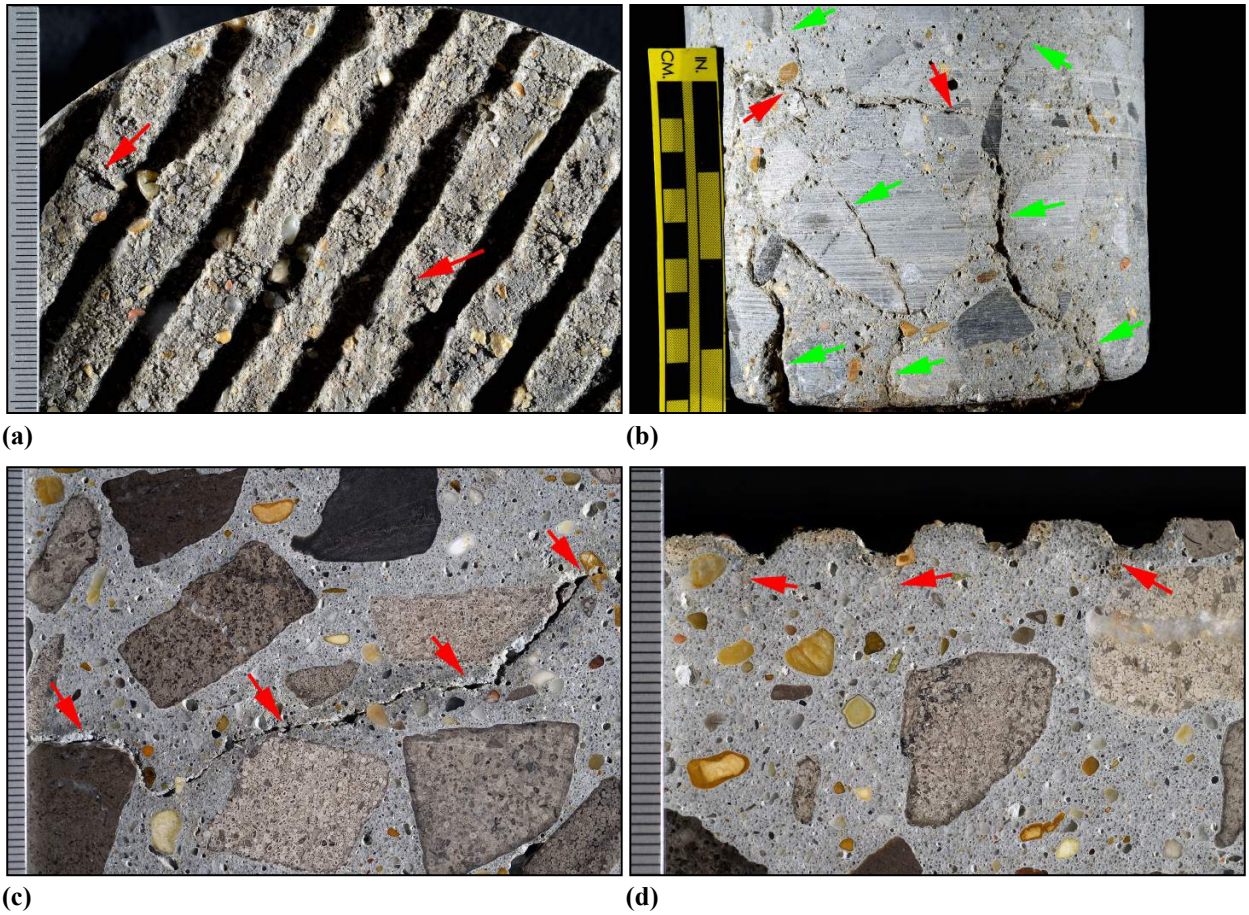

(a) (b)

(c) (d)

Figure 8. Photographs of cracking in Core 1. (a) Linear cracks (red arrows) on the top surface. (b) Sub-vertical cracks (green arrows) and sub-horizontal cracks (red arrows) near the bottom of the core. (c) Sub-horizontal crack (red arrows) about 75 mm (3 in.) below the top surface. (d) Sub-vertical microcracks (red arrows) at the top of the core. Scale in millimeters in all photos except (b).

Core 2 Core 2 shows cracks up to 750 µm (30 mil) wide that cut across the the top surface and cracks up to 500 µm (20 mil) wide and 75-200 mm (3 - 8 in.) long on the side of the core. On the polished surface sub-vertical cracks up to 500 µm (20 mil) wide cut from the top surface where they intersect sub-horizontal cracks ~ 38 mm (1 ½ in.) below the top surface. A hairline crack cuts sub-vertically from the top surface through a chert particle where it terminates in a dolomitic aggregate particle at ~ 15 mm (⅝ in.). These cracks show minor discoloration of the paste along their walls but are generally free of secondary deposits. A crack ranging from 250 µm (10 mil) to 2 mm (80 mil) wide cuts from the bottom surface to 100 mm (4 in.). Deposits of ettringite and ASR gel were observed along segments of the crack. Several microcracks ranging up to 100 µm (4 mil) wide cut sub-vertically from the top surface to depths of 3-6 mm (⅛-¼ in.). These microcracks lack secondary deposits. Fine peripheral microcracks less than 25 µm (1 mil) wide were observed in occasional particles of limestone.

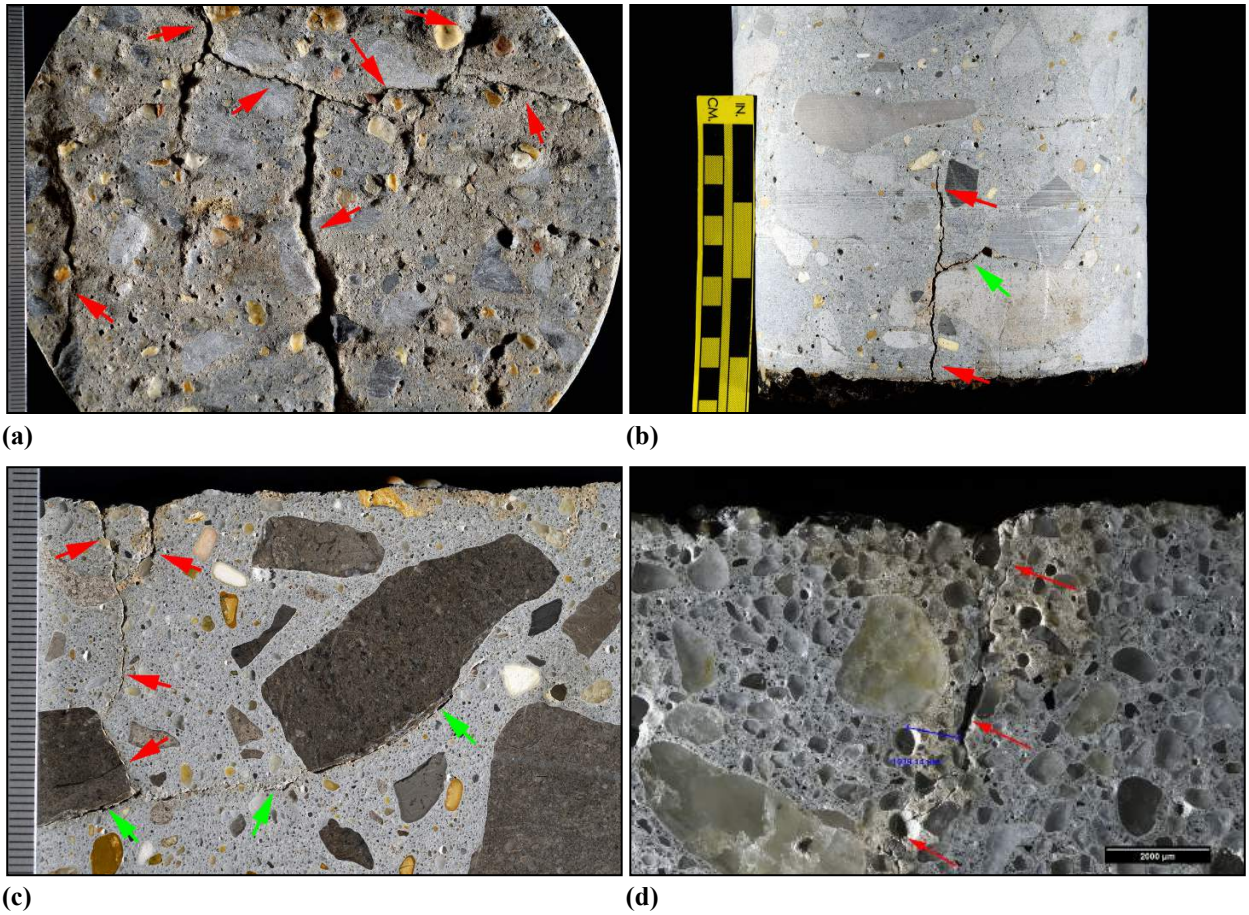

Figure 9. Photographs of cracking in Core 2. (a) Linear cracks (red arrows) on the top surface. (b) Sub-vertical crack (red arrows) and sub-horizontal crack (green arrow) near the bottom of the core. (c) Sub-horizontal crack (green arrows) and sub-vertical cracks red arrows near the top of the core. (d) Reflected light photomicrograph of a sub-vertical microcrack (red arrows) at the top of the core. Scale in millimeters in (a) and (c).

Core 3 Core 3 shows cracks up to 250 µm (0 mil) wide that cut across the the top surface and cracks up to 500 µm (20 mil) wide and 160 mm (6 ¼ in.) long on the side of the core. On the polished surface sub-vertical cracks up to 500 µm (20 mil) wide cut from the top surface 50-70 mm (2-2 ¾ in.). Several sub-horizontal cracks were observed that range up to 750 µm (30 mil) wide and cut up to the full width of the polished slab. Several sub-vertical microcracks up to 100 µm (4 mil) wide cut to depths of 3-6 mm (⅛-¼ in.). These cut around aggregates and are free of secondary deposits. Extensive microcracking was observed in reaction rims in dolomitic aggregate particles. Most of these are less than 25 µm (1 mil) wide. Occasional microcracks cut from these aggregate particles into the paste; these are mostly free of secondary deposits but some contain deposits of ettringite.

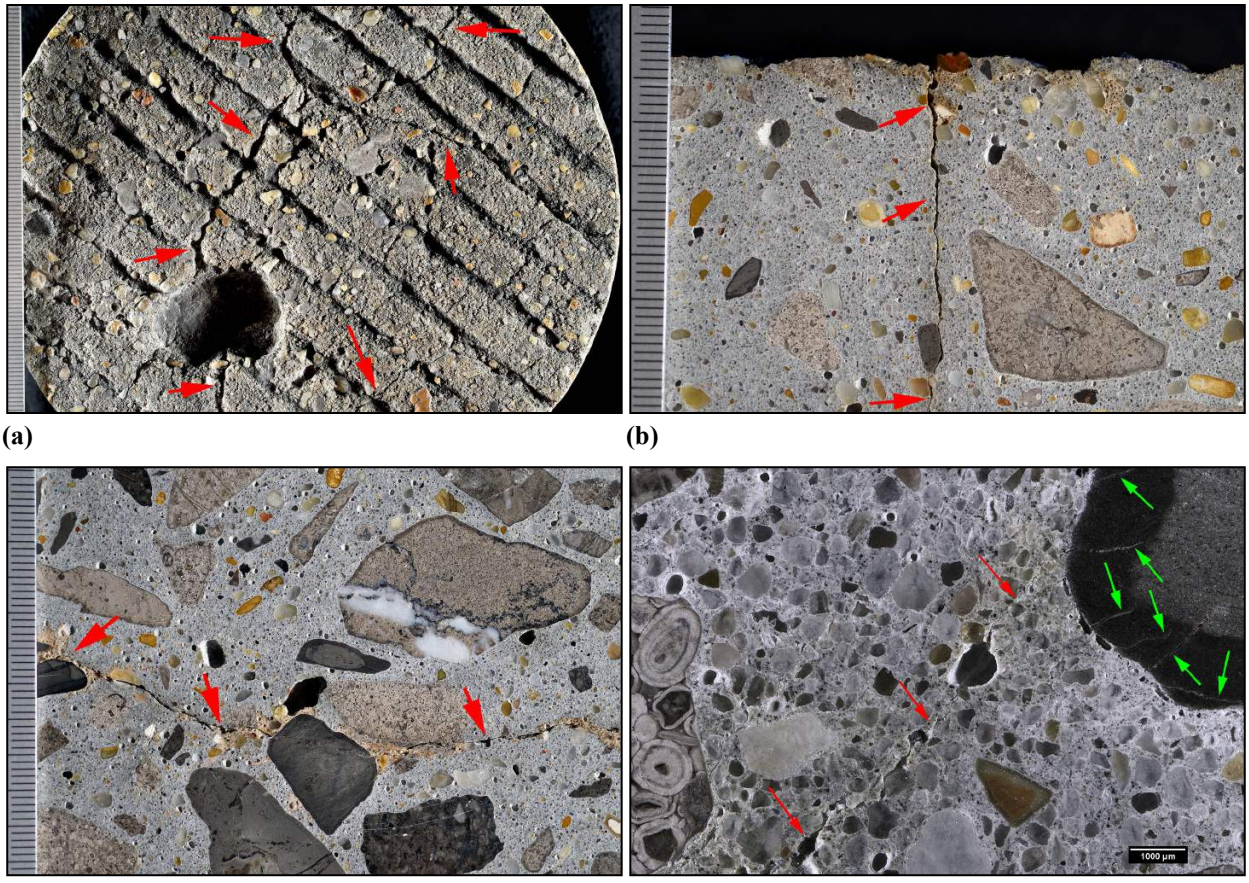

Figure 10. Photographs of cracking in Core 3. (a) Linear cracks (red arrows) on the top surface. (b) Sub-vertical crack (red arrows) at the top of the core. (c) Sub-horizontal crack (red arrows) about 165 mm (6 ½ in.) below the top surface. (d) Reflected light photomicrograph of dolomitic limestone particle with peripheral microcracks (green arrows) and hairline crack cutting through the paste (red arrows) about 110 mm (4 ⅜ in.) below the top surface.

3.6 ***Secondary Deposits—Carbonation*** No significant carbonation was detected by phenolphthalein staining or thin section microscopy; which indicate negligible carbonation (< 1 mm or 40 mil; **Figure 11**).

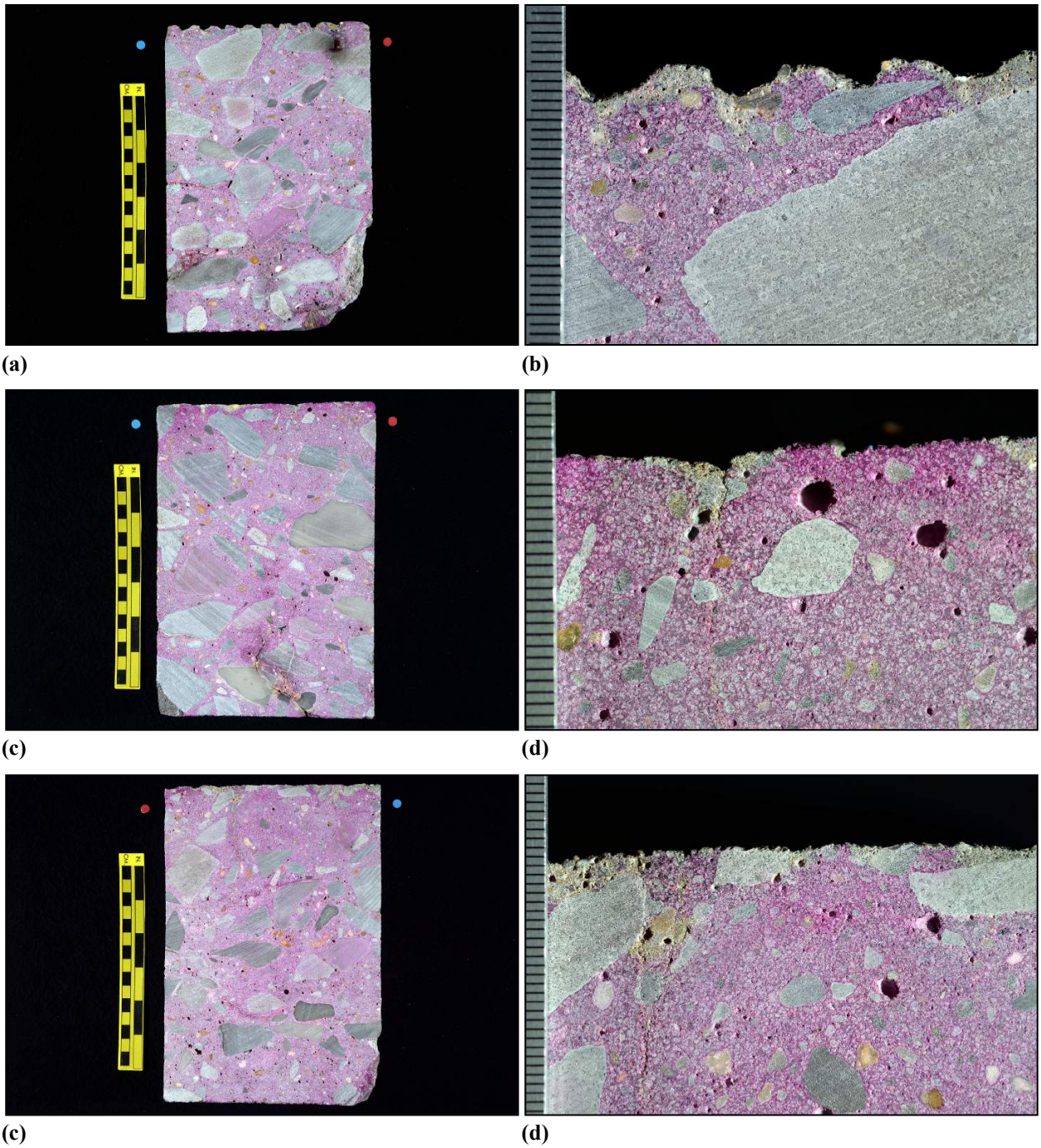

Figure 11. Photographs of the phenolphthalein stained surfaces. (a), (b) Core 1. (c), (d) Core 2. (e), (f) Core 3. The yellow scale bar is ~ 150 mm (6 in.) long; the scale is in millimeters in (b), (d) and (f).

3.7 ***Secondary Deposits—Ettringite*** Ettringite was observed in all three cores but is more abundant in Core 1 and Core 3 than in Core 2. The ettringite occurs primarily in air voids but was also observed lining and filling segments of cracks and microcracks as well as discrete deposits in the paste (**Figure 12**). No cracking or microcracking due to ettringite mineralization was observed.

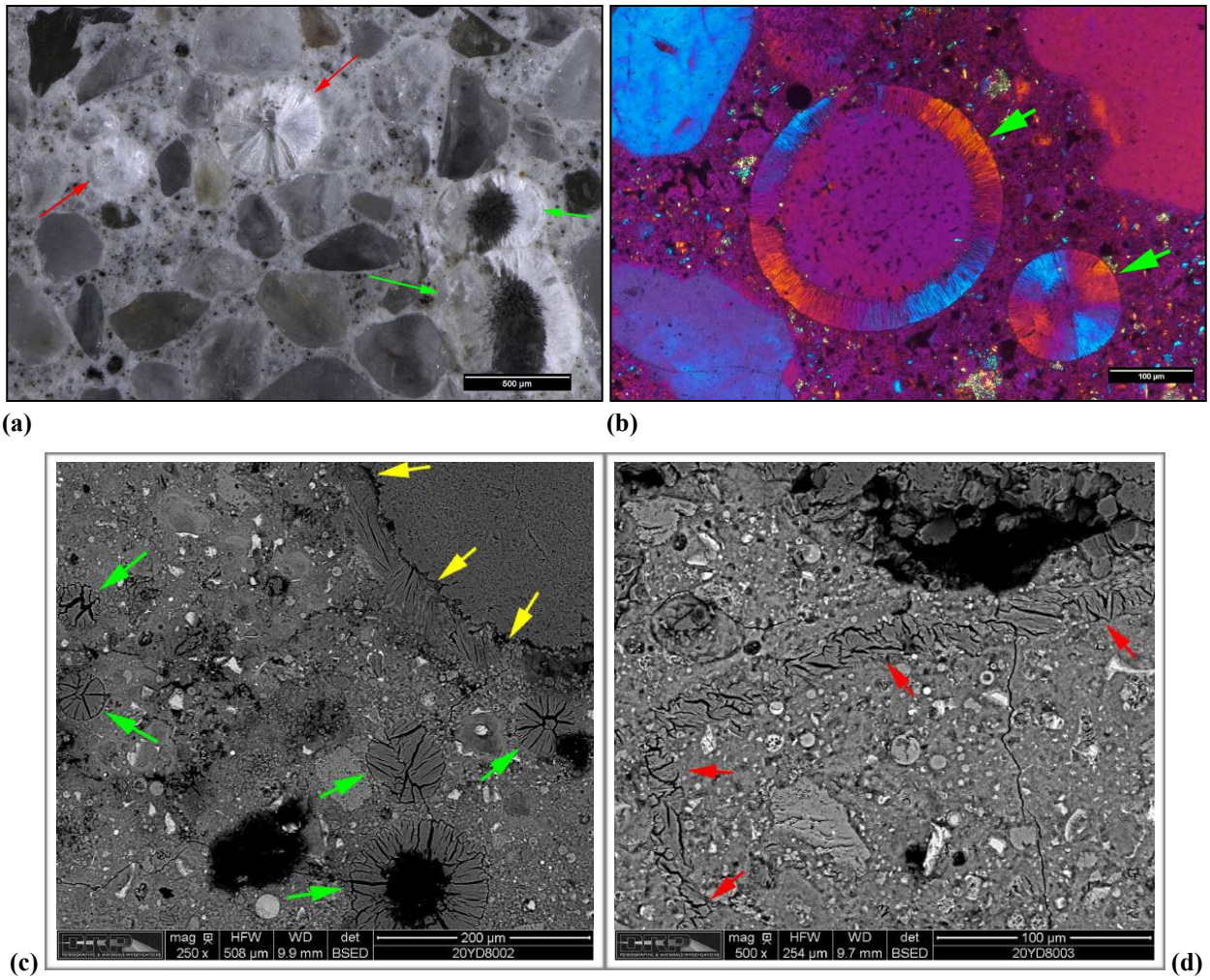

(a) (b) (c) (d)

Figure 12. (a) Reflected light photomicrograph of the polished surface of Core 1 showing ettringite filling air voids (red arrows) and lining air voids (green arrows). (b) Cross-polarized transmitted light photomicrograph of thin section from Core 3 showing voids lined and filled with ettringite (green arrows). (c) BSE micrograph of polished surface from Core 1 showing voids with ettringite (green arrows) and ettringite in the interfacial transition zone (yellow arrows) between an aggregate particle and the paste. (d) BSE micrograph of the polished surface from Core 2 showing microcrack filled with ettringite (red arrows).

3.7 ***Secondary Deposits—ASR Gel*** Deposits of gel were observed in all three cores (**Figure 13**) but they are most abundant in Core 1, followed by Core 3 and are relatively scarce in Core 2. In all three cores analysis of gel compositions by EDS indicated they consist primarily of calcium and silicon. This indicates the gels are fairly mature, as calcium tends to diffuse into gels over time. This also suggests that the concrete shows evidence of alkali cycling, which may promote continued AAR. The reactive components in these cores primarily involves fossiliferous and oolitic limestones, which also contain interstitial quartz and chert, some of which is chalcedonic. Minor reaction was also observed with chert particles in the fine aggregate.

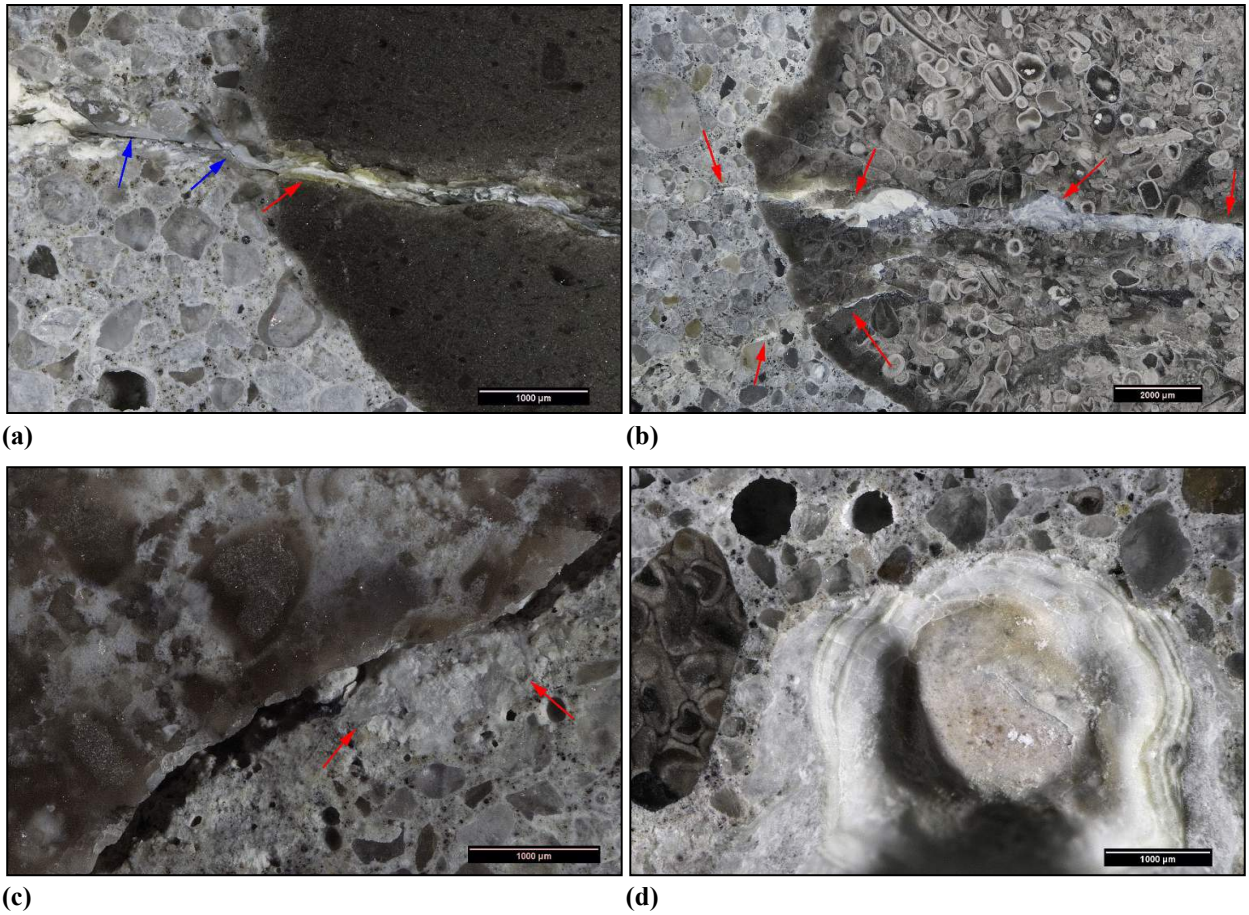

(a) **(b)**

(c) **(d)**

Figure 13. Reflected light photomicrographs of the polished surfaces of (a), (b) Core 1 and (c), (d) Core 3 showing deposits of ASR gel. In (a) the red arrow indicates white gel in a dolomitic limestone particle about 110 mm (4 ⅜ in.) below the top surface and the blue arrows indicate translucent gel in the paste. In (b) the red arrows show deposits of gel about 150 mm (6 in.) below the top surface. In (c) the red arrows show a deposit of gel in the ITZ of a limestone particle about 90 mm (3 ½ in.) below the top surface. (d) Laminated gel deposit in void about 135 mm (5 ⅜ in.) below the top surface. All of these deposits were analyzed by EDS and found to consist primarily of calcium and silicon (see Appendices for details).

3.8 ***Alkali-Carbonate Reaction*** All three cores show evidence of ACR but it is most advanced in Core 3, where numerous limestone particles show peripheral microcracking in reaction rims. The cores show and cracks and microcracks that cut from particles of dolomitic limestone into the paste (**Figure 14**). The reactive components involve the dark brown dolomitic limestone observed in the coarse aggregate.

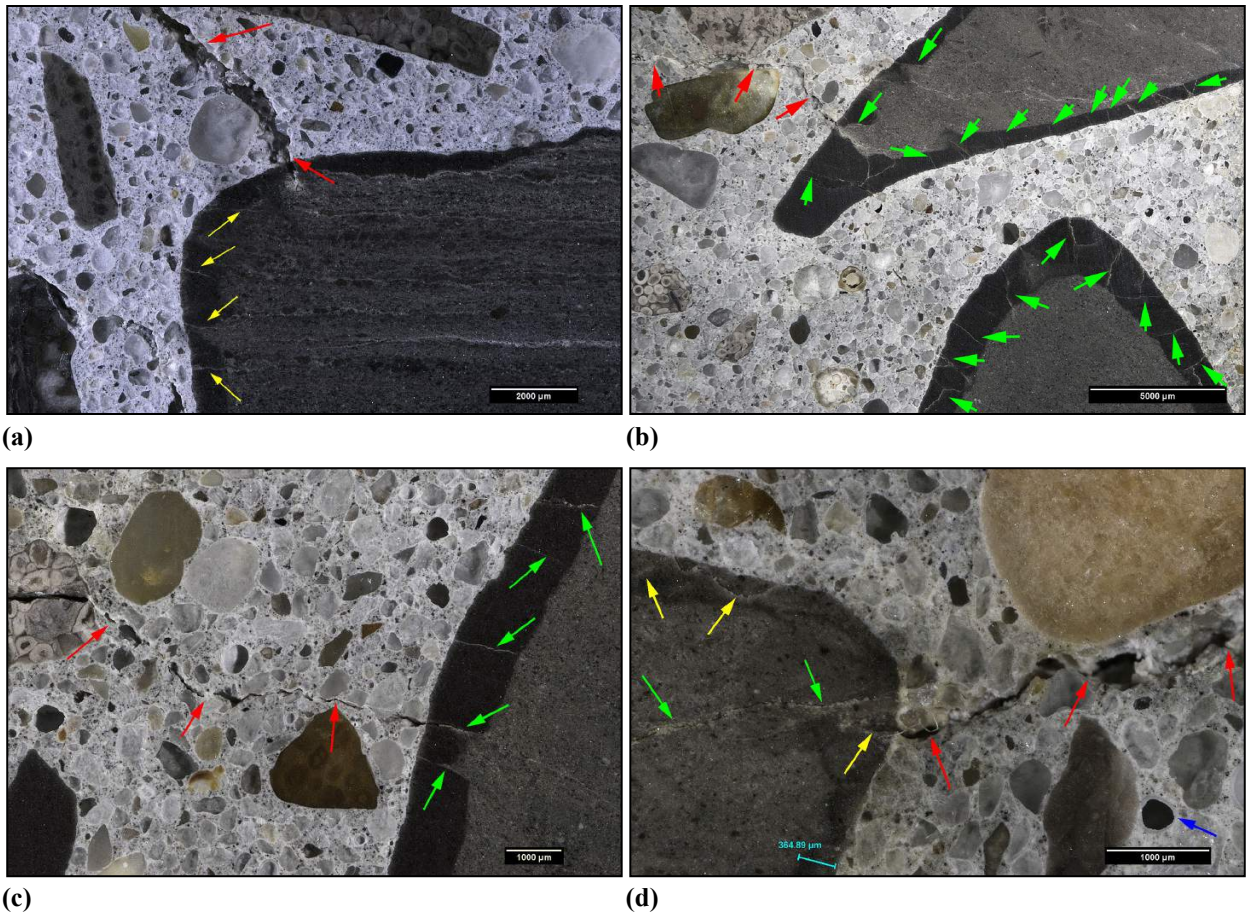

(a) **(b)**

(c) **(d)**

Figure 14. Evidence of ACR. (a) Reflected light photomicrograph of polished surface of Core 2 showing limestone particle with peripheral microcracks (yellow arrows) and crack (red arrows) that cuts from the particle and into the paste about 65 mm (2 ½ in.) below the top surface. (b)-(c) Reflected light photomicrographs of the polished surface of Core 3 showing peripheral microcracks (green arrows) in dolomitic limestone particles about (b) 80 mm (3 ⅛ in.) and (c) 85 mm (3 ⅜ in.) below the top surface. Red arrows show cracks that cut from the particle into the paste. (d) Reflected light photomicrograph of polished surface of Core 3 showing peripheral microcracks (yellow arrows) in dolomitic limestone particle about 165 mm (6 ½ in.) below the top surface. The green arrows highlight a sub-horizontal microcrack in the particle, the red arrows show a crack that cuts from the particle into the paste. The blue bar measures the width of a reaction rim and the blue arrow indicates a void lined by ettringite.

4.0 DISCUSSION & CONCLUSIONS

Based on the findings described above, the concrete represented by the cores is made from similar components. The paste consists of hydrated portland cement with fly ash; no slag cement or other supplemental cementitious materials observed. The physical and optical properties of the paste observed in all the cores indicate broad consistency in the proportioning of water and cementitious materials. The cores are not purposefully air entrained but Core 1 and Core 3 contain 3-4% air whereas Core 4 contains less than 2% air as estimated from visual and microscopical observations (not measured per ASTM C457). The coarse aggregate is a limestone gravel with a 38 mm (1 ½ in.) nominal top size and the fine aggregate is a natural siliceous sand. All three cores show significant gap grading in the coarse aggregate.

Extensive cracking and microcracking was observed over the full thickness of all three cores. The mechanisms associated with the cracking involve drying shrinkage and AAR. The shrinkage cracks and microcracks are typical of concrete with significant gap grading. Extensive sub-horizontal cracking and microcracking typical of AAR was observed in all three cores but is most prevalent in Core 1 and Core 3. These cores also show the most extensive ettringite mineralization, which is consistent with higher internal relative humidity.

The reactive components for AAR were observed primarily in the coarse aggregate. Rocks that show evidence of ASR include fossiliferous and oolitic limestone particles that contain interstitial quartz and chert. Minor ASR was also observed in association with some of the chert particles observed in the fine aggregate. Brown dolomitic limestones observed in the coarse aggregate are associated with ACR where extensive peripheral microcracks are present and cracks cut from these particles into the paste.

This concludes work performed on this project to date.

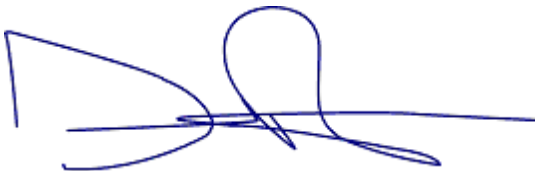

David Rothstein, Ph.D., P.G., FACI

LTRC 16-1TA-C Pavement Core Petrography

Appendices

Appendix A	**Core #1 Petrography (ASTM C856/ASTM C1723)**
Appendix B	**Core #2 Petrography (ASTM C856/ASTM C1723)**
Appendix C	**Core #3 Petrography (ASTM C856/ASTM C1723)**
Appendix D	**Procedures**

1. Received Condition

Orientation	Vertical core through pavement slab measures 150 mm (6 in.) in diameter and 220 mm (~ 8 ⅝ in.) in length (**Figure A1, A2**).
Surfaces	The top surface is tined (**Figure A3**) and the lower surface is cast on asphalt such that the core represents the full thickness of the portland cement concrete pavement.
General Condition	The concrete is hard and compact and rings lightly when sounded with a hammer. A section of the core is missing from the top surface; the missing section reaches down to 55 mm (2 ⅛ in.) below the top surface (**Figure A4**).

2. Embedded Objects

General	None observed.

3. Cracking

Macroscopic	Several cracks were observed on as-received surfaces. On the top surface two cracks measuring ~ 250 µm (10 mil) wide and 40 mm (1 ⅝ in.) long were observed (**Figure A5**). These cracks do not significantly penetrate into the core as viewed form as-received surfaces. On the side of the core several cracks were observed that range from horizontal to vertical in orientation (**Figure A6**). The larger cracks range from 70-200 mm (2 ¾-8 in.) long and are up to 1.5 mm (60 mil) wide. On the polished slab sub-horizontal cracks were observed at 75 mm (3 in.), 110 mm (4 ⅜ in.) and 145 mm (5 ¾ in.) to 150 mm (6 in.) below the top surface (**Figure A7**). The crack at 110 mm (4 ⅜ in.) is ~ 50 mm (2 in.) long and 1-1.5 mm (40-60 mil) wide over most of its strike length. The crack cuts through a limestone particle in the coarse aggregate and contains green and white deposits of ASR gel. The sub-horizontal crack at 145-155 mm (5 ¾-6 ⅛ in.) below the top surface strikes across the full width of the polished slab and ranges from 1-2 mm (40-80 mil) wide over most of the strike length. Deposits consisting of gel were observed in the crack (**Figure A8**).
Microscopic	A few different types of microcracks were observed in the core but the overall extent of microcracking is fairly minor. Several microcracks cut sub-vertically from the top surface to depths that reach up to 6 mm (¼ in.); these are up to 50 µm (2 mil) wide, cut around aggregate particles and lack secondary deposits (**Figure A9**). Minor microcracking was observed in the periphery of some coarse aggregate particles with reaction rims. Most of these microcracks are sub-parallel to the perimeter of the particles and do not cut into the adjacent paste. Occasional microcracks filled with gel cut from limestone particles into the paste (**Figure A10, Figure A11**).

4. Voids

Void System	Concrete is marginally air-entrained and contains 3-4% total air as estimated from visual and microscopical observations (**Figure A12**). The concrete is well consolidated with no significant entrapped voids or water voids observed.
Void Fillings	Voids commonly contain deposits of ettringite.

5. Coarse Aggregate

Physical Properties	The coarse aggregate is a limestone gravel with a nominal top size of 38 mm (1 ½ in.; **Figure A13**). The rocks are hard and competent. The particles are sub-equant to oblong in shape with sub-rounded to sub-angular edges. The aggregate shows major gap grading with few particles below 25 mm (1 in.) across observed such that the sand content is high. The distribution is somewhat uneven.
Rock Types	The aggregate is carbonate in composition and consists of various types of limestone that range from dark brown micritic rocks to pale tan oolitic limestones to brown fossiliferous packstones and brown dolomitic limestones. Many particles show well-defined reaction rims and some contain fine-grained siliceous material that includes chert, some of which is chalcedonic.
Other Features	No deleterious coatings or incrustations observed. No low w/c mortar coatings observed. Minor internal microcracking observed. Well-developed reaction rims are commonly observed and some particles are cut by microcracks and that contain gel and cut into the paste.

6. Fine Aggregate

Physical Properties	The fine aggregate is a natural sand that consists of rocks that are hard and competent (**Figure A14**). The sand consists primarily of siliceous rocks but minor amounts of limestone (carbonate) similar to those in the coarse aggregate were observed. The particles are sub-equant to oblong in shape with rounded to sub-angular edges. The grading and distribution are even.
Rock Types	The consists primarily of quartz and quartzite; chert is a minor component and limestone is also present.
Other Features	No deleterious coatings or incrustations observed and no low w/c mortar coatings observed. The chert commonly shows well-developed reaction rims; the quartz and quartzite particles are intact. Thin section analysis shows that some chert particles show internal microcracks with gel that cut into the paste.

7. Paste Observations

Polished Surface	Paste is light gray (Munsell 10YR/7/1), has a smooth texture and weakly sub-vitreous luster (**Figure A15**). The paste is moderately hard (Mohs 3-3.5). The paste is gray (10YR/6/1) for 1-2 mm (40-80 mil) from the top surface and irregularly distributed zones of yellow (2.5Y/7/4) to light red (2.5YR/7/4) paste are present for up to 6 mm (¼ in.) from the top surface.
Fresh Fracture	Fracture surface is gray, has a hackly texture and a sub-vitreous luster (**Figure A16**). The fracture cuts through coarse aggregate particles. No significant deposits were observed on the surface.
Thin Section/ SEM*	The paste contains hydrated portland cement and fly ash; no slag cement or other SCM were observed. The hydration is normal with 3-6% RRCG that consist mostly of belite and interstitial ferrite and aluminate (**Figure A17, Figure A18**). Minor amounts of very fine crystals of calcite are present in the paste. CH makes up 8-15% of the paste, is fine to medium grained and distributed fairly evenly.

** Abbreviations as follows: RRCG = relict and residual cement grains; SCM = supplemental cementitious materials; CH = calcium hydroxide; ITZ = interfacial transition zone. Modal abundances are based on visual estimations.*

8. Secondary Deposits

Phenolphthalein	Entire surface stains purple except along irregular zones (microcracks) at the top of the core where not staining was observed to 6 mm (¼ in.) depth (**Figure A19**).
Deposits	No significant carbonation observed. Deposits of ettringite observed commonly in voids throughout core and in microcracks that cut through the paste and in the ITZ along aggregate particles (**Figure A20**). Deposits of ASR gel observed in occasional microcracks, commonly in association with coarse aggregate particles. Occasional cracks and numerous microcracks filled with gel observed cutting from chert particles into the paste (**Figure A8, A10, A11, A21**). SEM/EDS analysis indicates the gels are richer in calcium than alkali, suggesting they are mature (**Figure A22, A23**).

FIGURES

(a)

(b)

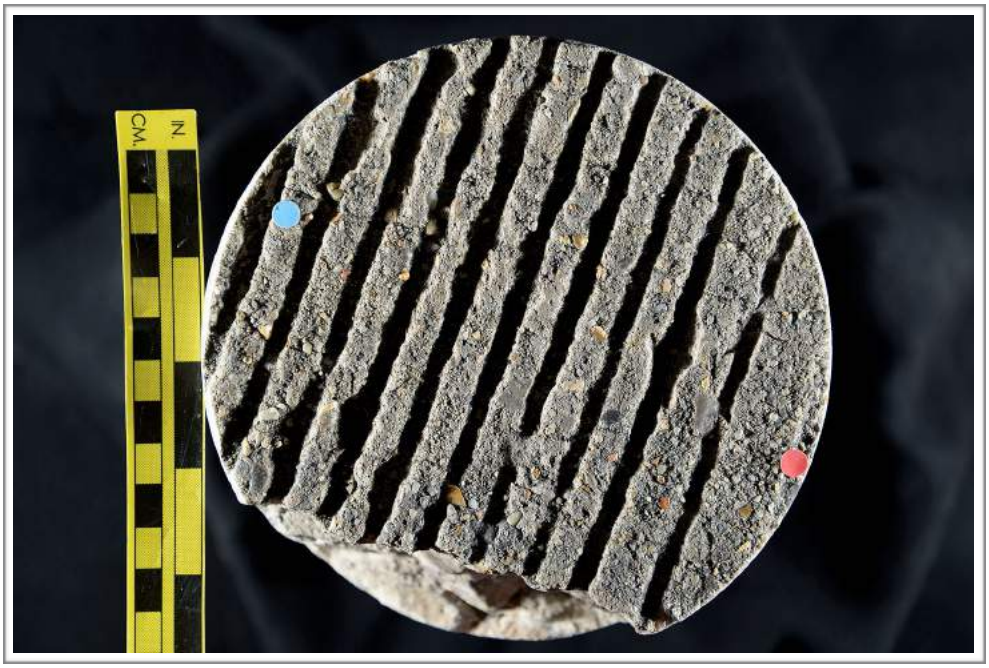

Figure A1. Photographs showing (a) oblique view of the top and side of the core with identification labels and (b) the top of the core. The red and blue dots in (b) show the orientation of the saw cuts used to prepare the sample. The yellow bar is ~ 150 mm (6 in.) long.

(c)

Figure A1 (cont'd). (c) Photograph showing the bottom surface of the core.

Figure A2. Photograph showing one of the polished surfaces of the core; both sides of the slab were polished. The yellow bar is ~ 150 mm (6 in.) long.

Figure A3. Photograph showing detail of tined top surface; scale in millimeters.

Figure A4. Photograph of top of core showing missing section.

Figure A5. Photograph of the top surface showing linear cracks (red arrows). Scale in millimeters.

(a)

Figure A6. (a) Photograph of the side of the core showing overview of cracks (red arrows). The yellow scale is ~ 150 mm (6 in.) long.

(b)

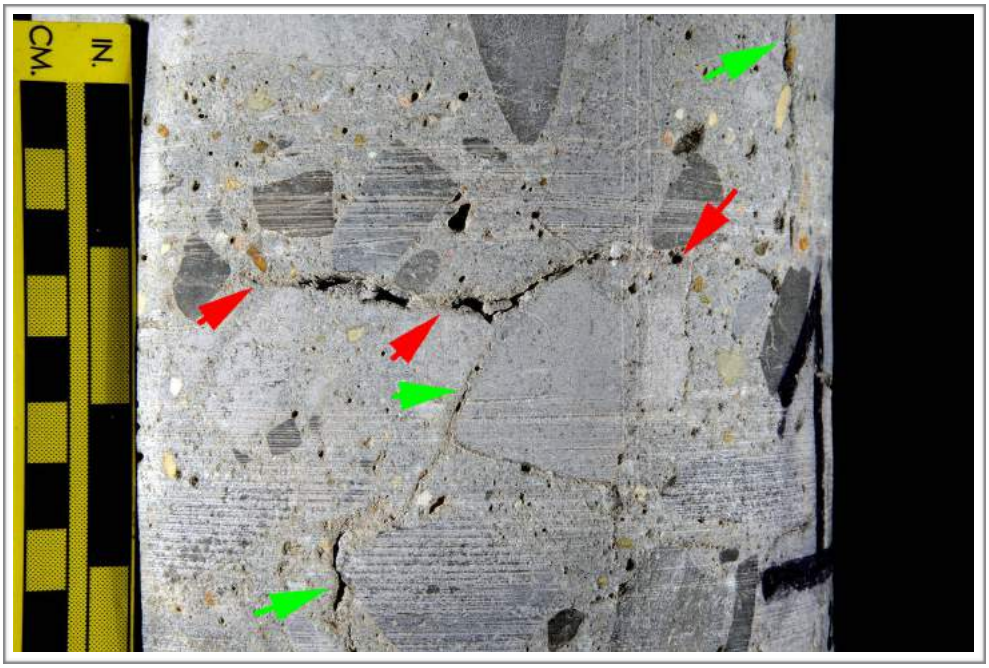

(c)

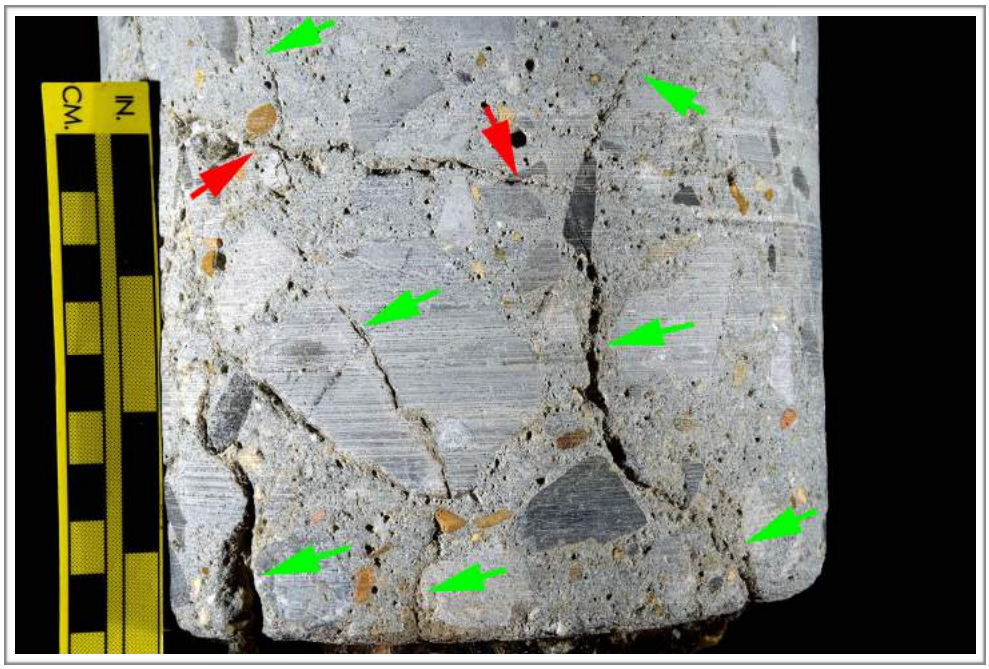

Figure A6 (cont'd). Photographs showing cracks on the side of the core. The red arrows indicate sub-horizontal cracks and the green arrows indicate sub-vertical cracks.

(a)

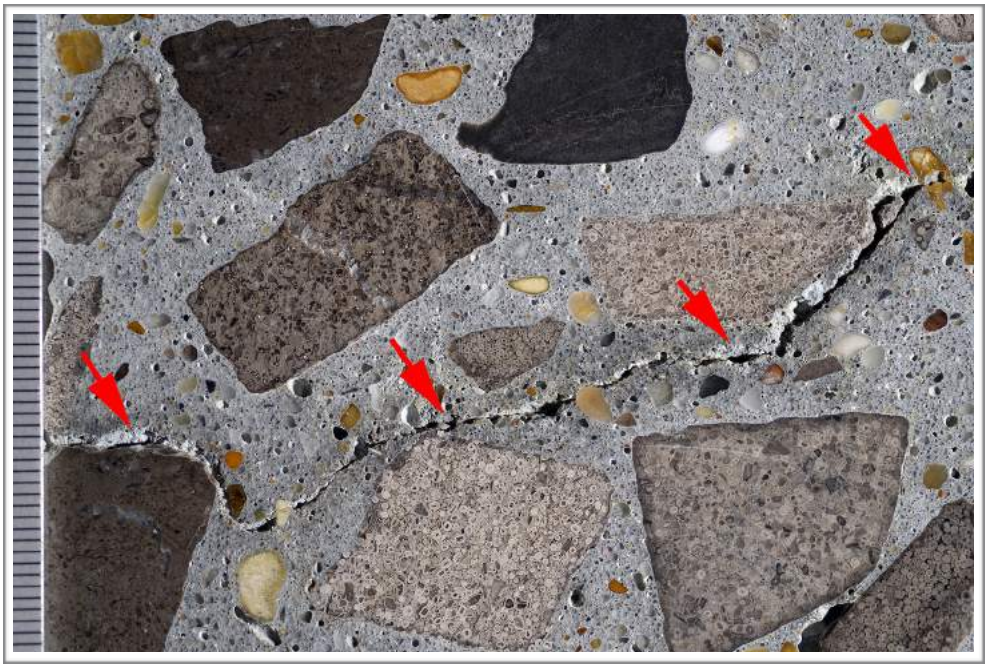

(b)

Figure A7. Photographs of the polished surface showing sub-horizontal cracks (red arrows) at (a) 75 mm (3 in.) and (b) 110 mm (4 ⅜ in.) below the top surface.

(a)

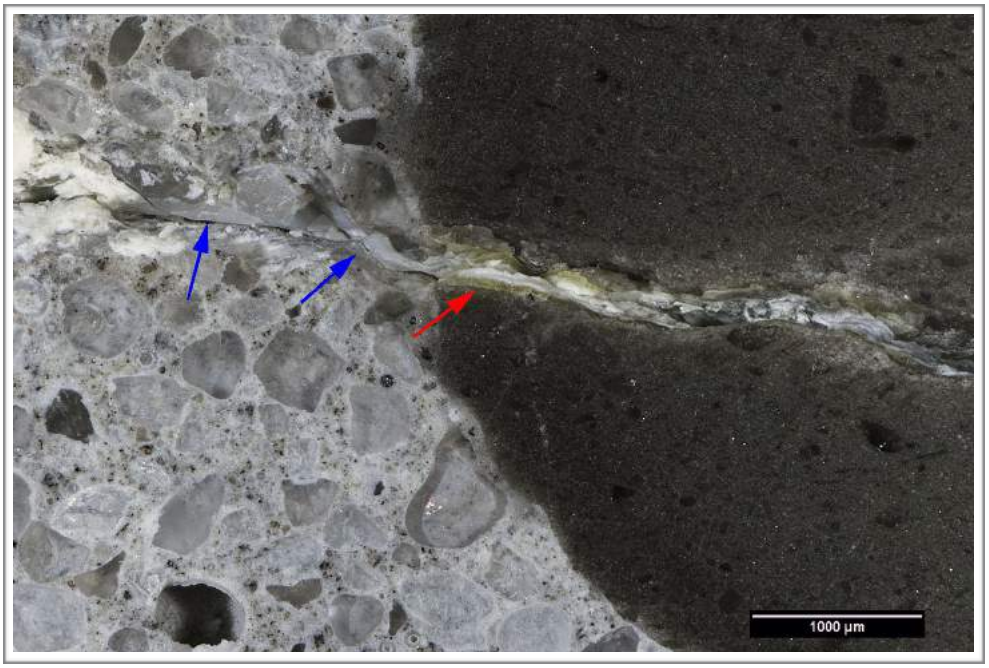

(b)

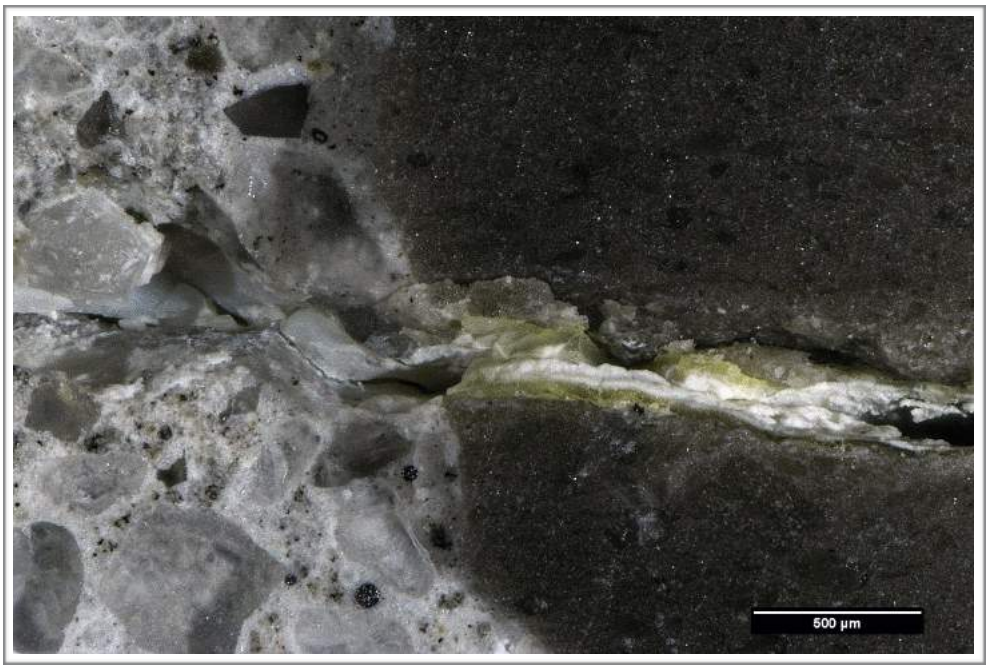

Figure A8. Reflected light photomicrographs of polished surface showing detail of gel in microcrack about 110 mm (4 ⅜ in.) below the top surface.

(a)

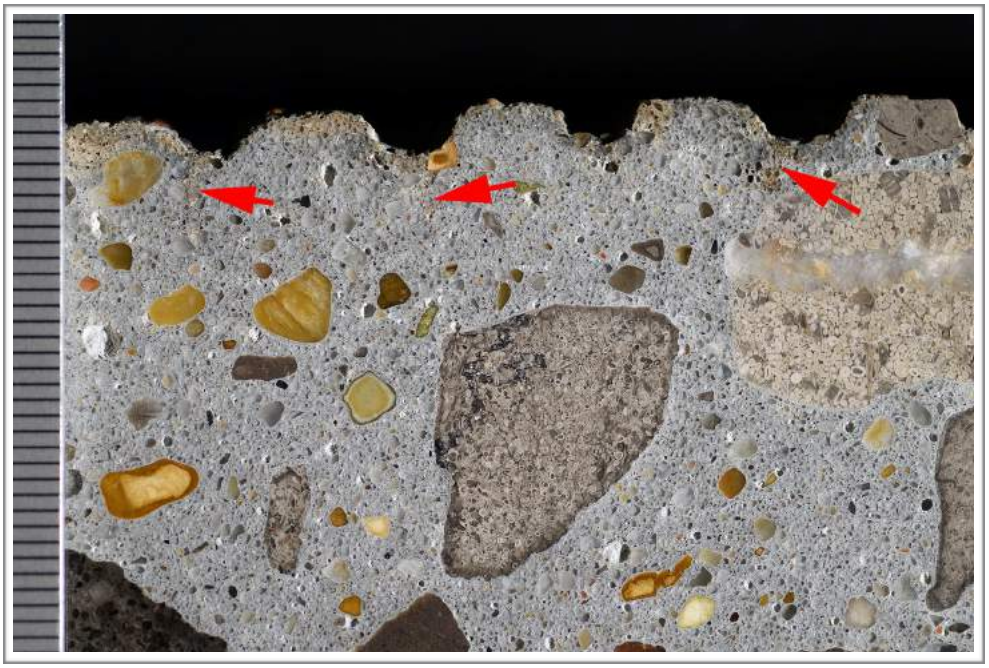

(b)

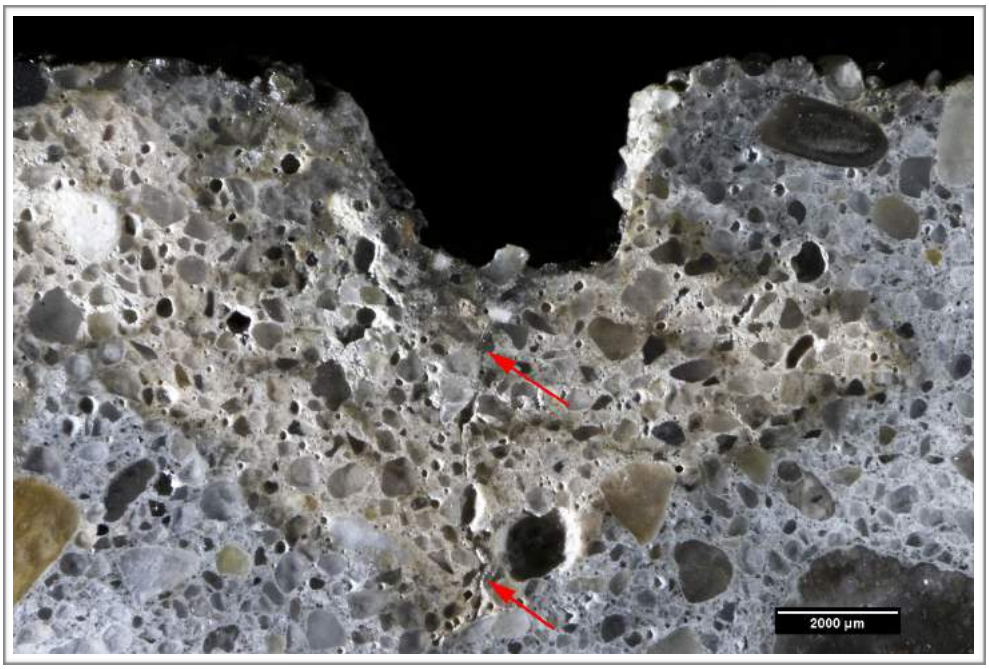

Figure A9. (a) Photograph showing overview of polished surface at the top of the core where red arrows highlight discolored paste in walls of sub-vertical microcracks. The scale is in millimeters. (b) Reflected light photomicrograph of the polished surface showing detail of sub-vertical microcrack (red arrows) at the top of the core.

(a)

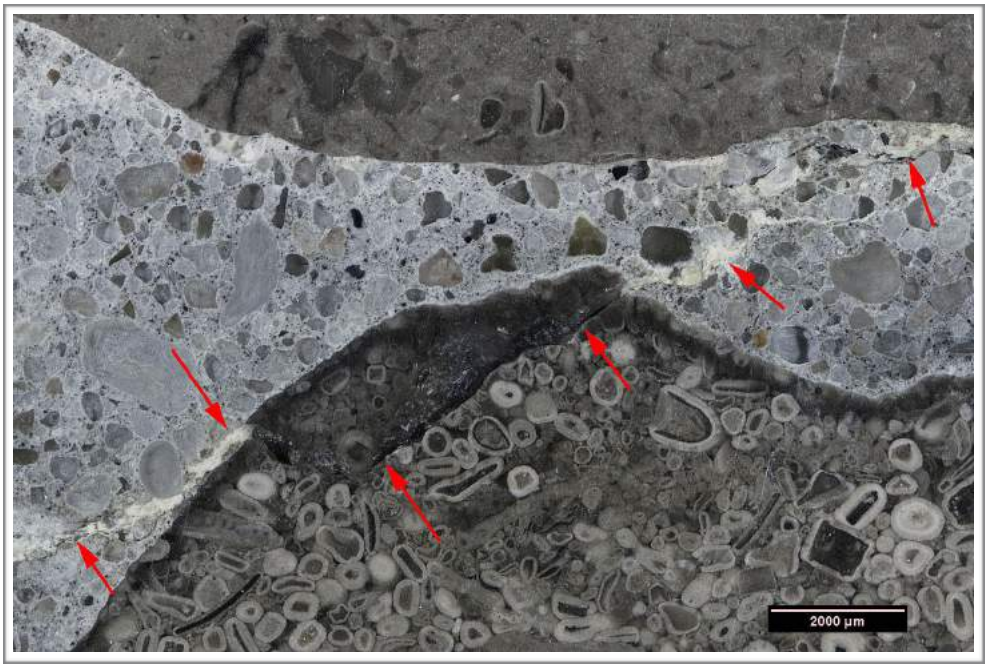

(b)

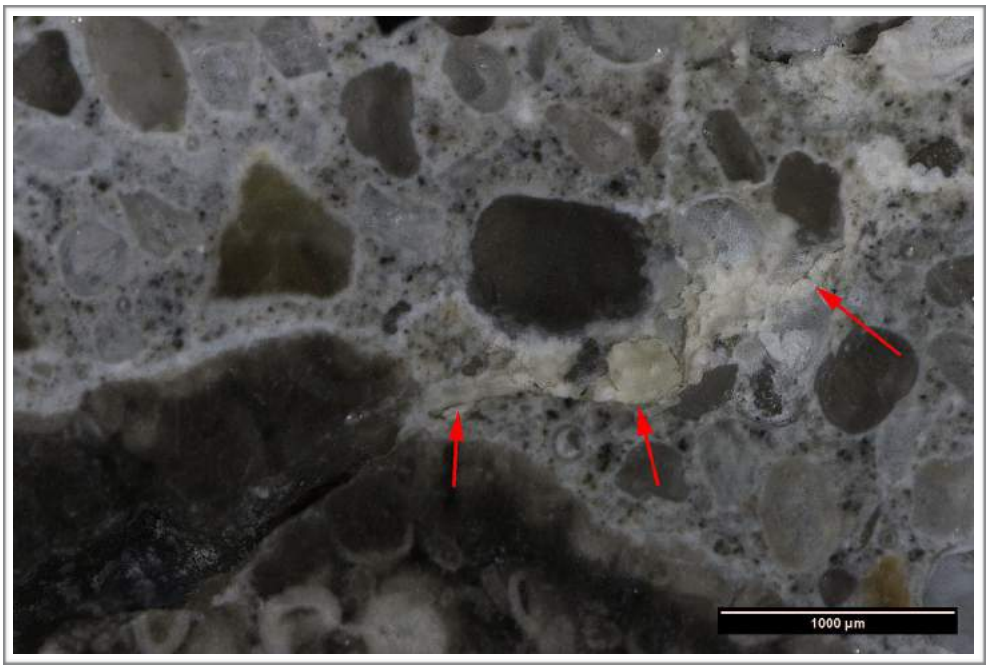

Figure A10. Reflected light photomicrographs of polished surface showing (a) overview and (b) detail of microcracks (red arrows) that cut from oolitic limestone particle into the paste about 65 mm (2 ½ in.) below the top surface. In (b) the red red arrows highlight deposits of gel.

(a)

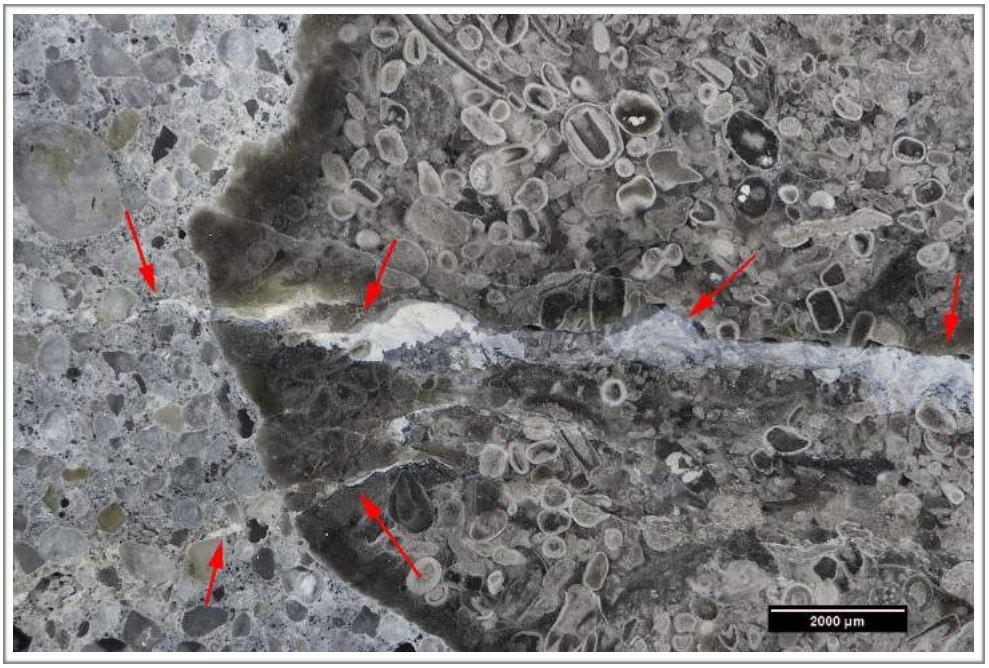

(b)

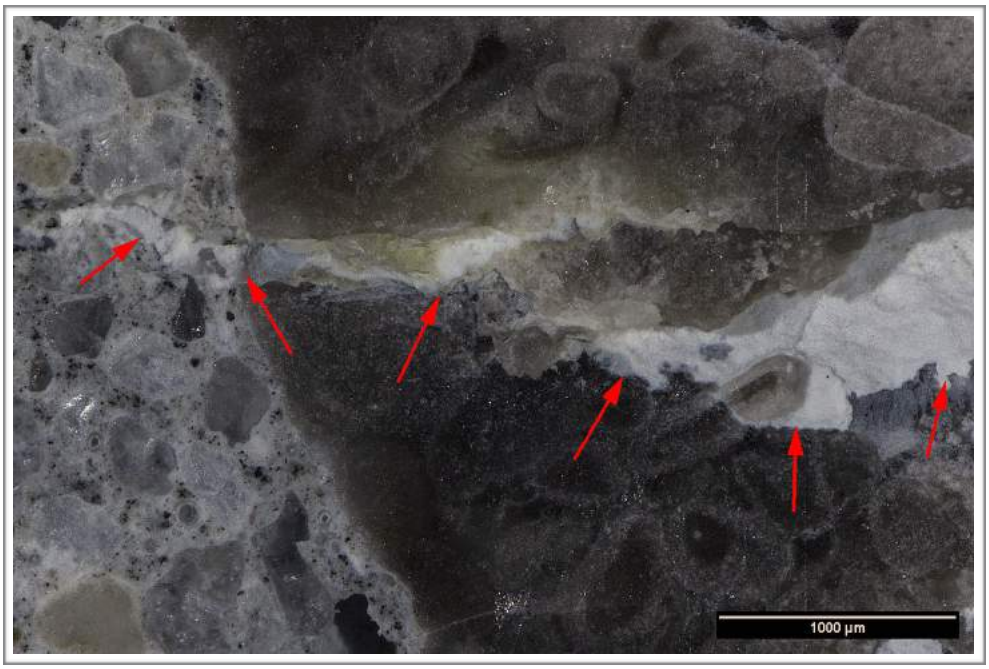

Figure A11. Reflected light photomicrographs of polished surface showing (a) overview and (b) detail of microcracks (red arrows) that cut from oolitic limestone particle into the paste about 150 mm (6 in.) below the top surface. In (b) the red red arrows highlight deposits of gel within the particle and in the microcrack in the paste.

(a)

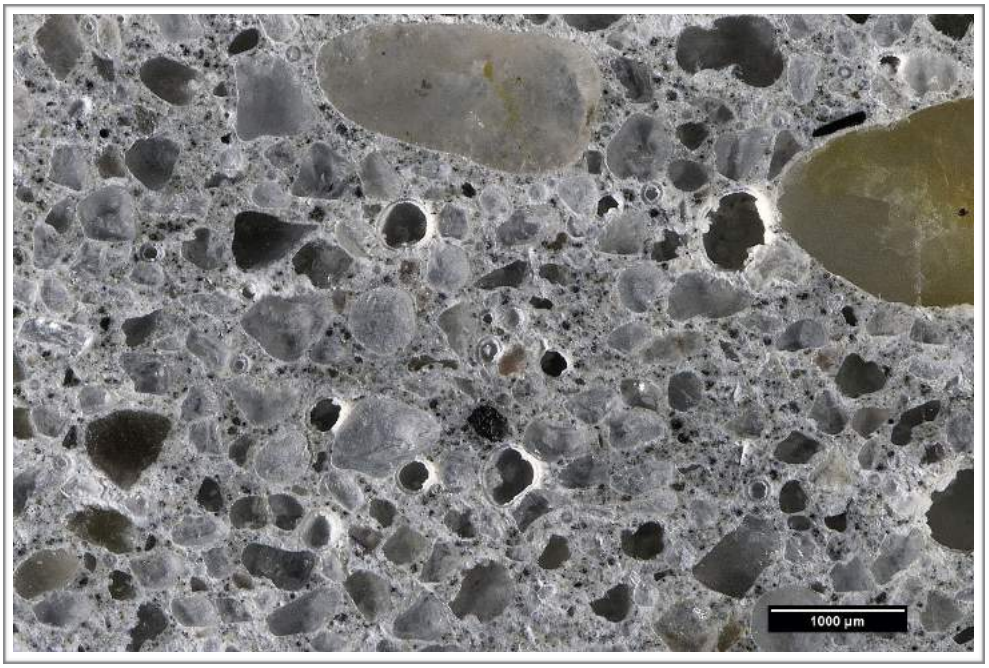

(b)

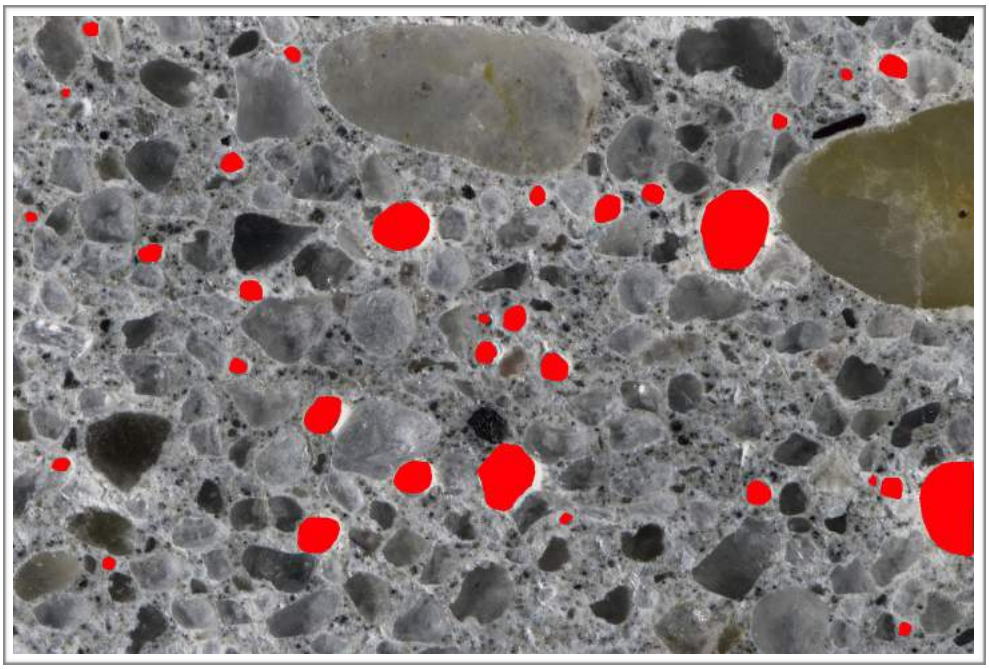

Figure A12. (a) Oblique reflected light photomicrographs of polished surface showing voids (dark circles). (b) Image of same area as (a) where red circles indicate voids. This image was analyzed and found to contain ~ 4% air.

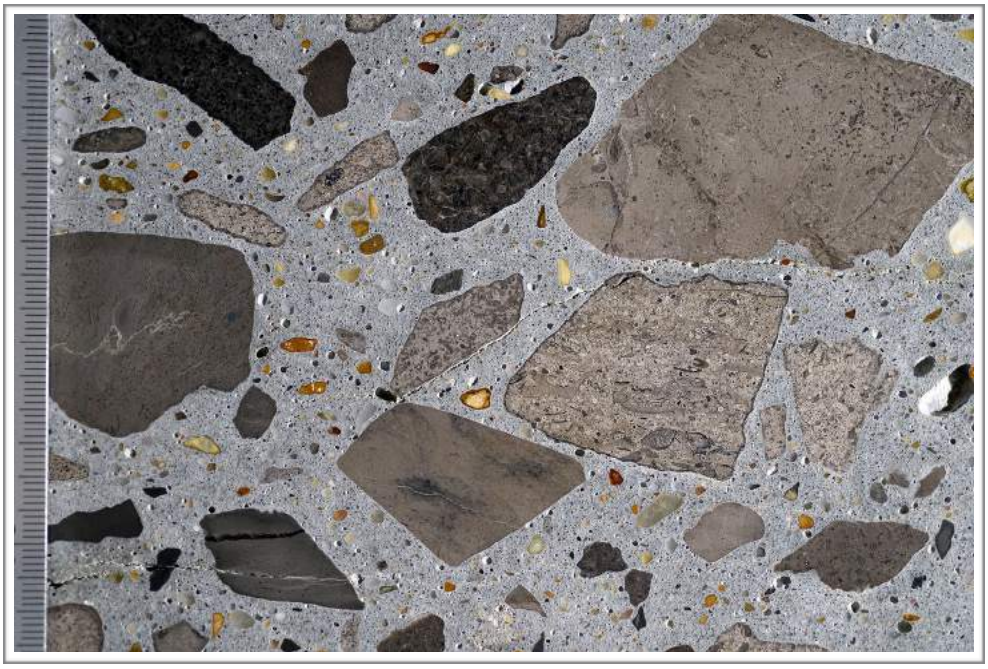

Figure A13. Photograph of polished surface showing overview of coarse aggregate; scale in millimeters.

Figure A14. Reflected light photomicrograph of polished surface showing fine aggregate.

(a)

(b)

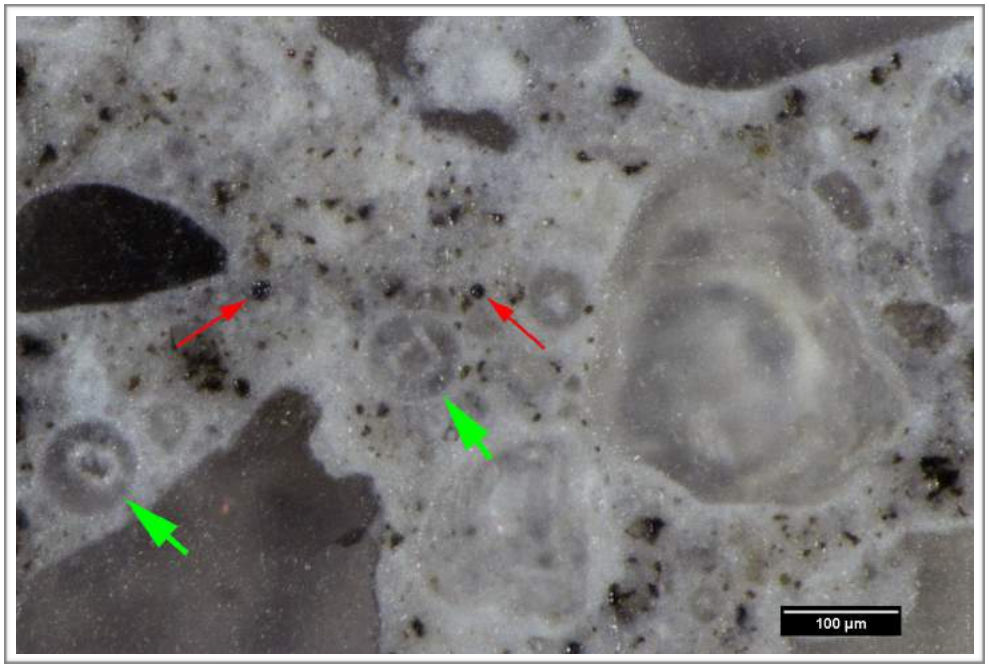

Figure A15. (a) Photograph of polished surface showing overview of paste in the middle of the core. The scale is in millimeters. (b) Reflected light photomicrograph of polished surface showing detail of paste texture and luster. The red and green arrows indicate fly ash and voids filled with ettringite, respectively.

(a)

(b)

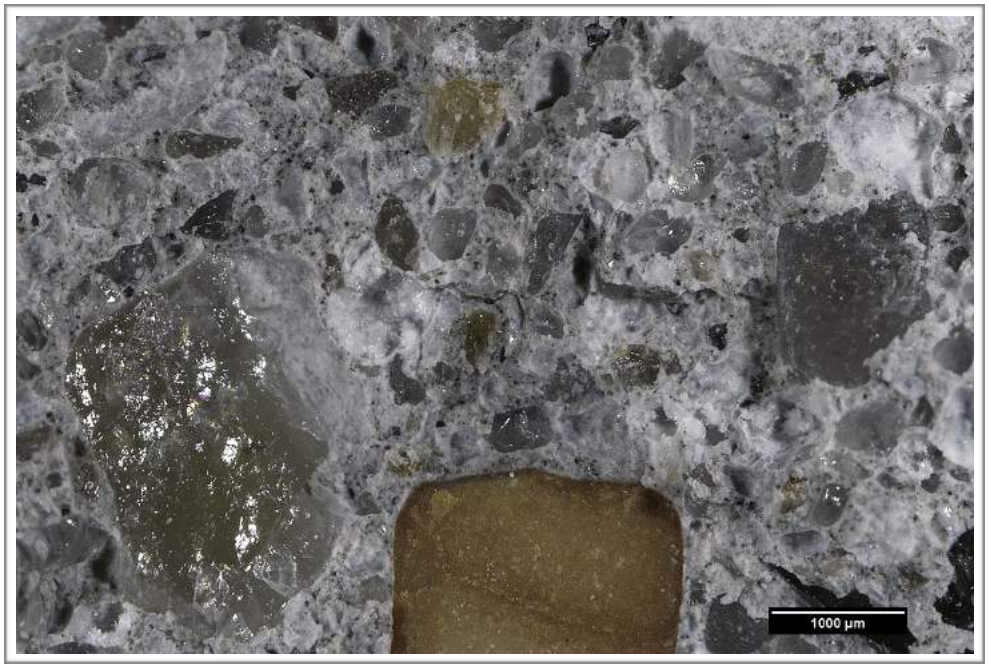

Figure A16. (a) Photograph and (b) reflected light photomicrograph of fresh fracture surface. The scale is in millimeters in (a).

(a)

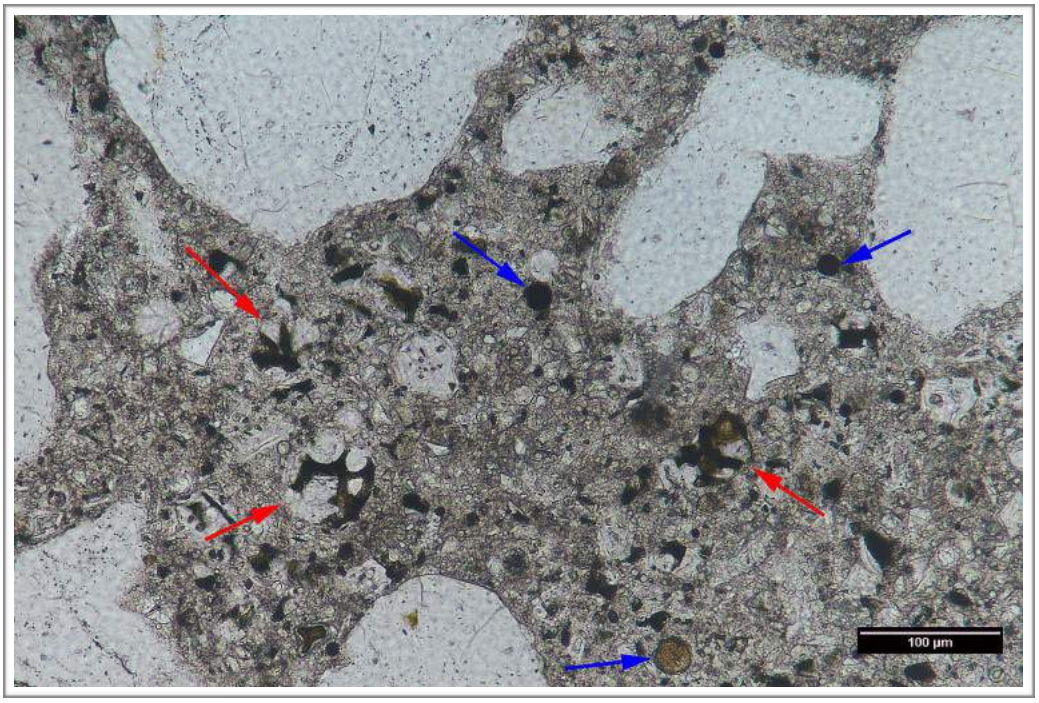

(b)

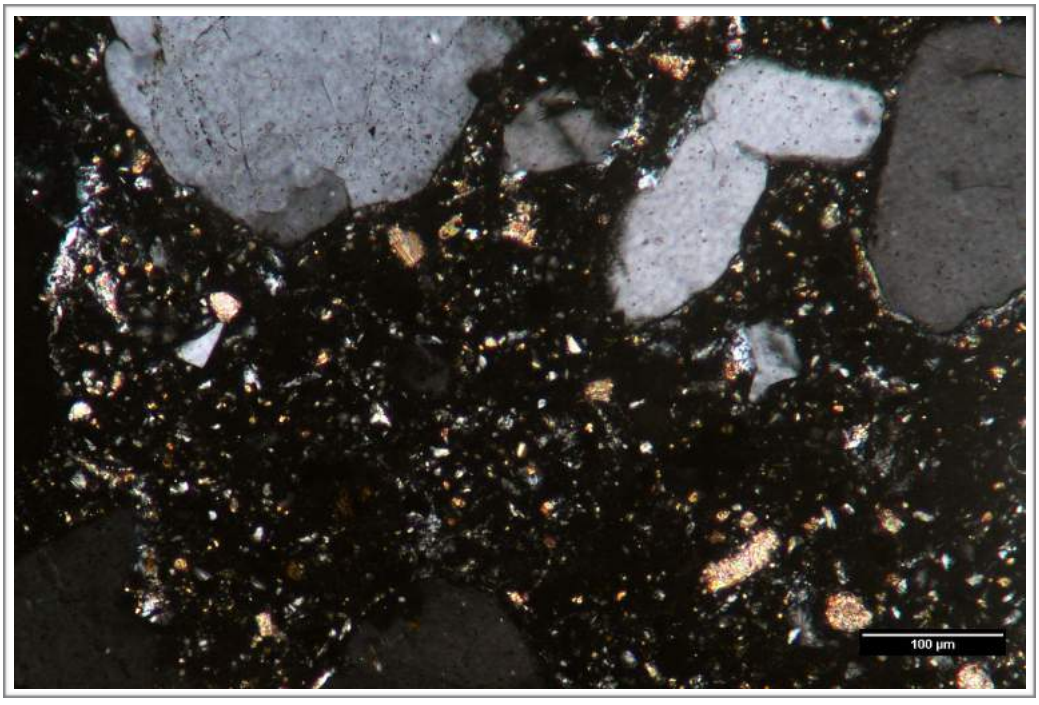

Figure A17. Transmitted light photomicrographs of thin section showing detail of paste in (a) plane-polarized and (b) cross-polarized light. The red and blue arrows in (a) indicate RRCG and fly ash, respectively.

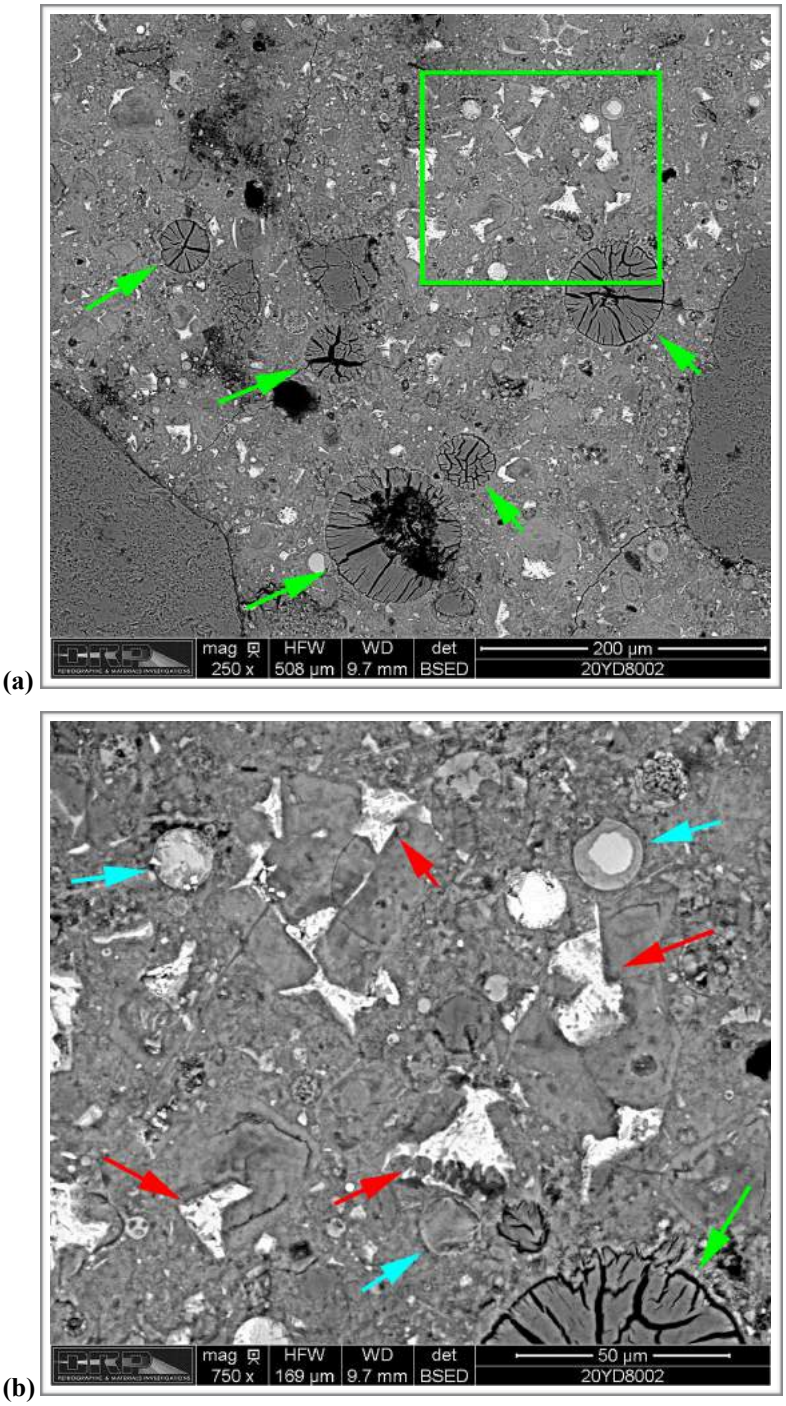

Figure A18. Backscatter electron (BSE) micrographs of polished surface showing (a) overview and (b) detail of paste. The green box in (a) shows the area of (b) and the green arrows in (a) indicate voids with ettringite. The red and blue arrows in (b) indicate RRCG and fly ash, respectively and the green arrow indicates ettringite in a void.

(a)

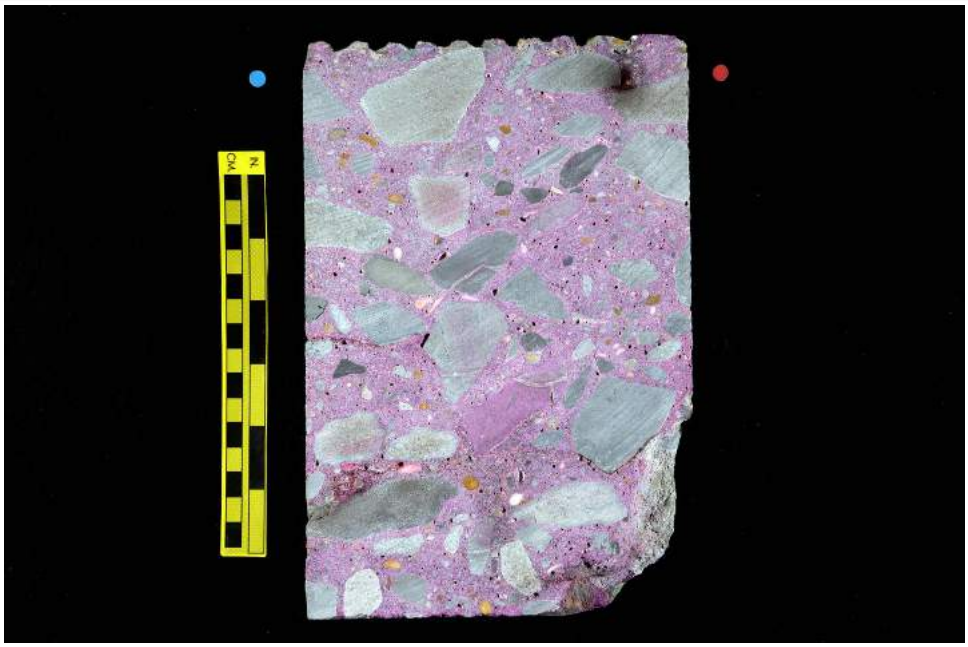

(b)

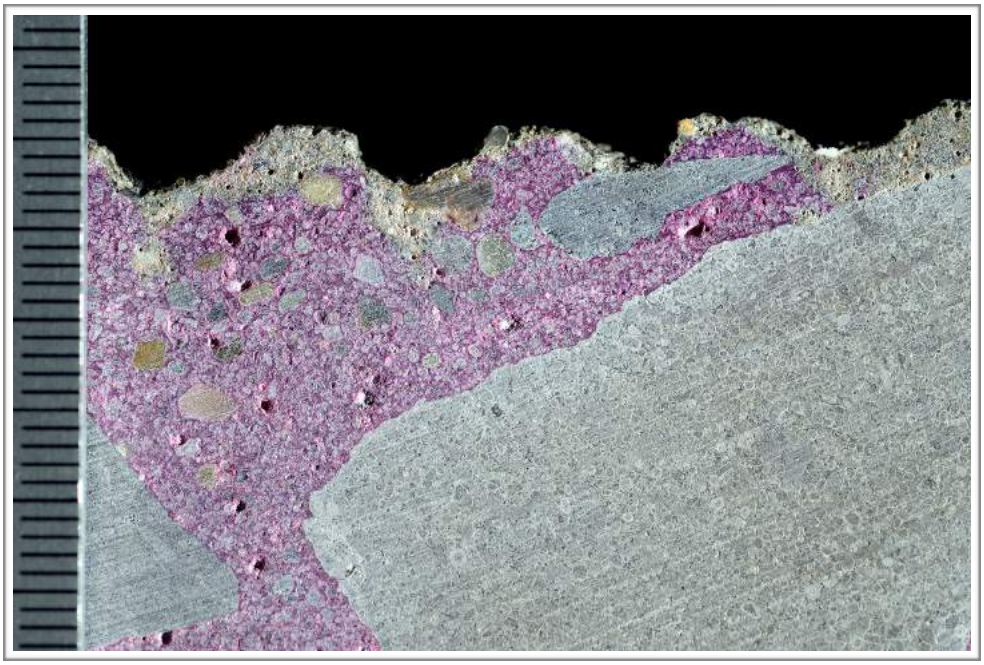

Figure A19. Photographs showing (a) overview of phenolphthalein stained surface and (b) detail of surface near the top of the core. Scale in millimeters in (b).

(a)

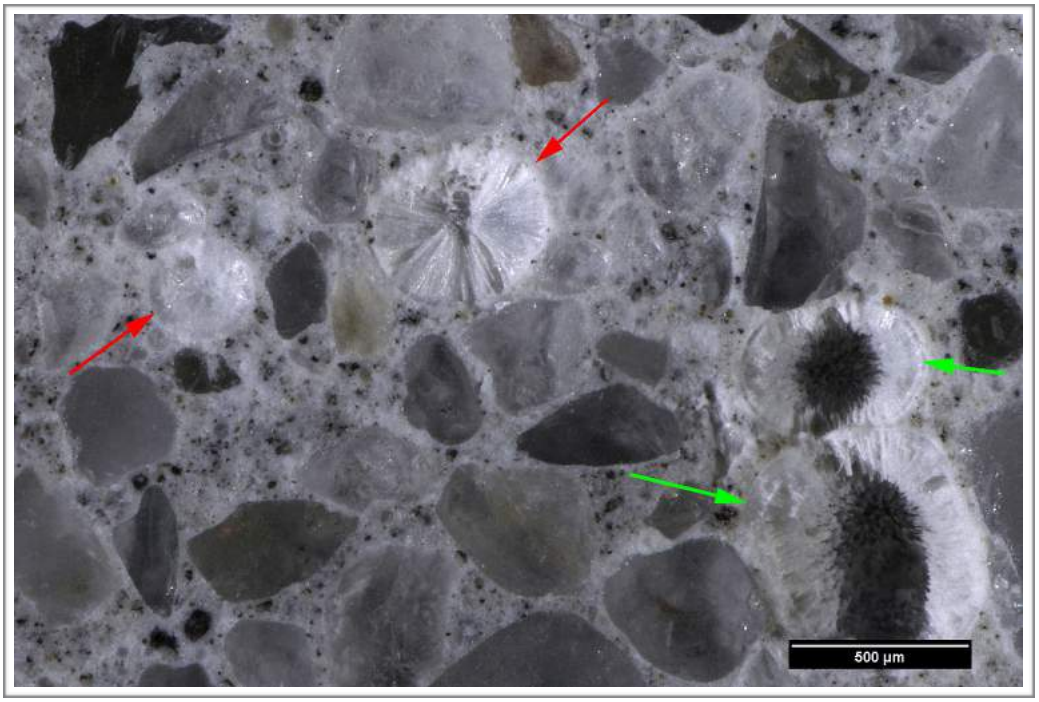

(b)

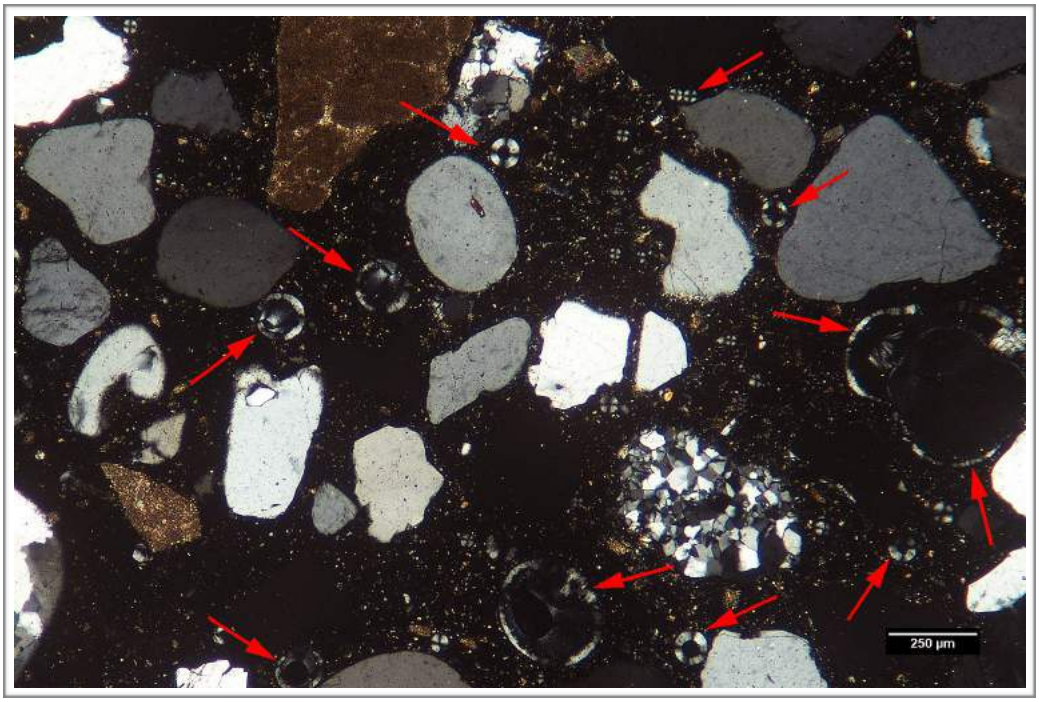

Figure A20. (a) Reflected light photomicrograph of the polished surface showing deposits of ettringite filling voids (red arrows) and lining voids (green arrows). (b) Cross-polarized transmitted light photomicrograph of thin section showing voids lined and filled with ettringite (red arrows).

(c)

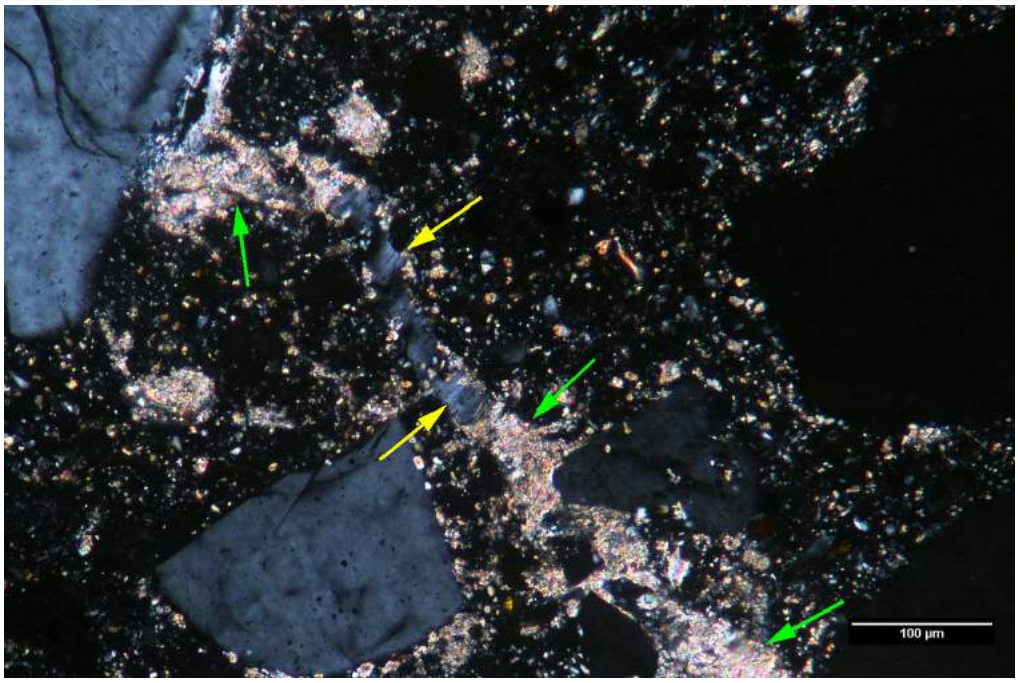

(d)

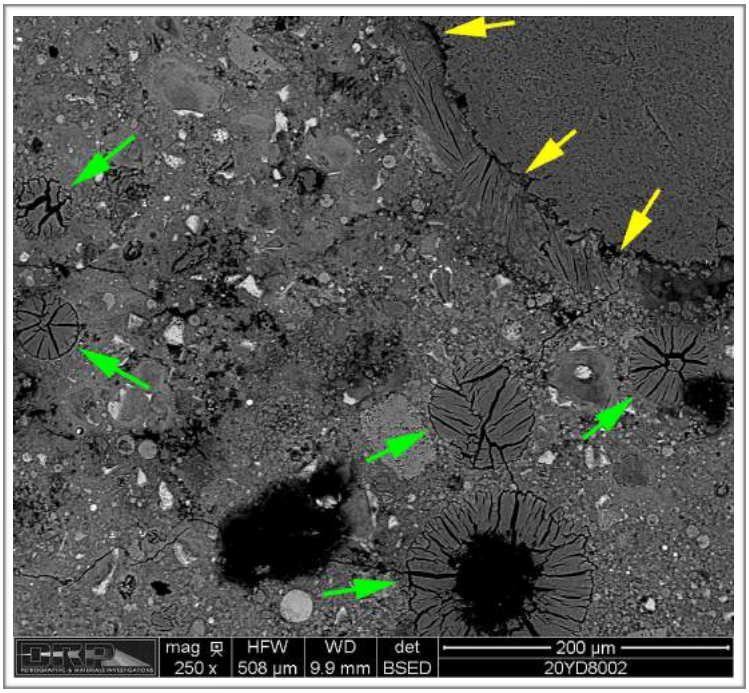

Figure A20 (cont'd). (c) Cross-polarized transmitted light photomicrograph of thin section showing microcrack with deposits of ettringite (yellow arrows) being replaced by calcium carbonate (green arrows). (d) BSE micrograph of polished surface showing ettringite in voids (green arrows) and along the ITZ of an aggregate particle (yellow arrows).

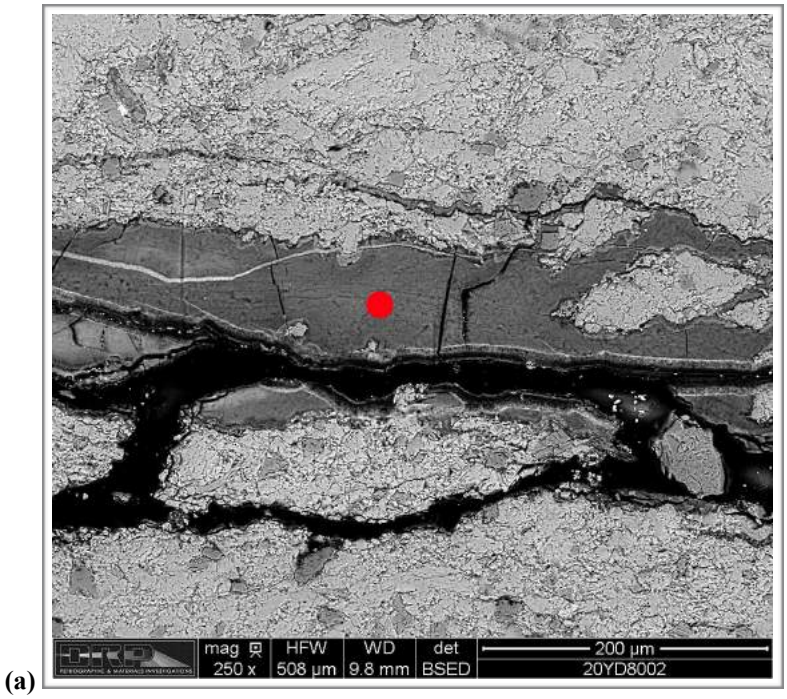

(a)

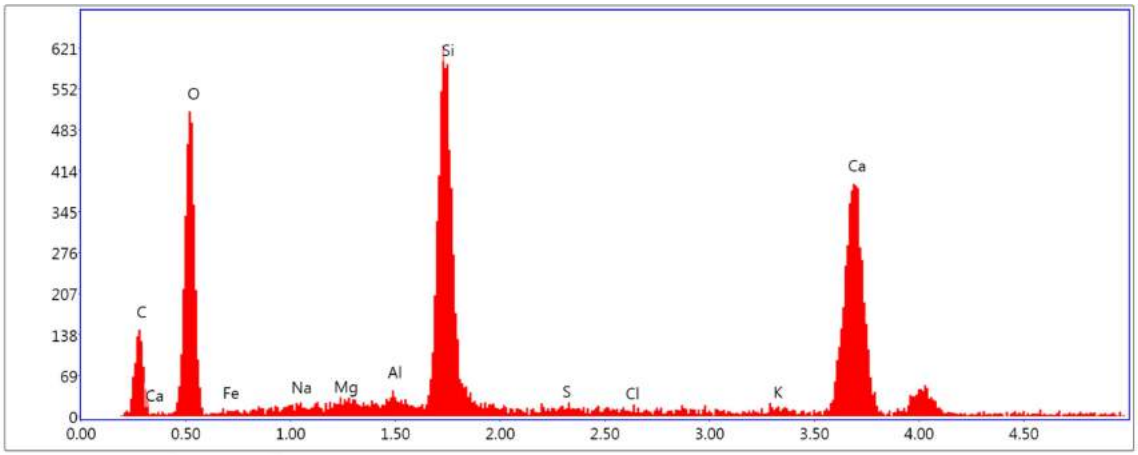

(b)

Figure A21. (a) BSE micrograph of gel in microcrack shown in Figure A8. The red dot in (a) shows area subject to EDS analysis that produced the spectra shown in (b). Similar spectra were obtained for the gel when it was scraped from the surface and analyzed separately. Note the high calcium content of the gel.

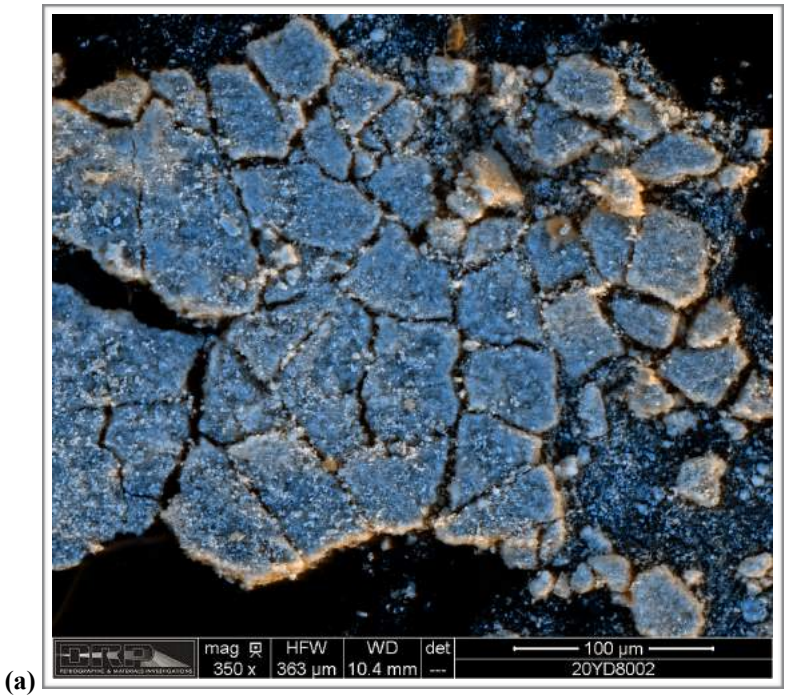

(a)

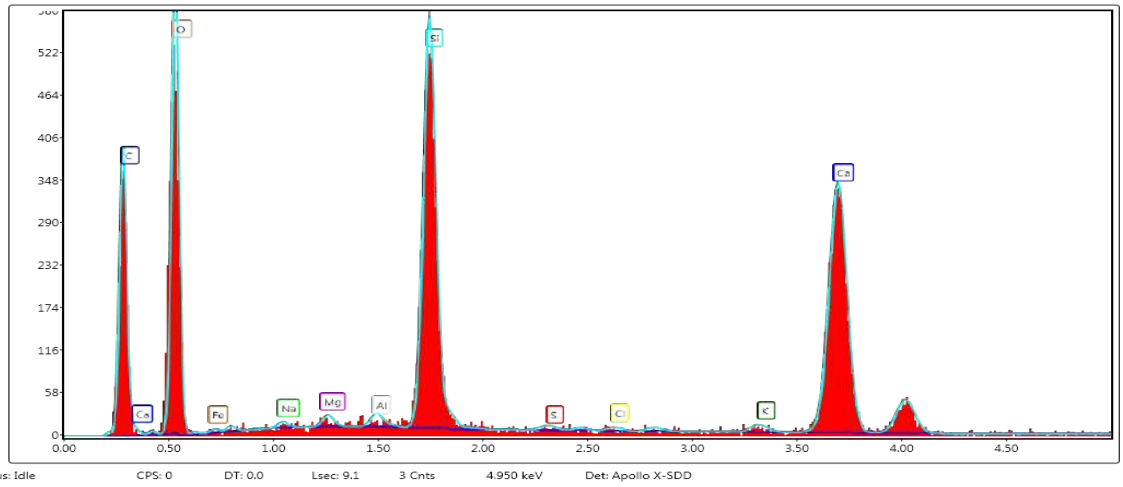

(b)

Figure A22. (a) Combined BSE and secondary electron micrograph of gel that was scraped from microcrack shown in Figure A10 and placed on a carbon tape for EDS analysis. (b). EDS spectra obtained for the gel. Note the high calcium content of the gel.

(a)

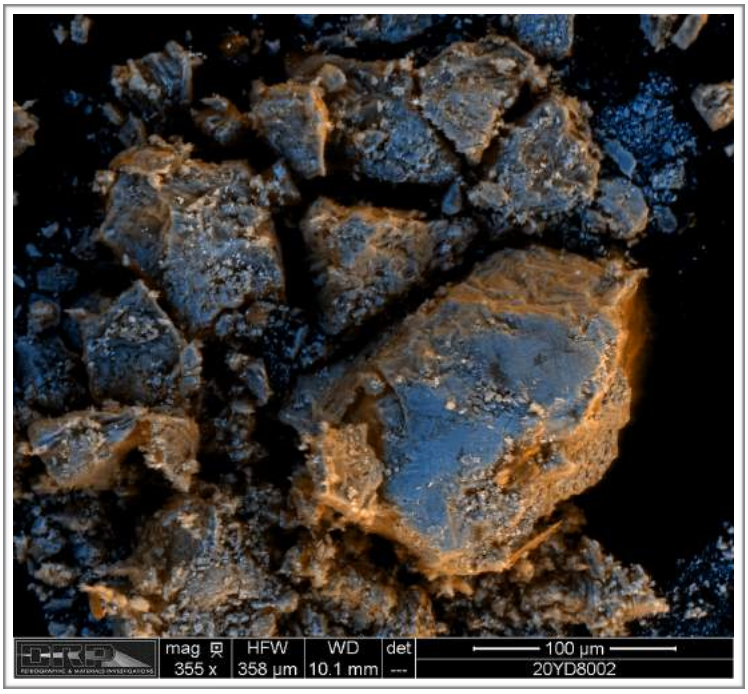

(b)

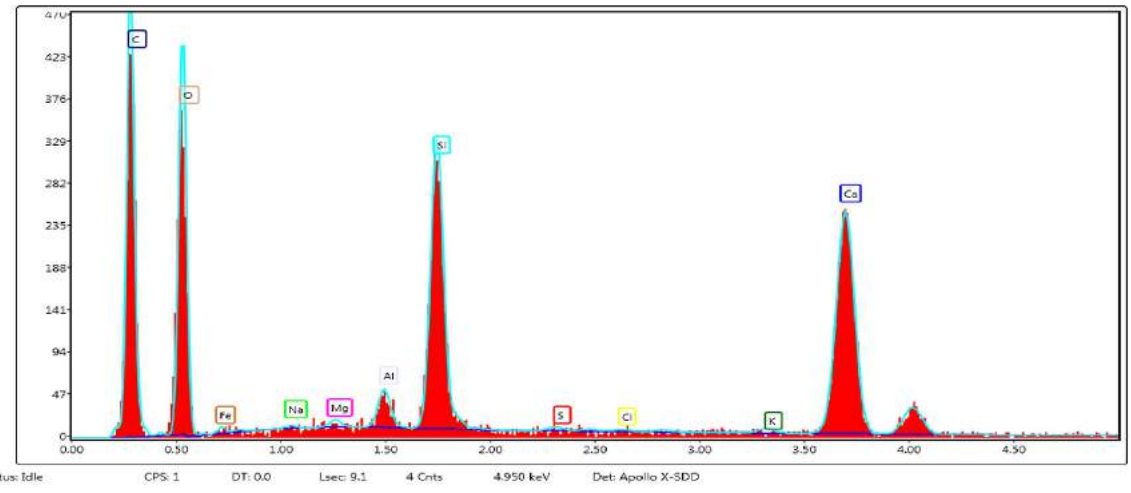

Figure A23. (a) Combined BSE and secondary electron micrograph of gel that was scraped from microcrack shown in Figure A11 and placed on a carbon tape for EDS analysis. (b). EDS spectra obtained for the gel. Note the high calcium content of the gel.

1. Received Condition

Orientation & Dimensions	Vertical core through pavement slab measures 150 mm (6 in.) in diameter and 220 mm (~ 8 ⅝ in.) in length (**Figure B1, B2**).
Surfaces	The top surface is quite worn with no remnant of an original texture and exposed, polished coarse aggregate particles (**Figure B3**) and the lower surface is cast on asphalt such that the core represents the full thickness of the portland cement concrete pavement.
General Condition	The concrete is hard and compact and rings lightly when sounded with a hammer.

2. Embedded Objects

General	None observed.

3. Cracking

Macroscopic	Several cracks were observed on as-received surfaces. On the top a triple-point crack measuring up to 750 µm (30 mil) wide cuts across the full diameter of the core (**Figure B4**). Several sub-vertical and sub-horizontal cracks were observed on the side of the core (**Figure B5**). These are up to 500 µm (20 mil) wide and range from ~ 75-200 mm (3-8 in.) as they are traced on the side of the core. On the polished slab a crack cuts sub-vertically from the top surface to a depth of ~ 38 mm (1 ½ in.) where it intersects a horizontal crack and cuts along it for ~ 19 mm (¾ in.) and then cuts sub-vertically for another ~ 12.5 mm (½ in.; **Figure B6**). This crack is up to 500 µm (20 mil) wide, cuts around aggregate particles and is free of secondary deposits although slight discoloration of the paste was observed along segments of its strike length. The crack is bifurcated in the top ~ 9.5 mm (⅜ in.) of the core. A hairline crack cuts sub-vertically from the top surface to ~ 15 mm (⅝ in.) where it terminates in a dolomitic aggregate particle (**Figure B7**). The crack is ~ 100 µm (4 mil) wide and cuts through a chert particle just below the top surface. There is minor discoloration of the paste in the walls of segments of the crack. A crack cuts from the bottom surface to ~ 100 mm (4 in.) above the surface (**Figure B8**). The crack cuts mostly around aggregate particles and ranges from ~ 250 µm (10 mil) to 2 mm (80 mil) wide. Deposits of ettringite and gel were observed along segments of the crack.
Microscopic	A few microcracks ranging up to 100 µm (4 mil) wide cut from the top surface to 3-6 mm (⅛-¼ in.); these cut around aggregates and are mostly free of secondary deposits (**Figure B9**). Peripheral microcracking was observed in occasional particles of limestone. Most of these microcracks are less than 25 µm (1 mil) wide. In one case a limestone particle with peripheral microcracks serves as the source of a sub-horizontal hairline crack that cuts from the particle into the past (**Figure B10**).

4. Voids

Void System	Concrete is not air-entrained and contains less than 3% total air as estimated from visual and microscopical observations. The concrete is well consolidated with no significant entrapped voids or water voids observed.
Void Fillings	Occasional voids contain minor deposits of ettringite.

5. Coarse Aggregate

Physical Properties	The coarse aggregate is a limestone gravel with a nominal top size of 38 mm (1 ½ in.; **Figure B11**). The rocks are hard and competent. The particles are sub-equant to oblong in shape with sub-rounded to sub-angular edges. The aggregate shows gap grading with few particles below 19 mm (¾ in.) across observed but the gradation is more even than Core C-1
Rock Types	The aggregate is carbonate in composition and consists of various types of limestone that range from dark brown micritic rocks to pale tan oolitic limestones to brown fossiliferous packstones and brown dolomitic limestones. Many particles show well-defined reaction rims and some appear to contain fine-grained siliceous material. Examination of some particles in thin section shows that deposits of chalcedonic chert are present in some of the limestone particles (**Figure B12**; chalcedonic chert is highly susceptible to alkali-silica reaction (ASR).
Other Features	No deleterious coatings or incrustations observed. Minor low w/c mortar coatings observed. A few particles show significant internal microcracking; minor microcracking of the paste around aggregates and other evidence of ACR was observed. Well-developed reaction rims are commonly observed and some particles are cut by microcracks and appear to contain gel.

6. Fine Aggregate

Physical Properties	The fine aggregate is a natural sand that consists of rocks that are hard and competent (**Figure B13**). The sand consists primarily of siliceous rocks but minor amounts of limestone (carbonate) similar to those in the coarse aggregate were observed. The particles are sub-equant to oblong in shape with rounded to sub-angular edges. The grading and distribution are even.
Rock Types	The consists primarily of quartz and quartzite; chert is a minor component and limestone is also present. Seams of chalcedonic chert were observed in limestones.
Other Features	No deleterious coatings or incrustations observed and no low w/c mortar coatings observed. The chert commonly shows well-developed reaction rims; the quartz and quartzite particles are intact. Occasional particles of limestone show peripheral microcracking (**Figure B14**).

7. Paste Observations

Polished Surface	Paste is light gray (Munsell 10YR/7/1), has a smooth texture and weakly sub-vitreous luster (**Figure B15**). The paste is moderately hard (Mohs 3-3.5). The paste is gray (10YR/6/1) for 1-2 mm (40-80 mil) from the top surface and irregularly distributed zones of yellow (2.5Y/7/4) to light red (2.5YR/7/4) paste are present for up to 3 mm (⅛ in.) from the top surface.
Fresh Fracture	Fracture surface is gray, has a hackly texture and a sub-vitreous luster (**Figure B16**). The fracture cuts through coarse aggregate particles. Significant deposits of ASR gel were observed on the surface.
Thin Section/ SEM*	The paste contains hydrated portland cement and fly ash; no slag cement or other SCM were observed. The hydration is normal with 5-10% RRCG that consist mostly of belite and interstitial ferrite and aluminate (**Figure B17, Figure B18**). Minor amounts of very fine crystals of calcite are present in the paste. CH makes up 8-15% of the paste, is fine grained and evenly distributed.

** Abbreviations as follows: RRCG = relict and residual cement grains; SCM = supplemental cementitious materials; CH = calcium hydroxide; ITZ = interfacial transition zone. Modal abundances are based on visual estimations.*

8. Secondary Deposits

Phenolphthalein	Entire surface stains purple except along irregular zones (microcracks) at the top of the core where not staining was observed to 6 mm (¼ in.) depth (**Figure B19**).
Deposits	No significant carbonation observed. Minor deposits of ettringite observed in occasional voids and microcracks (**Figure B20**). Traces of gel observed but much less gel than in Core C-1. A few cracks cut from limestone particles with peripheral microcracking into the paste (**Figure B21**). Minor deposits of Mg-rich material detected by EDS around some limestone particles with peripheral microcracking (**Figure B22**).

FIGURES

(a)

(b)

Figure B1. Photographs showing (a) oblique view of the top and side of the core with identification labels and (b) the top of the core. The red and blue dots show the orientation of the saw cuts used to prepare the sample. The yellow bar is ~ 150 mm (6 in.) long.

(c)

Figure B1 (cont'd). (c) Photograph showing the bottom surface of the core.

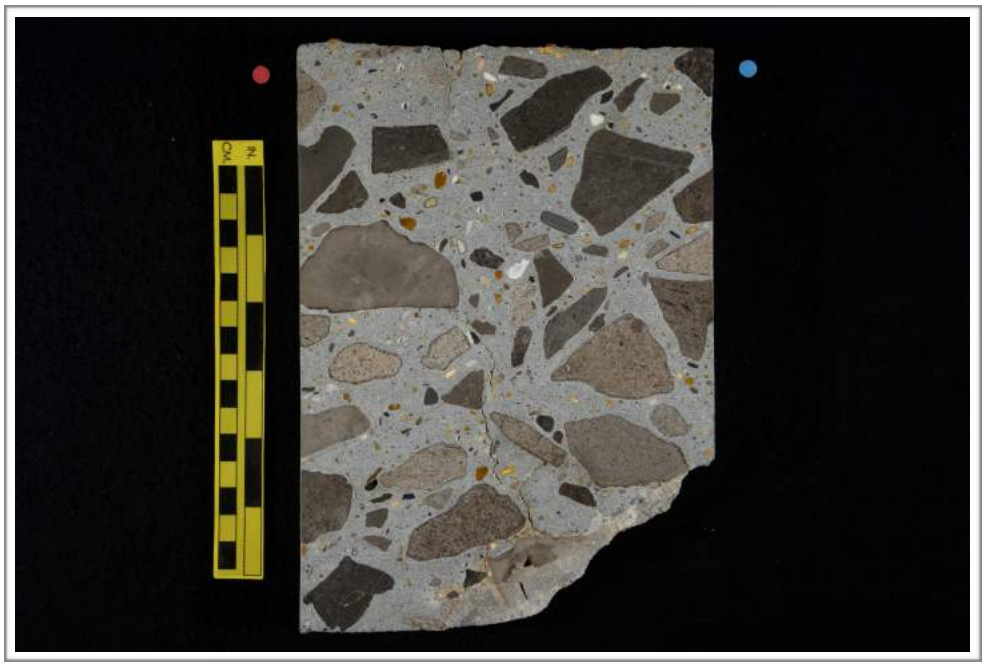

Figure B2. Photograph showing one of the polished surfaces of the core; both sides of the slab were polished. The yellow bar is ~ 150 mm (6 in.) long.

Figure B3. Photograph showing detail of top surface; scale in millimeters.

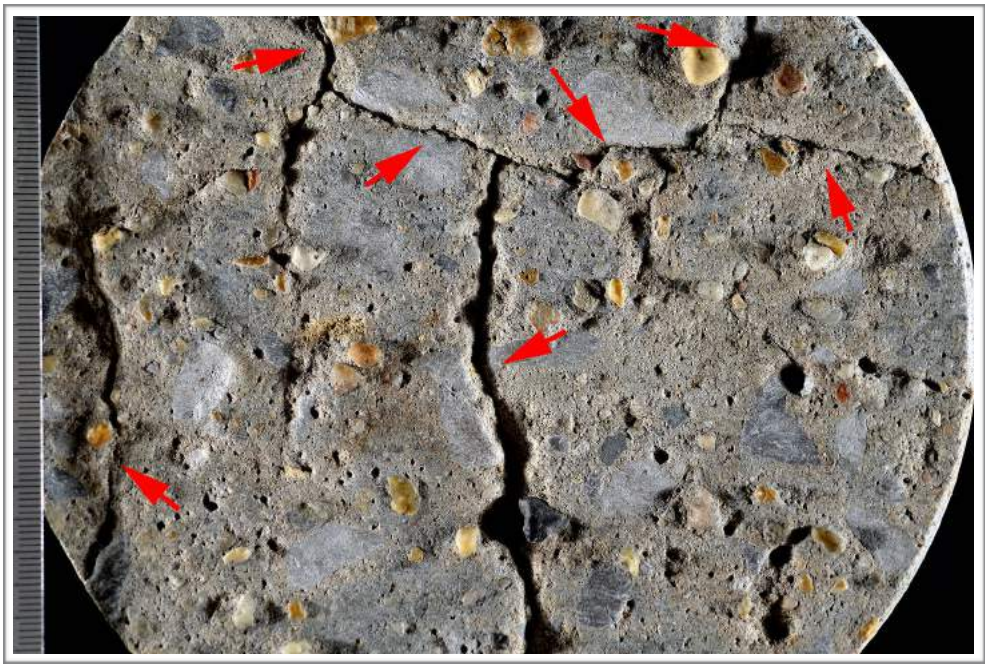

Figure B4. Photograph of top of core showing cracks (red arrows); scale in millimeters.

(a)

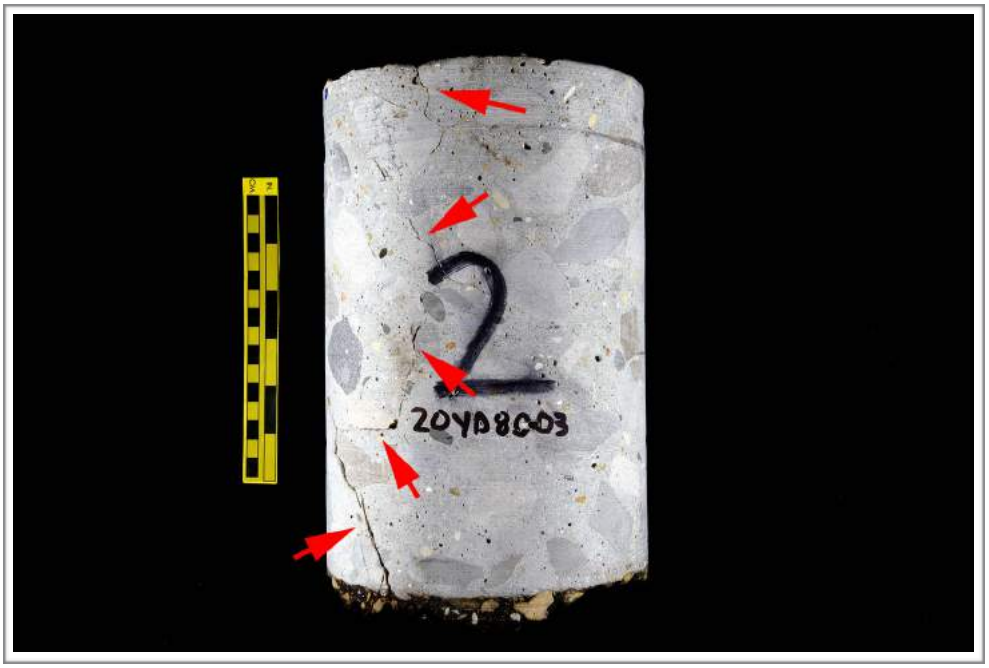

(b)

Figure B5. Photographs of the side of the core showing (a) overview and (b) detail of cracks (red arrows). The yellow scale is ~ 150 mm (6 in.) long.

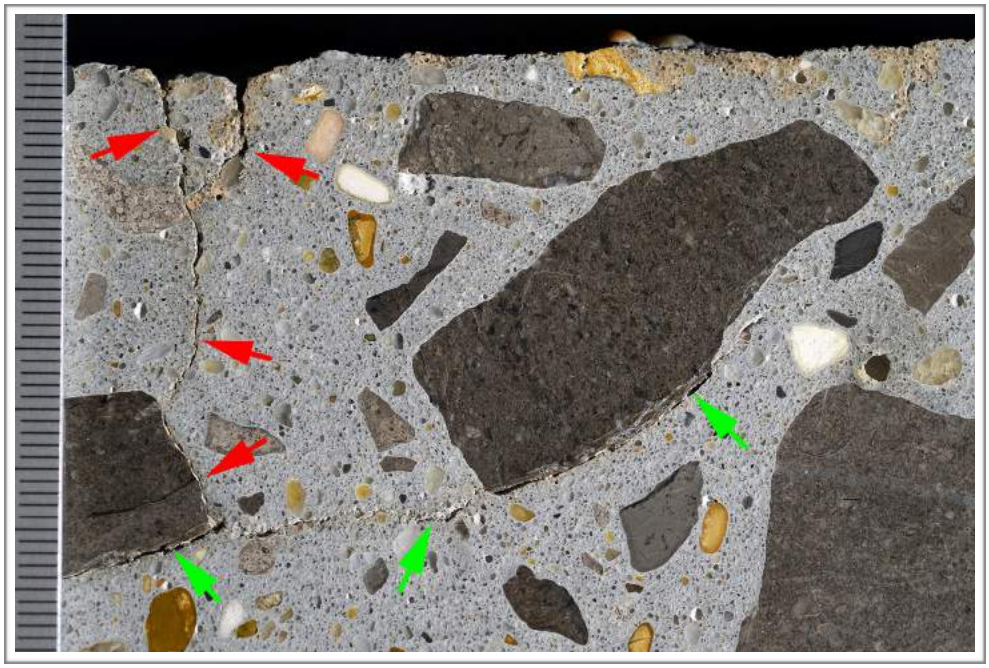

Figure B6. Photograph of polished surface showing sub-vertical crack (red arrows) at the top of the core and the sub-horizontal crack (green arrows) where it terminates.

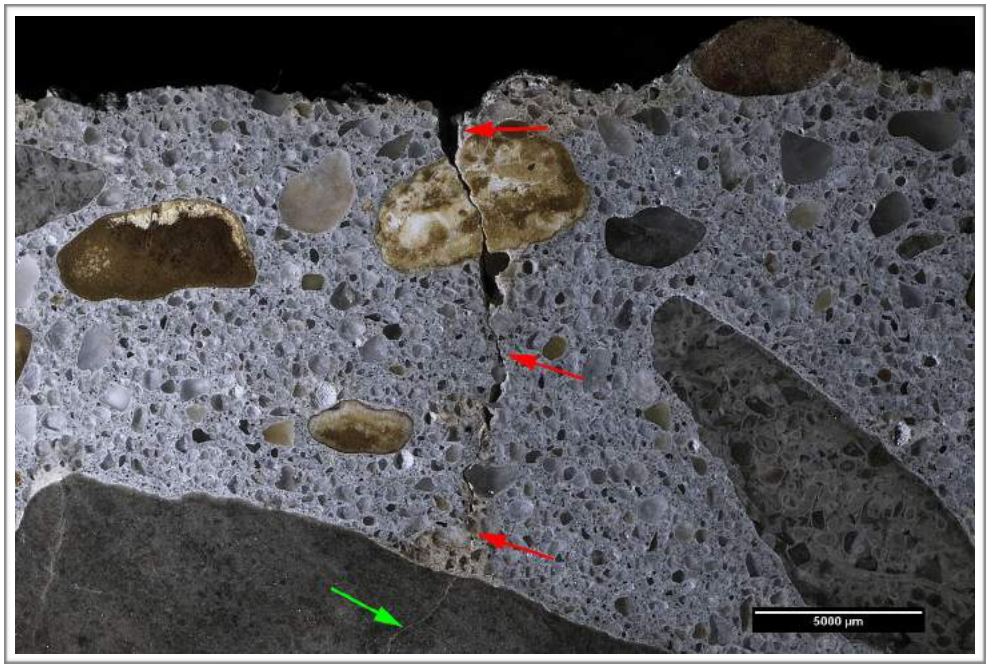

Figure B7. Reflected light photomicrograph of the top surface showing hairline crack (red arrows) that cuts sub-vertically from the top surface to a limestone particle with an internal microcrack (green arrow).

(a)

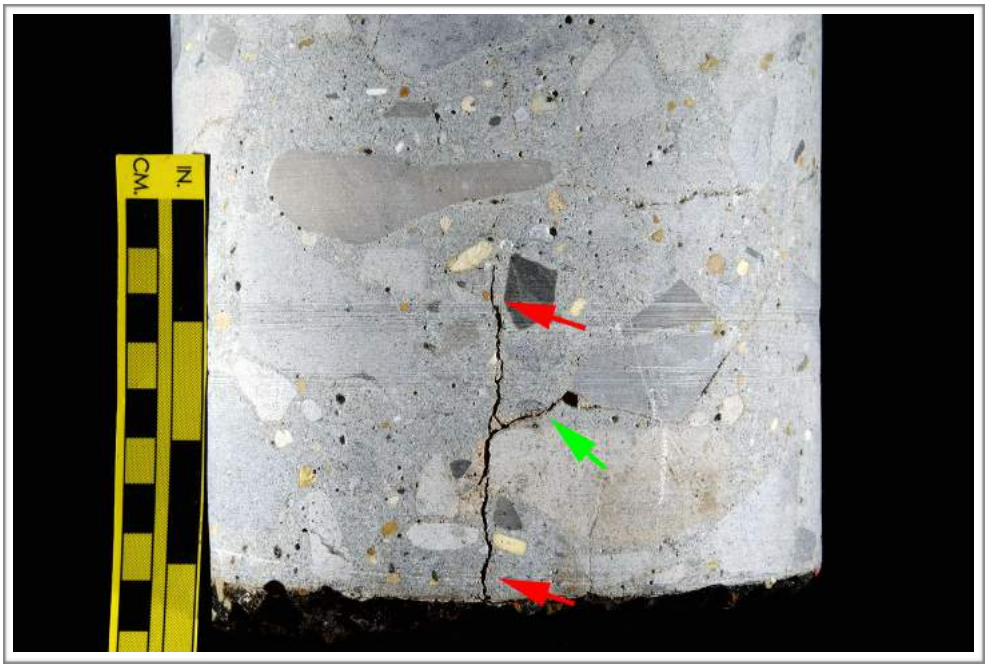

(b)

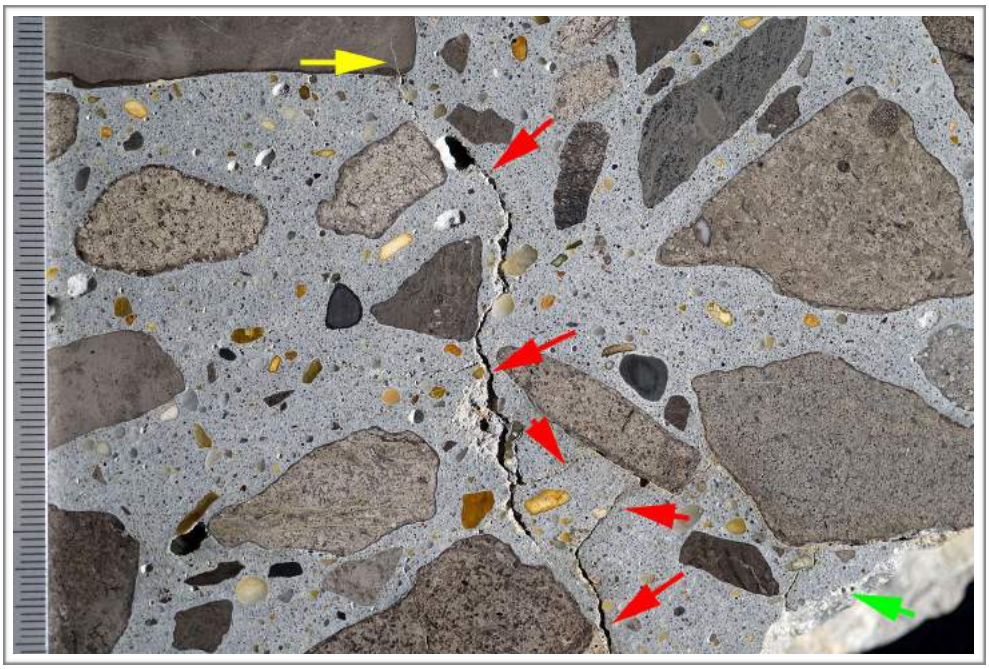

Figure B8. Photographs of the (a) side of the core and (b) the polished surface showing cracks (red arrows) at the bottom of the core (green arrow in (b). In (b) the yellow arrow highlights a hairline crack in a dolomitic limestone particle and the scale is in millimeters.

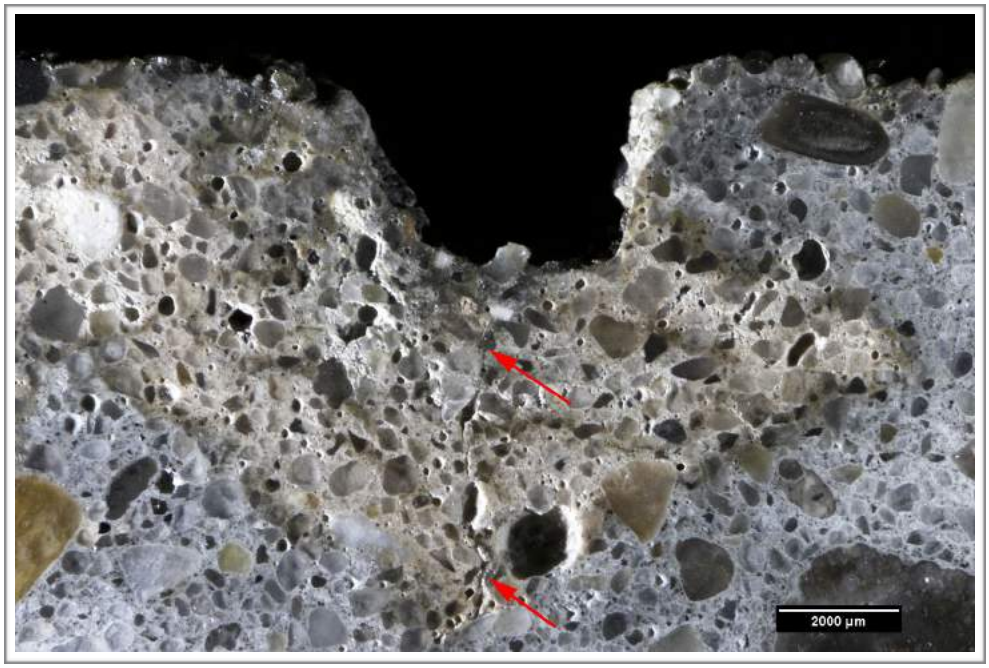

Figure B9. Reflected light photomicrograph of the polished surface showing sub-vertical microcrack (red arrows) at the top of the core. Note the discoloration of the paste around the microcrack, which is typical of carbonation.

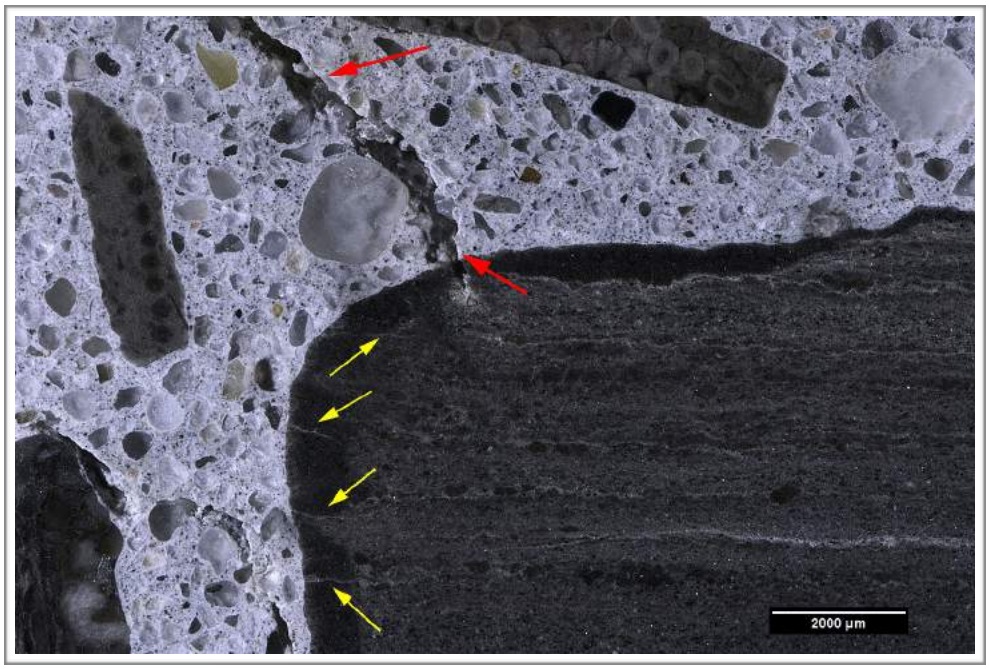

Figure B10. Reflected light photomicrograph of the polished surface showing microcracks (yellow arrows) in a reaction rim of a dolomitic limestone particle and a crack (red arrows) cutting from particle into the paste.

Figure B11. Photograph of the polished surface showing overview of coarse aggregate; scale in millimeters.

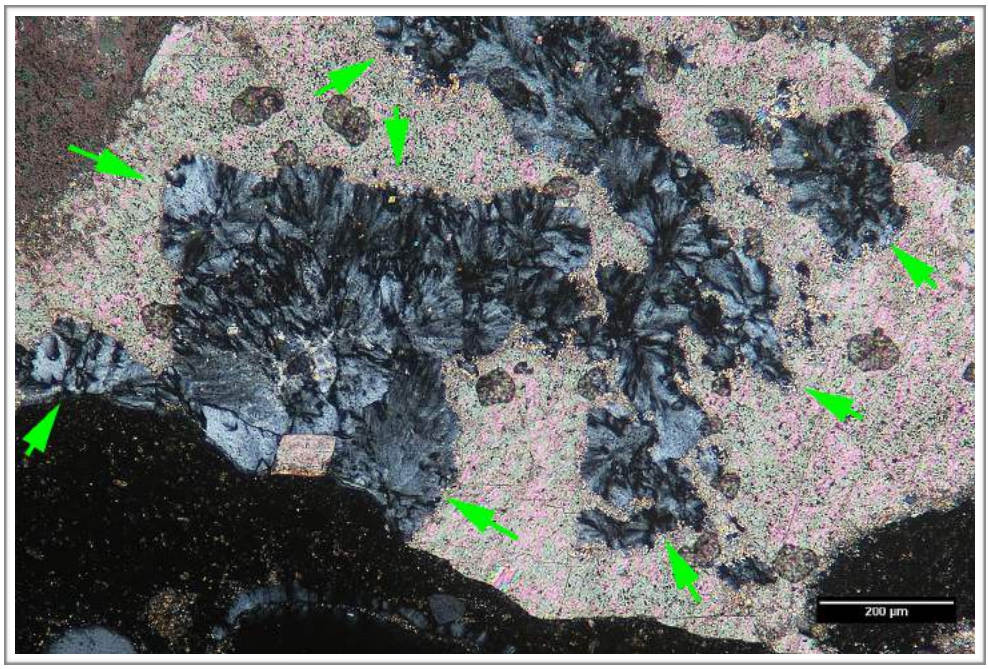

Figure B12. Cross-polarized transmitted light photomicrograph of thin section showing detail of limestone particle. The green arrows highlight area where chalcedonic chert is present.

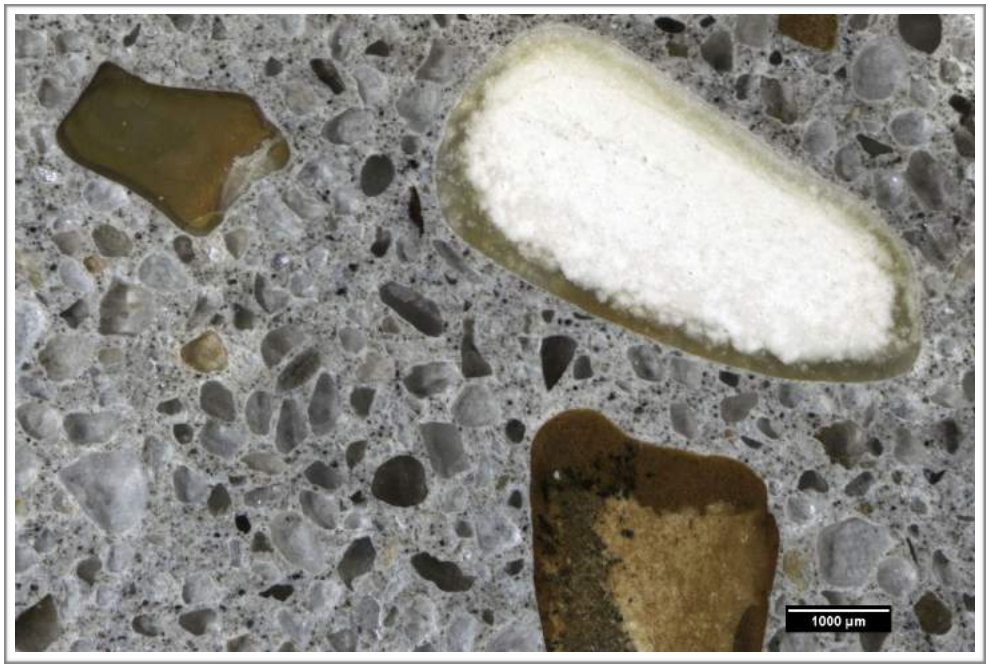

Figure B13. Reflected light photomicrographs of the polished surface showing overview of the sand. The larger particles consist of chert.

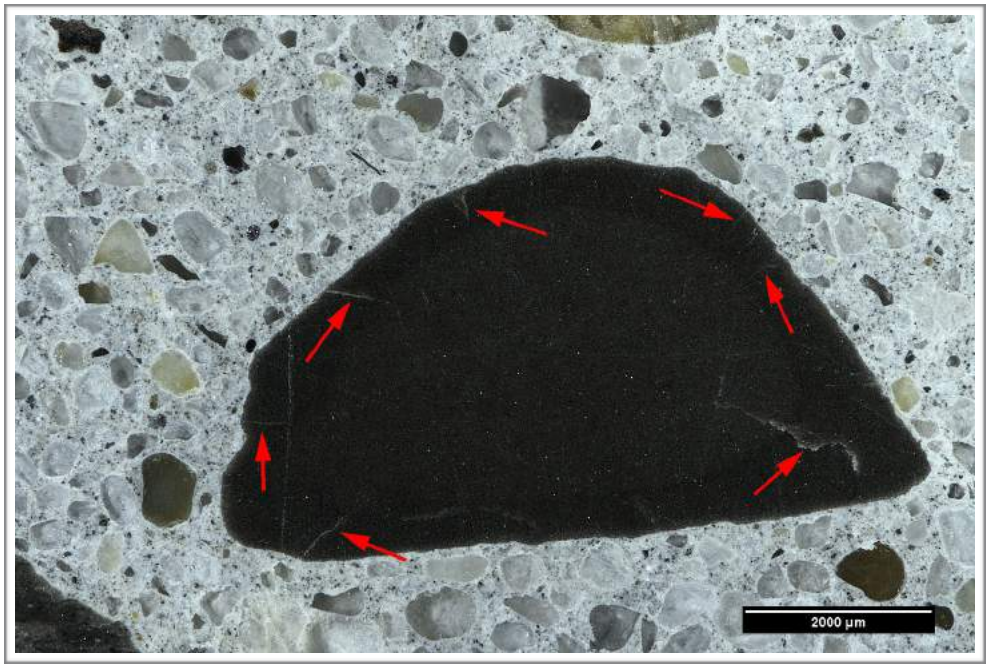

Figure B14. Reflected light photomicrographs of the polished surface showing limestone particle with internal microcracks (red arrows).

(a)

(b)

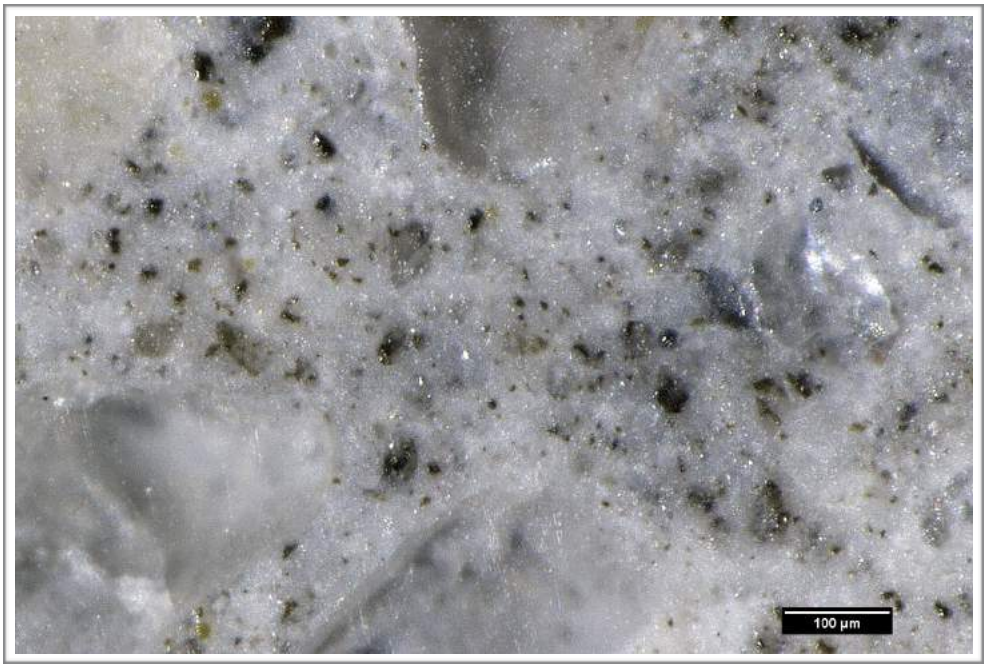

Figure B15. (a) Photograph of polished surface showing overview of paste in the middle of the core. The scale is in millimeters. (b) Reflected light photomicrograph of polished surface showing detail of paste texture and luster.

(a)

(b)

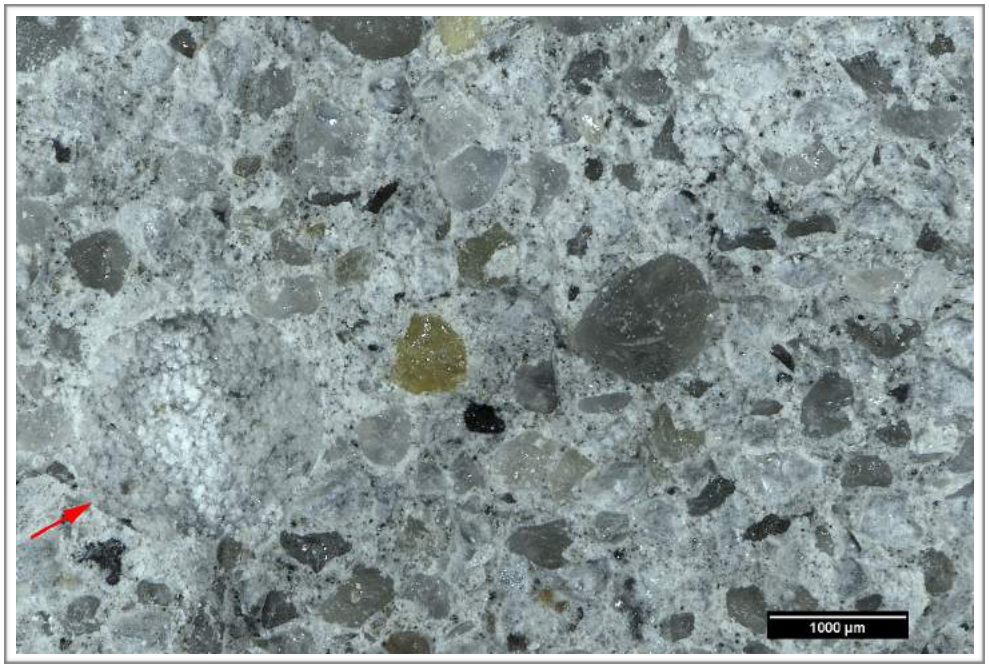

Figure B16. (a) Photograph and (b) reflected light photomicrograph of fresh fracture surface. The scale is in millimeters in (a). In (b) the red arrow shows a void with ettringite.

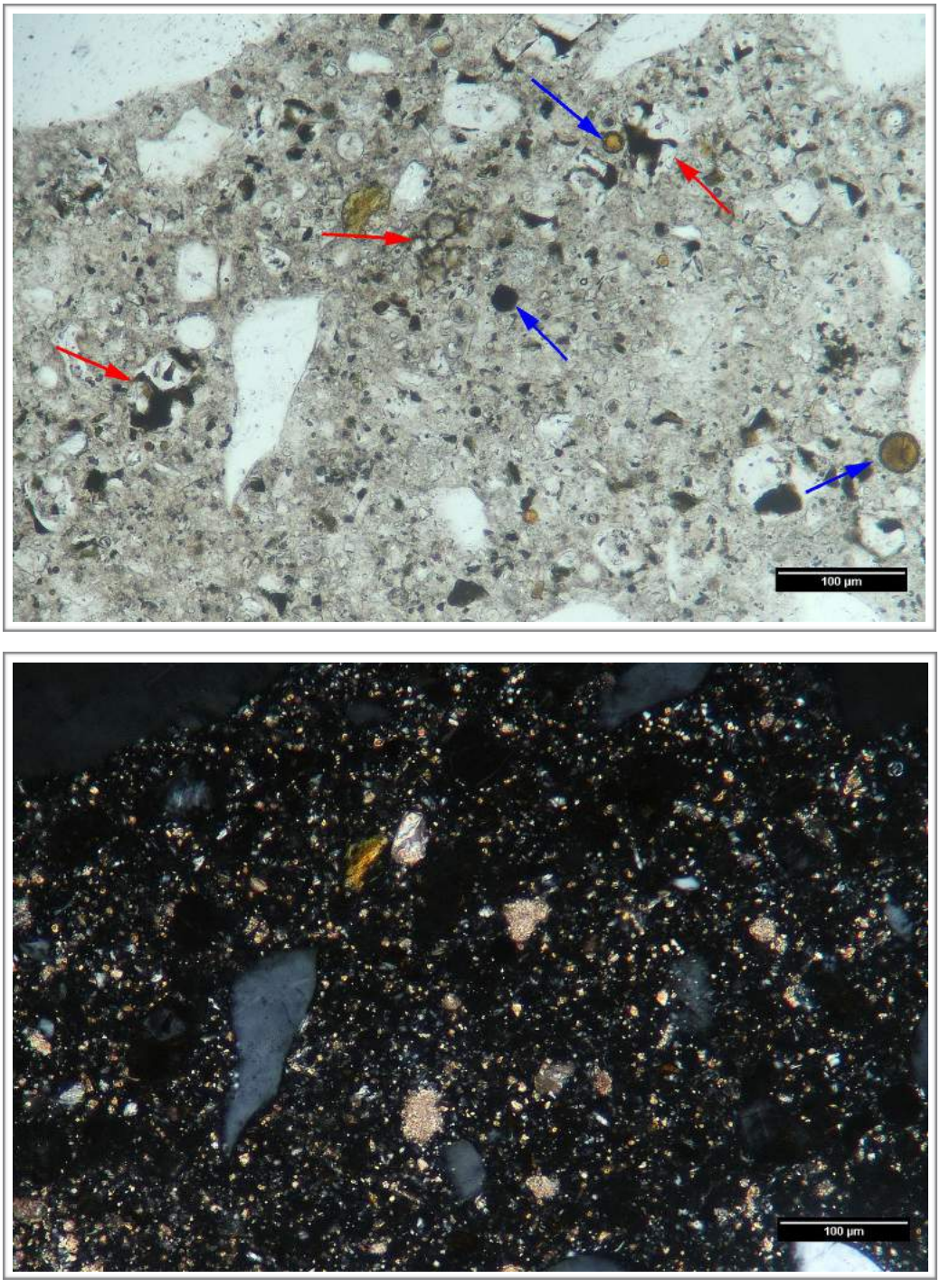

(a)

(b)

Figure B17. Transmitted light photomicrographs of thin section showing detail of paste in (a) plane-polarized and (b) cross-polarized light. The red and blue arrows in (a) indicate RRCG and fly ash, respectively.

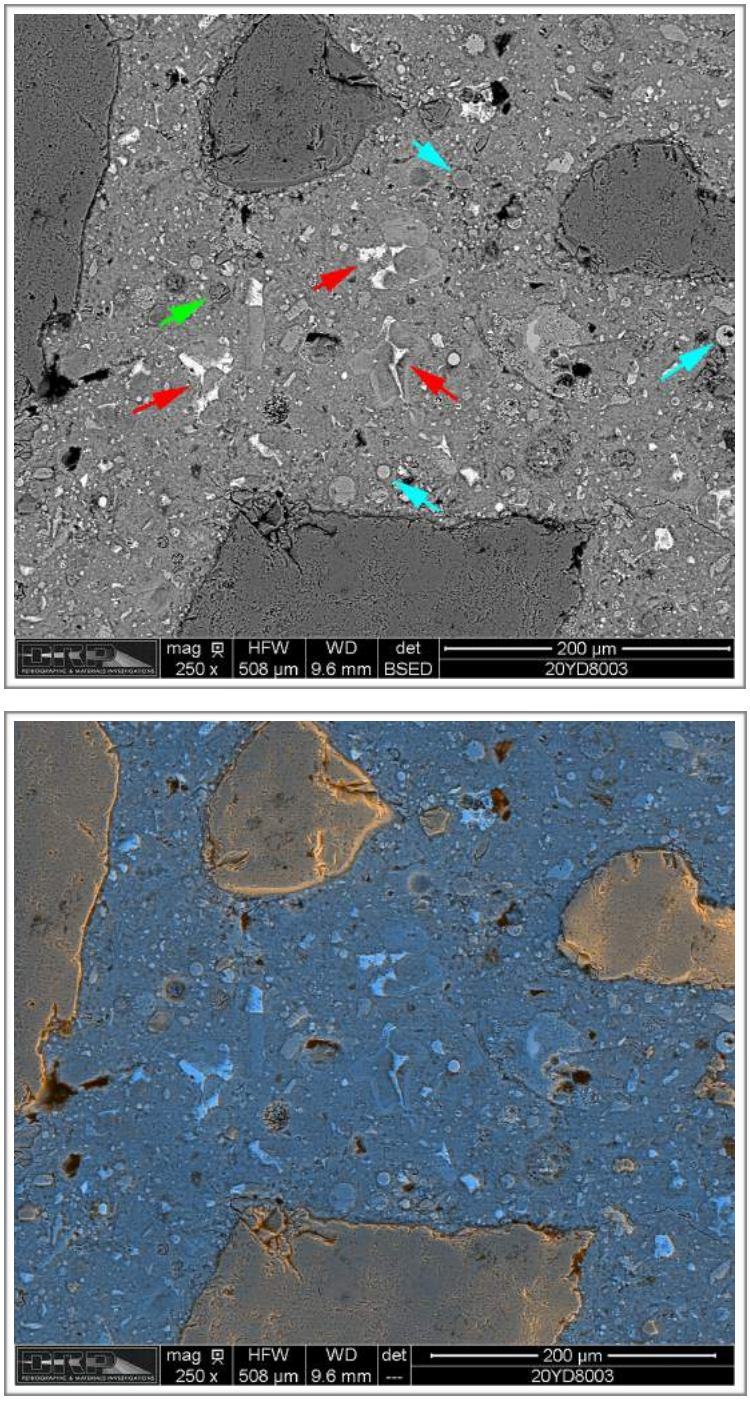

Figure B18. Backscatter electron (BSE) and combined BSE/secondary electron (SE) micrographs of polished surface showing detail of paste. The red and blue arrows in (a) indicate RRCG and fly ash, respectively and the green arrow indicates ettringite in a void.

(a)

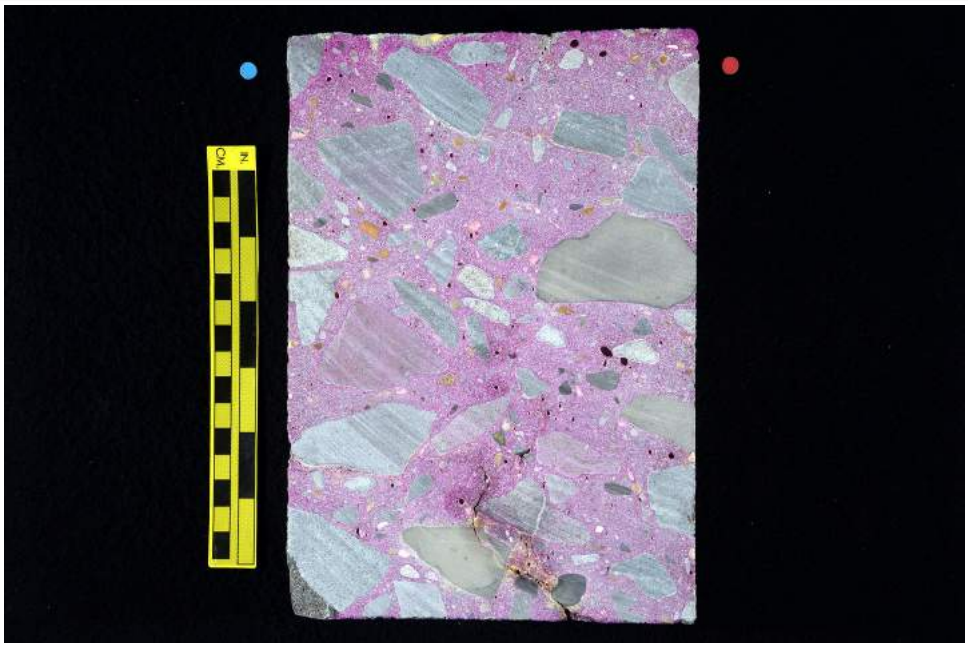

(b)

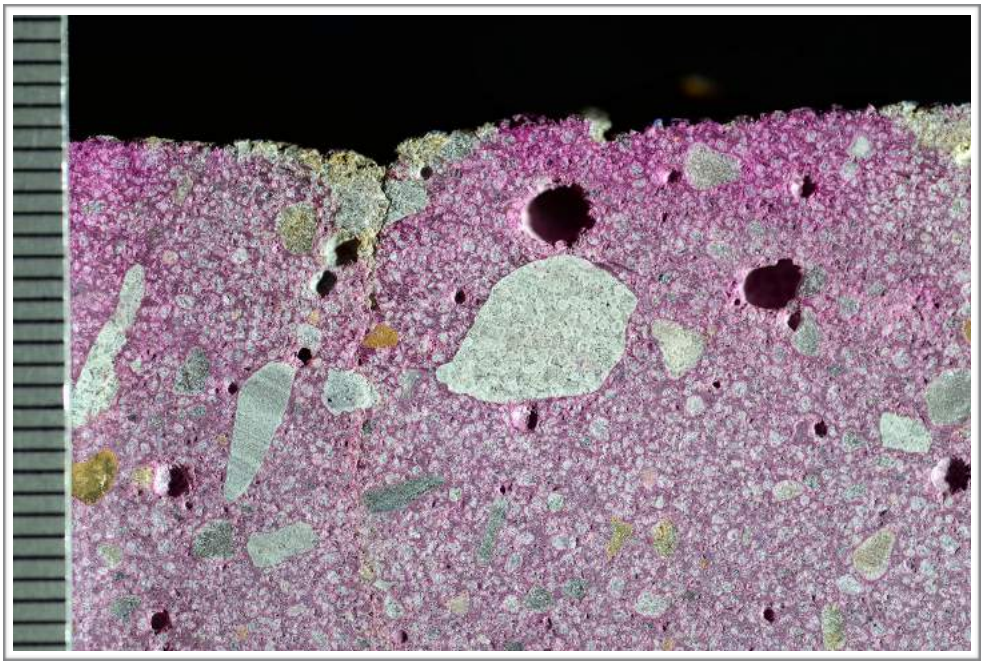

Figure B19. Photographs showing (a) overview of phenolphthalein stained surface and (b) detail of surface near the top of the core. Scale in millimeters in (b).

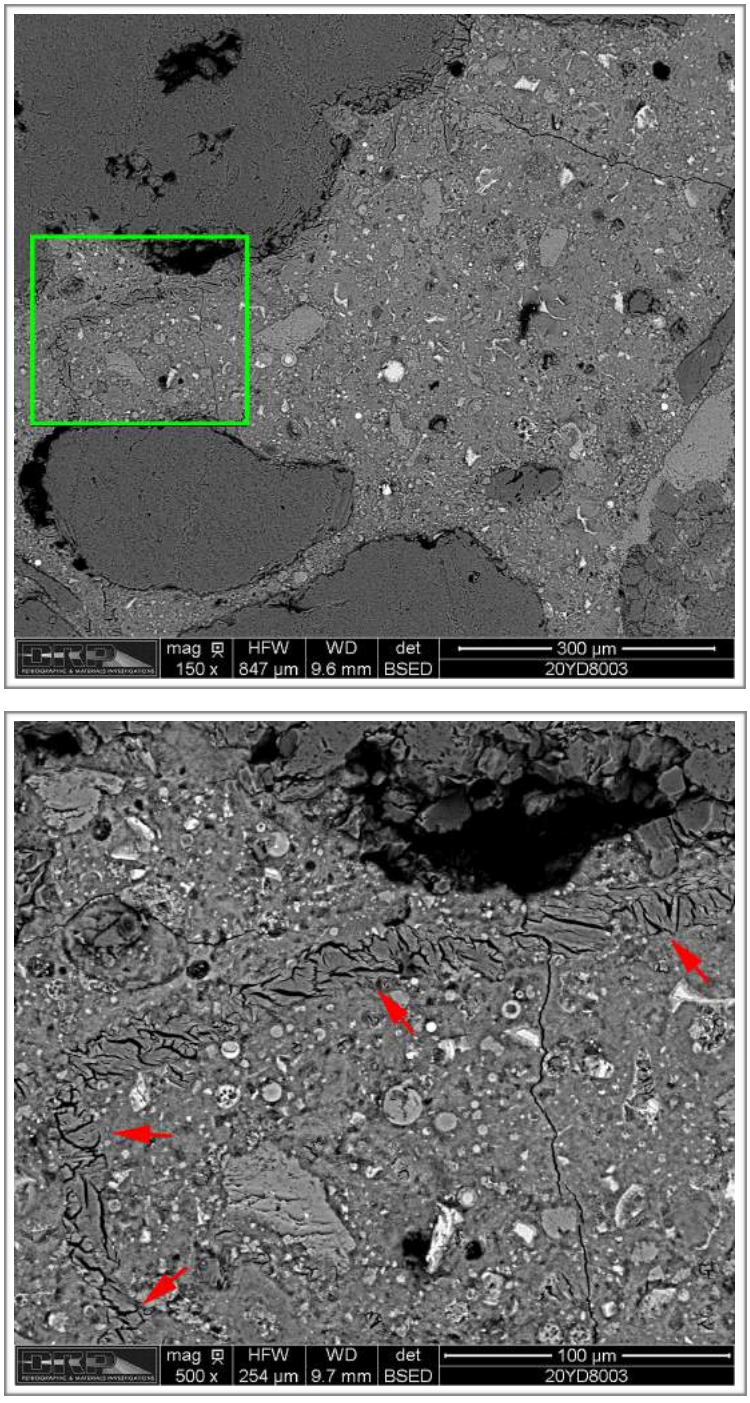

(a)

(b)

Figure B20. BSE micrographs showing (a) overview and (b) detail of microcrack with ettringite (red arrows) in the paste.

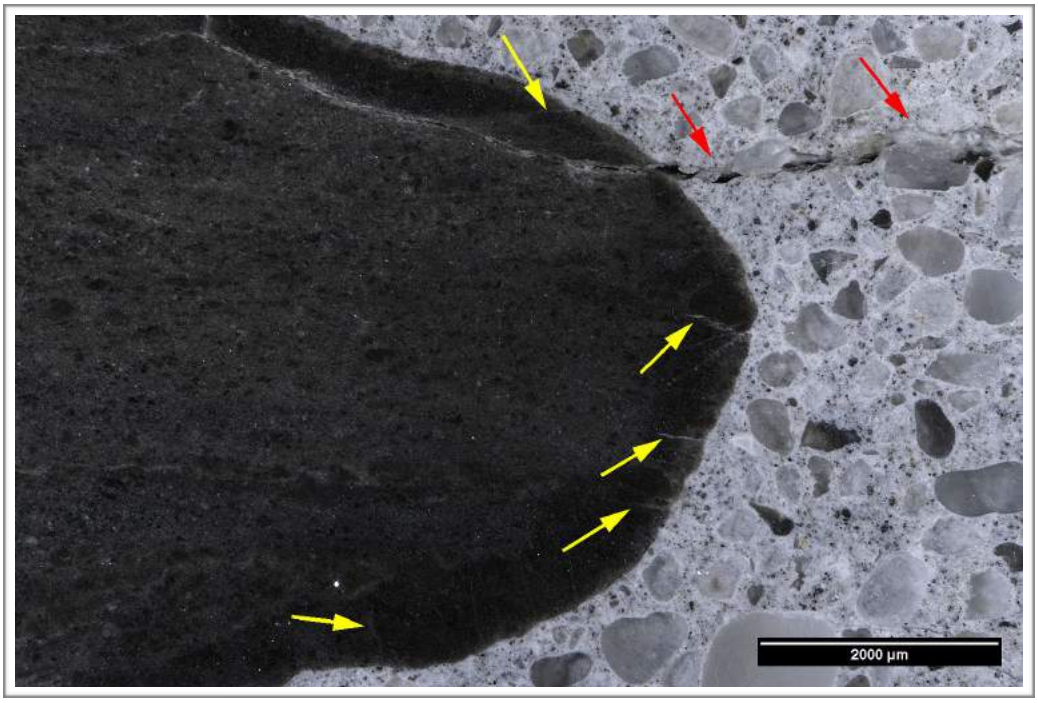

Figure B21. Reflected light photomicrograph of the polished surface showing hairline crack (red arrows) cutting from dolomitic limestone particle with microcracks in reaction rim (yellow arrows).

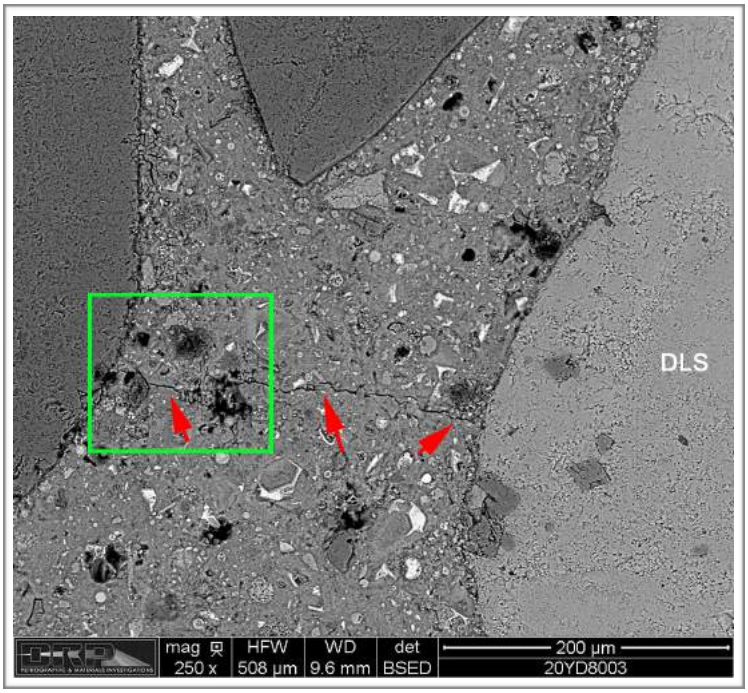

(a)

Figure B22. (a) BSE micrograph of polished surface showing location of area where EDS analyses were performed. The green box shows the area of (b). The red arrows indicate a microcrack that cut from the dolomitic limestone particle (DLS) on the right side of the image.

(b)

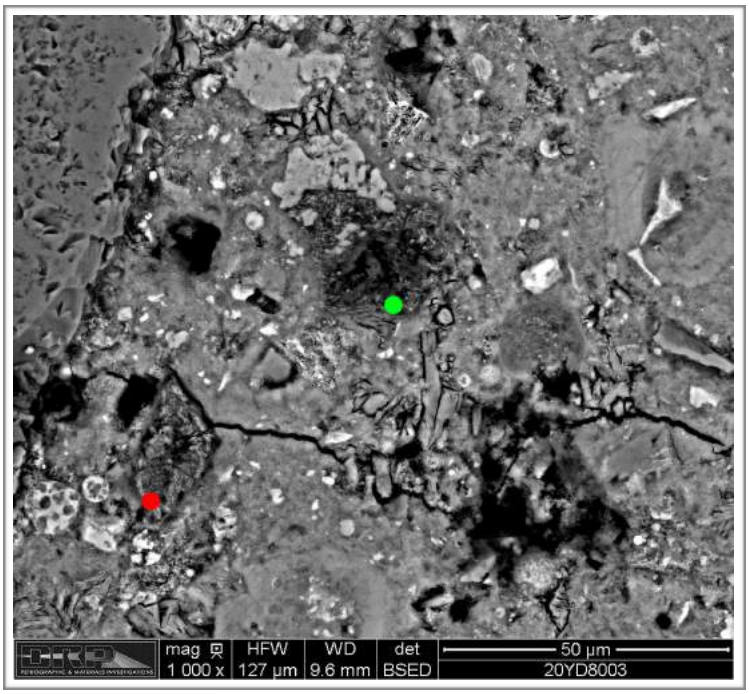

(c)

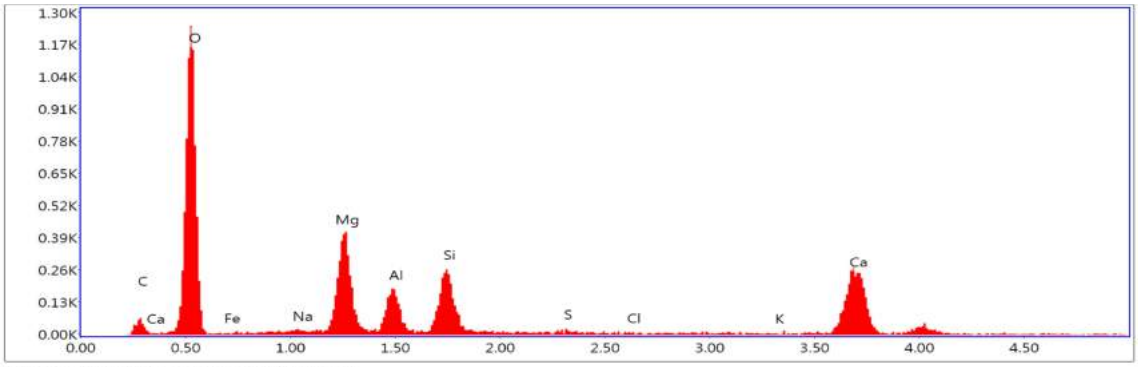

(d)

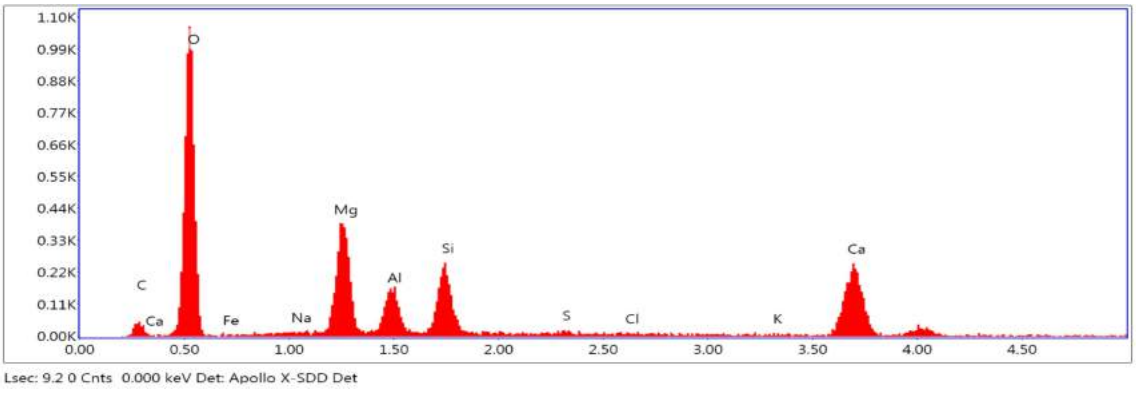

Figure B22 (cont'd). (b) BSE micrograph of polished surface showing location of EDS analyses. (c) and (d) are EDS spectra obtained from areas indicated by the red and green dots, respectively. These spectra show much higher concentrations of magnesium (Mg) than other areas, suggesting mobilization of Mg consistent with alkali-carbonate reaction.

1. Received Condition

Orientation	Vertical core through pavement slab measures 150 mm (6 in.) in diameter and 225 mm (~ 9 in.) in length (**Figure C1, C2**).
Surfaces	The top surface is tined and worn with exposed fine aggregate particles on the surface (**Figure C3**) and the lower surface is cast on asphalt such that the core represents the full thickness of the portland cement concrete pavement.
General Condition	The concrete is hard and compact and rings lightly when sounded with a hammer. A pit measuring ~ 19 x 35 mm (¾-1 ⅜ in.) in area is present on the top surface (**Figure C4**).

2. Embedded Objects

General	None observed.

3. Cracking

Macroscopic	Several cracks were observed on as-received surfaces. On the top a triple-point crack measuring up to 250 µm (10 mil) wide cuts across the full area of the surface (**Figure C5**). Several sub-vertical and sub-horizontal cracks were observed on the side of the core (**Figure C6**). These are up to 500 µm (20 mil) wide and 160 mm (~ 6 ¼ in.) long as they are traced on the side of the core. Most of these cracks cut around aggregate particles. Numerous cracks were observed on the polished surface. The most significant are as follows. Two (2) cracks ranging up to 500 µm (20 mil) wide cut sub-vertically from the top surface of the core (**Figure C7**). One crack cuts to a depth of ~ 50 mm (2 in.) where it narrows to a microcrack that is ~ 50 µm (2 mil) wide that cuts obliquely and terminates at a depth of ~ 60 mm (2 ⅜ in.). The other crack cuts to a depth of ~ 70 mm (2 ¾ in.) where it terminates in a sub-horizontal crack. These cracks cut around aggregate particles and are mostly free of secondary deposits. Several sub-horizontal cracks were observed. One cuts for ~ 100 mm (4 in.) across the surface 65-75 mm (2 ½-3 in.) below the top surface. The crack is up to 750 µm (30 mil) wide and contains deposits of gel and ettringite. Another cuts sub-horizontally and obliquely for ~ 100 mm (4 in.) across the core about 160 mm (6 ¼ in.) below the top surface (**Figure C8**). The crack is up to 500 µm (20 mil) wide but is ~ 100 µm (4 mil) wide over most of its length. The crack cuts mostly around aggregates and lacks significant deposits but the paste along the walls is discolored for segments of its length.
Microscopic	A few microcracks ranging up to 100 µm (4 mil) wide cut from the top surface to 3-6 mm (⅛-¼ in.); these cut around aggregates and are mostly free of secondary deposits. Extensive peripheral microcracking was observed in occasional particles of dolomitic limestone (**Figure C9**). Many of these microcracks are orthogonal to the perimeter of the particles and some cut into the paste where they cut mostly around but occasionally through aggregate particles. Most of these microcracks are free of secondary deposits but some contain deposits of ettringite.

4. Voids

Void System	Concrete is marginally air-entrained and contains ~ 3% total air as estimated from visual and microscopical observations (**Figure C10**). The concrete is well consolidated with no significant entrapped voids or water voids observed.
Void Fillings	Voids commonly contain deposits of ettringite that rim and fill the voids.

5. Coarse Aggregate

Physical Properties	The coarse aggregate is a limestone gravel with a nominal top size of 38 mm (1 ½ in.; **Figure C11**). The rocks are hard and competent. The particles are sub-equant to oblong in shape with sub-rounded to sub-angular edges. The aggregate shows gap grading with most particles between 19-25 mm (¾-1 in.) across.
Rock Types	The aggregate is carbonate in composition and consists of various types of limestone that range from dark brown micritic rocks to pale tan oolitic limestones to brown fossiliferous packstones and brown dolomitic limestones. Many particles show well-defined reaction rims and some appear to contain fine-grained siliceous material.
Other Features	No deleterious coatings or incrustations observed. Minor low w/c mortar coatings observed. Numerous particles show intense internal microcracking and peripheral microcracking that is typical of ACR. Microcracks cut from these particles into the paste.

6. Fine Aggregate

Physical Properties	The fine aggregate is a natural sand that consists of rocks that are hard and competent (**Figure C12**). The sand consists primarily of siliceous rocks but minor amounts of limestone (carbonate) similar to those in the coarse aggregate were observed. The particles are sub-equant to oblong in shape with rounded to sub-angular edges. The grading and distribution are even.
Rock Types	The consists primarily of quartz and quartzite; chert is a minor component and limestone is also present. Seams of chalcedonic chert were observed in limestones.
Other Features	No deleterious coatings or incrustations observed and no low w/c mortar coatings observed. The chert commonly shows well-developed reaction rims; the quartz and quartzite particles are intact.

7. Paste Observations

Polished Surface	Paste is light gray (Munsell 10YR/7/1), has a smooth texture and weakly sub-vitreous luster (**Figure C13**). The paste is moderately hard (Mohs 3-3.5). The paste is gray (10YR/6/1) for 1-2 mm (40-80 mil) from the top surface and irregularly distributed zones of yellow (2.5Y/7/4) to light red (2.5YR/7/4) paste are present for up to 12.5 mm (½ in.) from the top surface along microcracks and cracks.
Fresh Fracture	Fracture surface is gray, has a hackly texture and a sub-vitreous luster (**Figure C14**). The fracture cuts through coarse aggregate particles. Deposits of ettringite were observed on the surface.
Thin Section/ SEM*	The paste contains hydrated portland cement and fly ash; no slag cement or other SCM were observed. The hydration is normal with 3-6% RRCG that consist mostly of belite and interstitial ferrite and aluminate (**Figure C15, Figure C16**). Minor amounts of very fine crystals of calcite are present in the paste. CH makes up 8-15% of the paste, is fine to medium grained and distributed fairly evenly.

** Abbreviations as follows: RRCG = relict and residual cement grains; SCM = supplemental cementitious materials; CH = calcium hydroxide; ITZ = interfacial transition zone. Modal abundances are based on visual estimations.*

8. Secondary Deposits

Phenolphthalein	Entire surface stains purple except along irregular zones (microcracks) at the top of the core where not staining was observed to 6 mm (¼ in.) depth (**Figure C17**).
Deposits	No significant carbonation observed. Minor deposits of ettringite observed in occasional voids (**Figure C18**). Deposits of ASR gel observed in ITZ of occasional aggregate particles and in occasional voids (**Figure C19, Figure C20**).

FIGURES

(a)

(b)

Figure C1. Photographs showing (a) oblique view of the top and side of the core with identification labels and (b) the top of the core. The red and blue dots in (b) show the orientation of the saw cuts used to prepare the sample. The yellow bar is ~ 150 mm (6 in.) long.

(c)

Figure C1 (cont'd). (c) Photograph showing the bottom surface of the core.

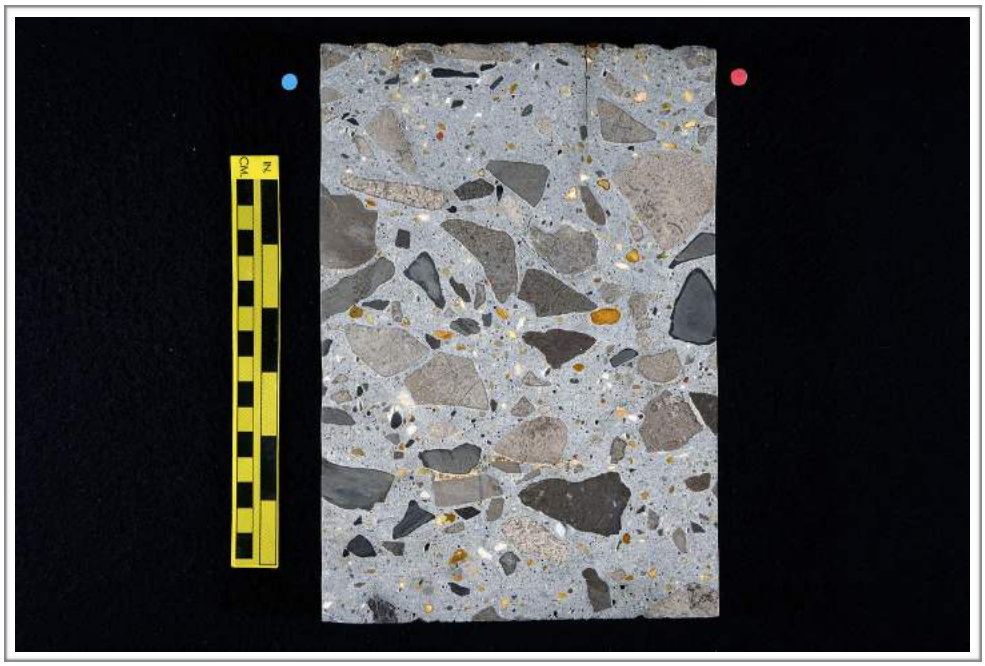

Figure C2. Photograph showing one of the polished surfaces of the core; both sides of the slab were polished. The yellow bar is ~ 150 mm (6 in.) long.

Figure C3. Photograph showing detail of top surface; scale in millimeters.

Figure C4. Photograph of top of core showing pit; scale in millimeters.

Figure C5. Photograph of the top surface showing overview of cracks (red arrows). Scale in millimeters.

Figure C6. Photograph of the side of the core showing overview of cracks (red arrows). The yellow scale is ~ 150 mm (6 in.) long.

(a)

(b)

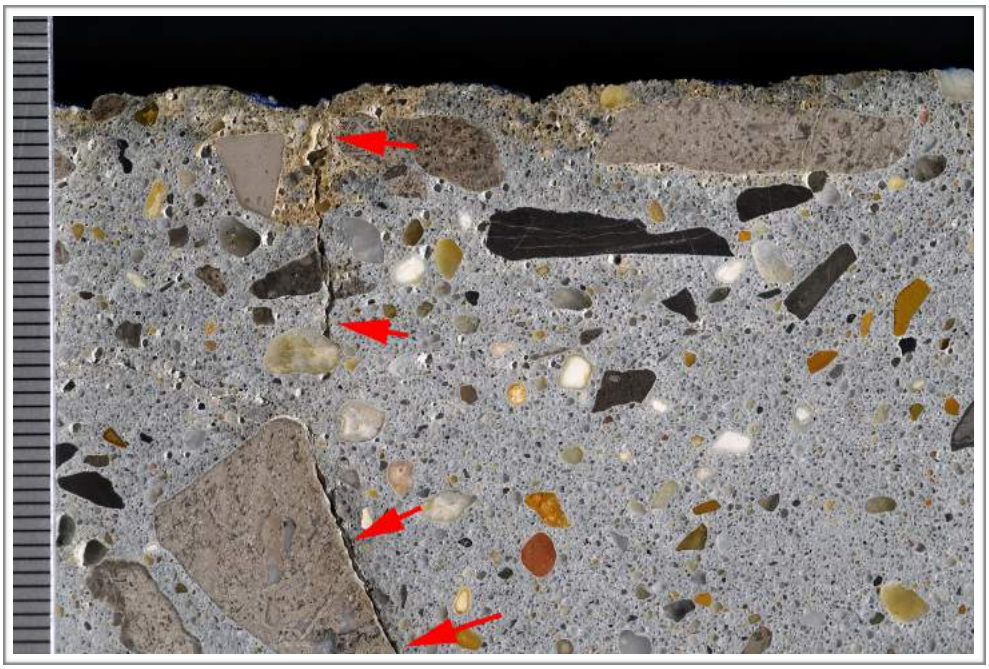

Figure C7. Photographs of the polished surface showing sub-vertical cracks at the top of the core. Scale in millimeters in both photos.

(a)

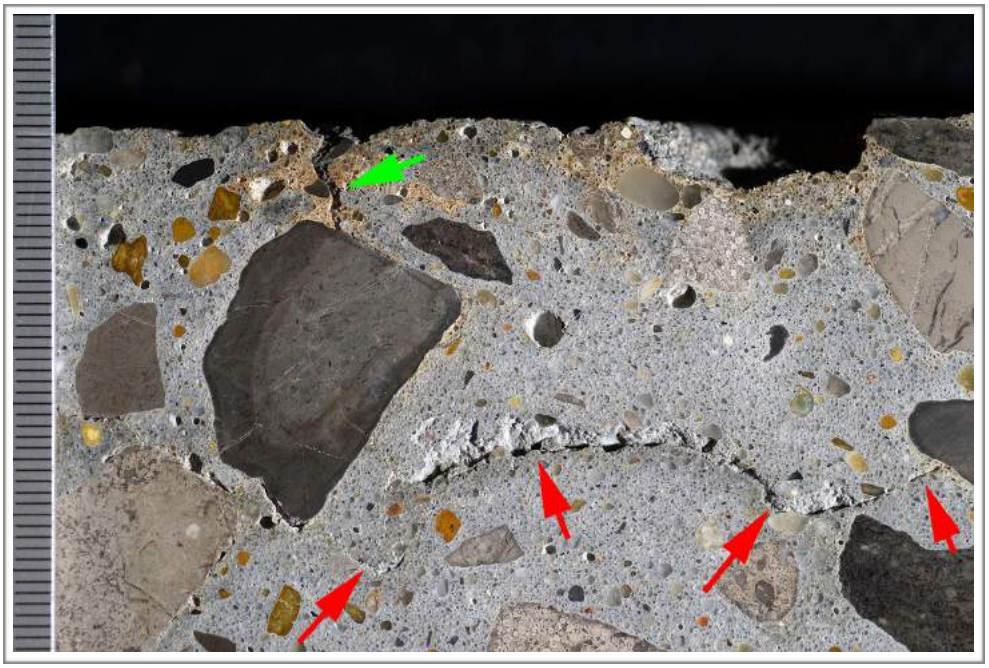

(b)

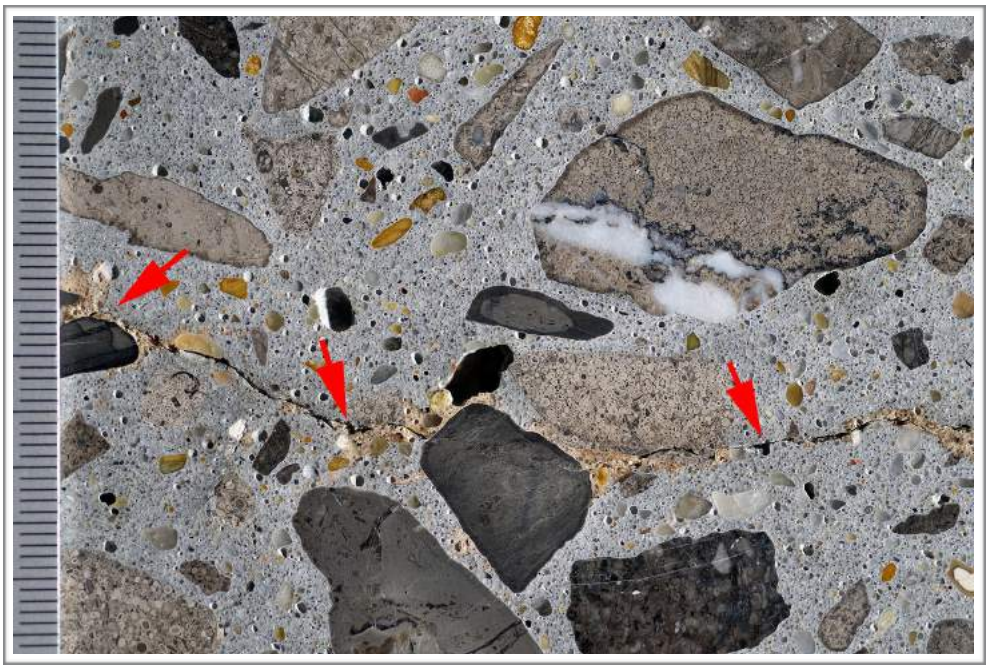

Figure C8. Photographs of the polished surface showing sub-horizontal cracks (red arrows). Scale in millimeters in both photos. The green arrow in (a) indicates sub-vertical crack.

(a)

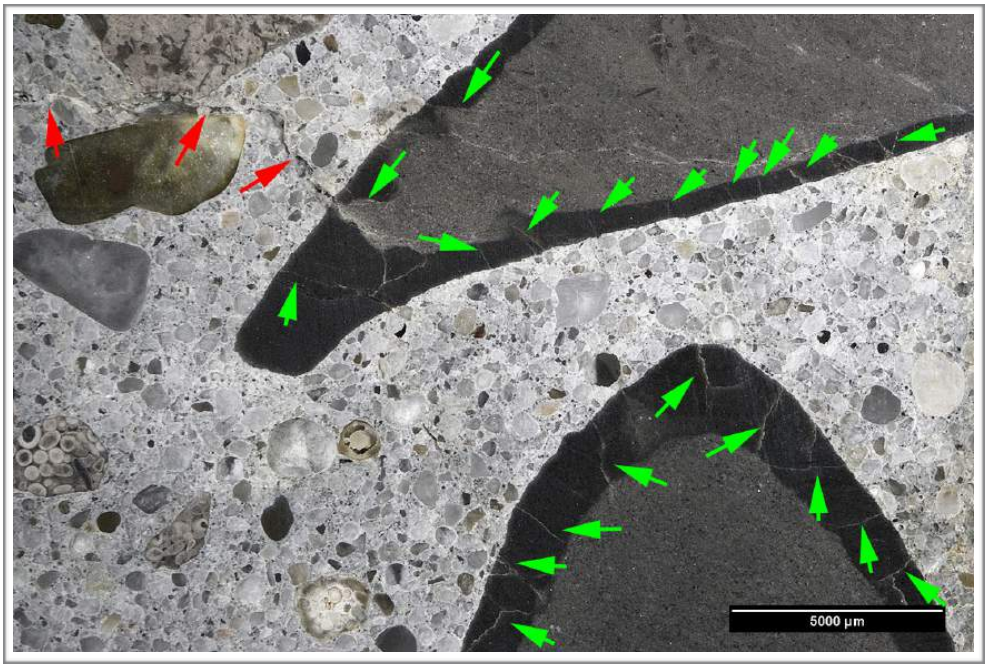

(b)

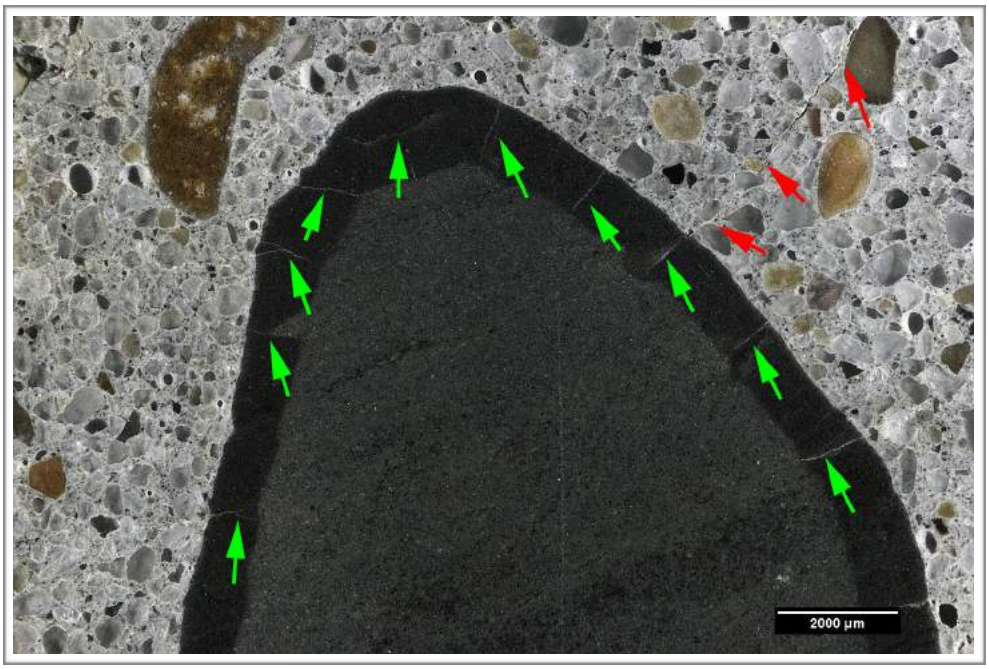

Figure C9. Reflected light photomicrographs of the polished surface showing (a) overview and (b) detail of peripheral microcracking (green arrows) in dolomitic limestone particles about 80 mm (3 ⅛ in.) below the top surface. The red arrows in both photos indicate microcracks that cut from the limestone into the paste.

(c)

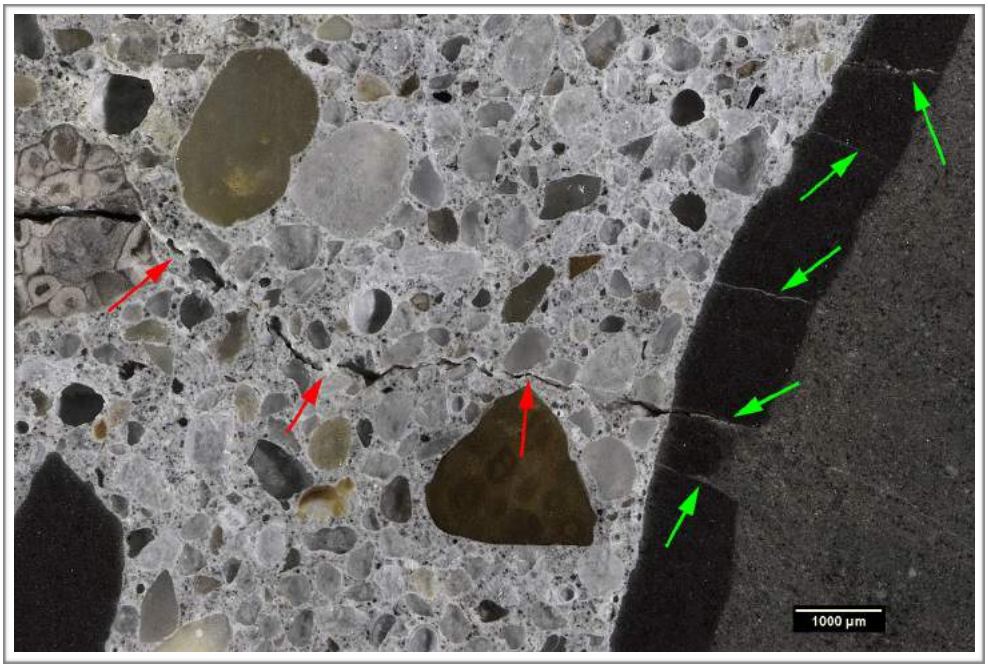

(d)

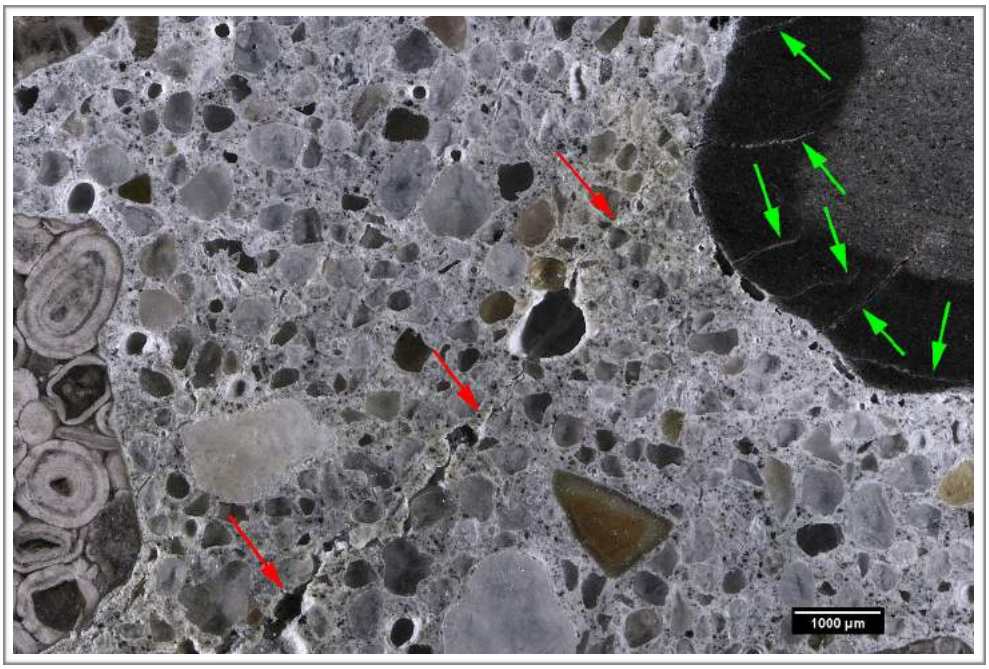

Figure C9 (cont'd). Reflected light photomicrographs of the polished surface showing peripheral microcracking (green arrows) in dolomitic limestone particles about (c) 85 mm (3 ⅜ in.) and (d) 110 mm (4 ⅜ in.) below the top surface. The red arrows in both photos indicate microcracks that cut from the limestone into the paste.

(e)

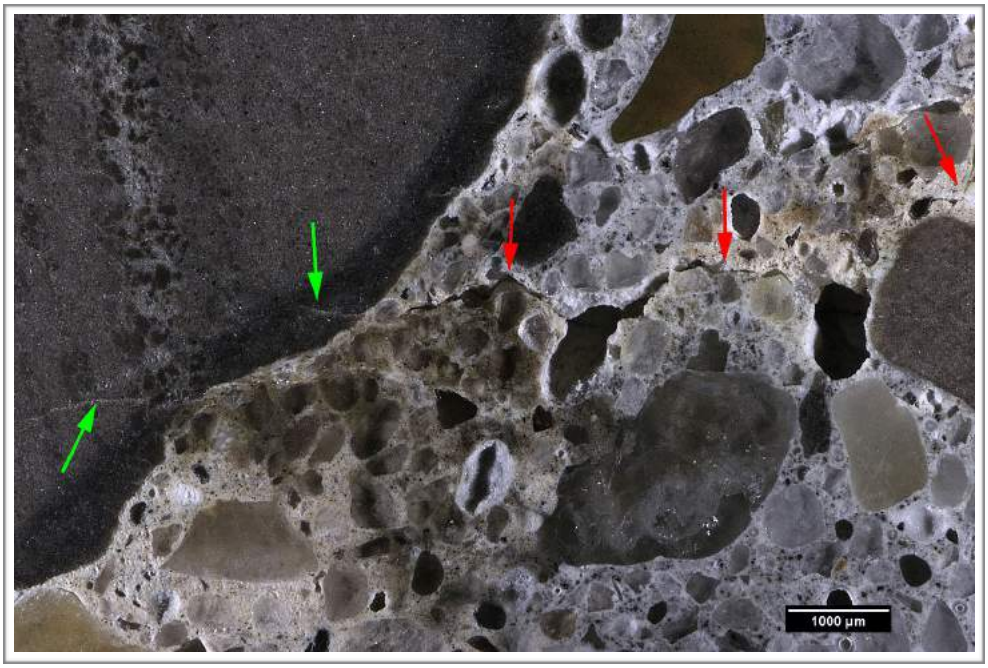

(f)

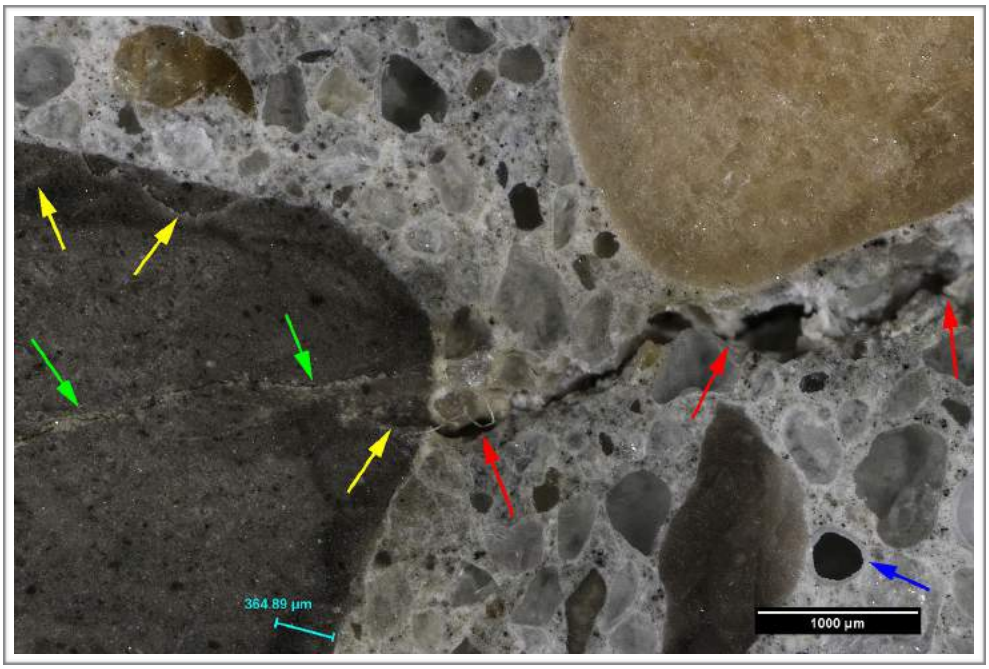

Figure C9 (cont'd). Reflected light photomicrographs of the polished surface showing microcracks (red arrows) that cut from dolomitic limestone particles into the paste about (e) 150 mm (6 in.) and (f) 165 mm (6 ½ in.) below the top surface. In (e) green arrows indicate peripheral microcracks that are mostly orthogonal to the perimeter of the particle. In (f) the yellow arrows indicate peripheral microcracks and the green arrow indicates an internal microcrack. The blue bar in (f) measures the width of a reaction rim and the blue arrow highlights a void lined by ettringite.

(a)

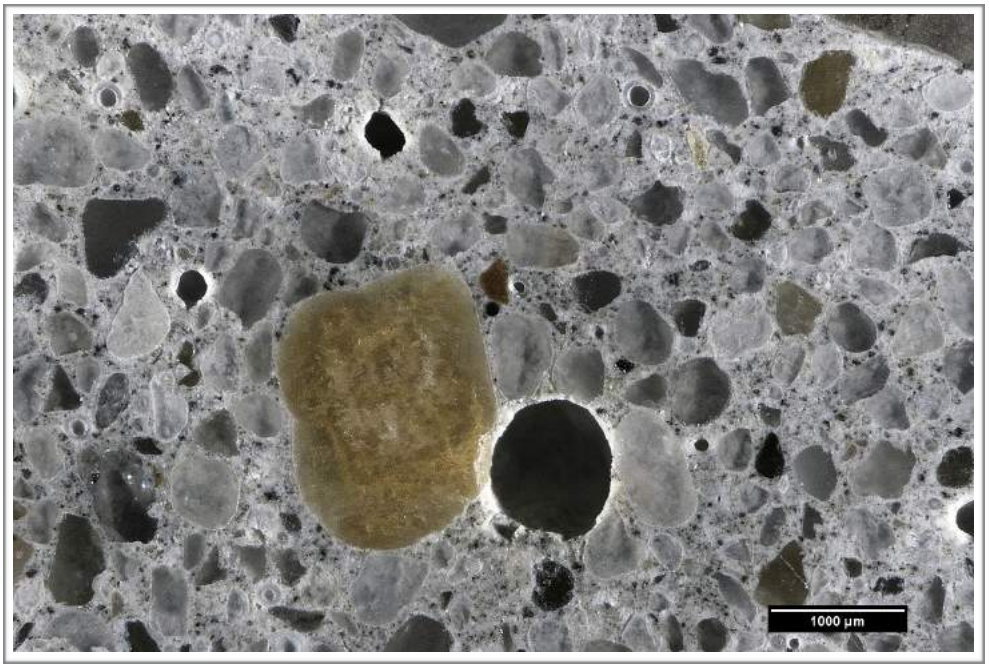

(b)

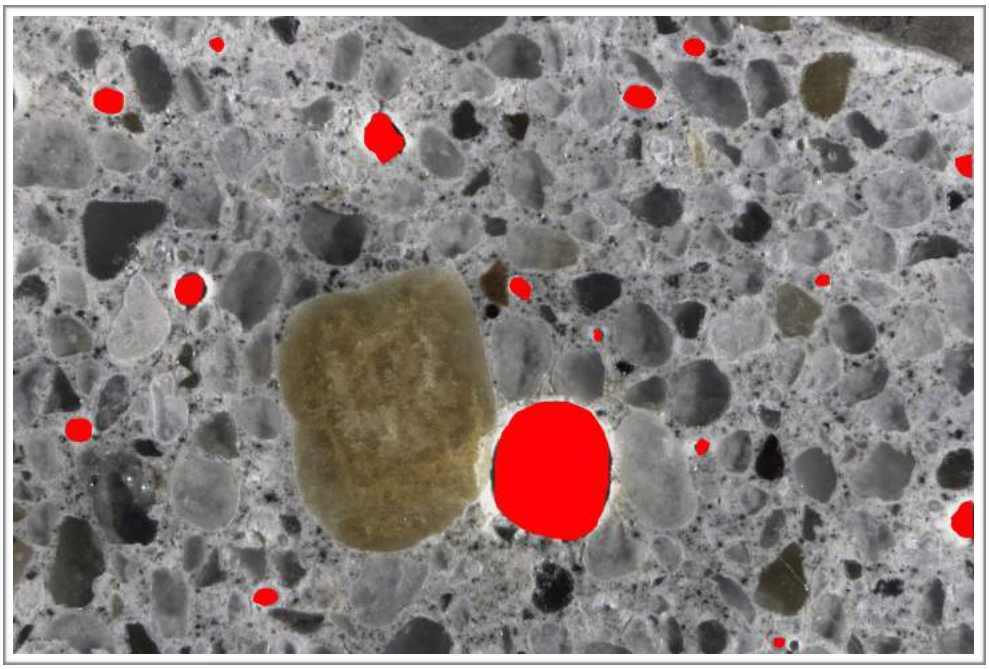

Figure C10. (a) Oblique reflected light photomicrographs of polished surface showing voids (dark circles). (b) Image of same area as (a) where red circles indicate voids. This image was analyzed and found to contain ~ 3% air.

Figure C11. Photograph of polished surface showing overview of coarse aggregate; scale in millimeters.

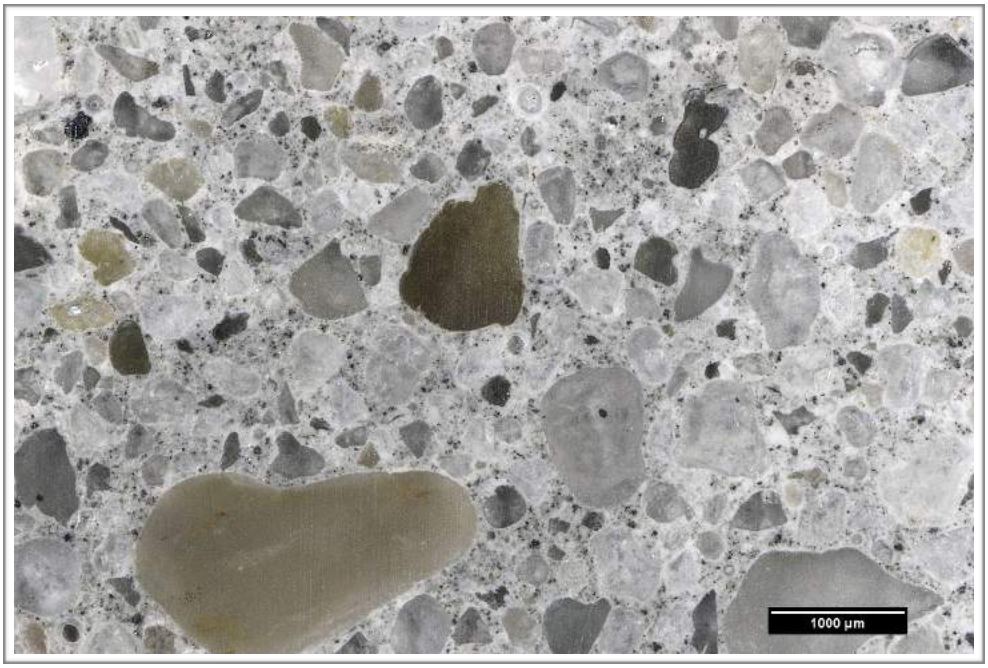

Figure C12. Reflected light photomicrograph of polished surface showing fine aggregate.

(a)

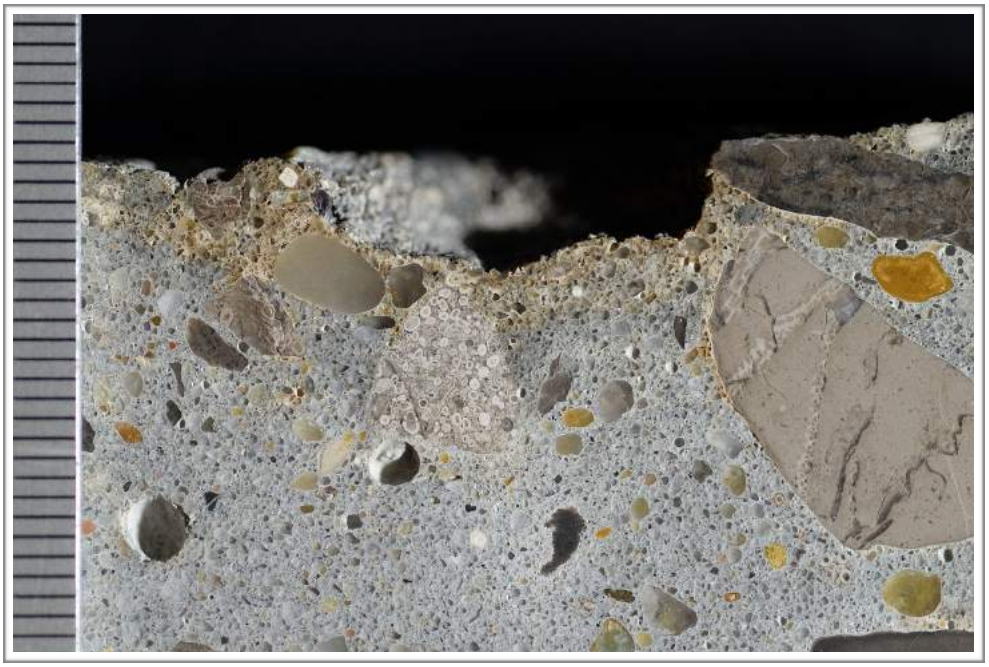

(b)

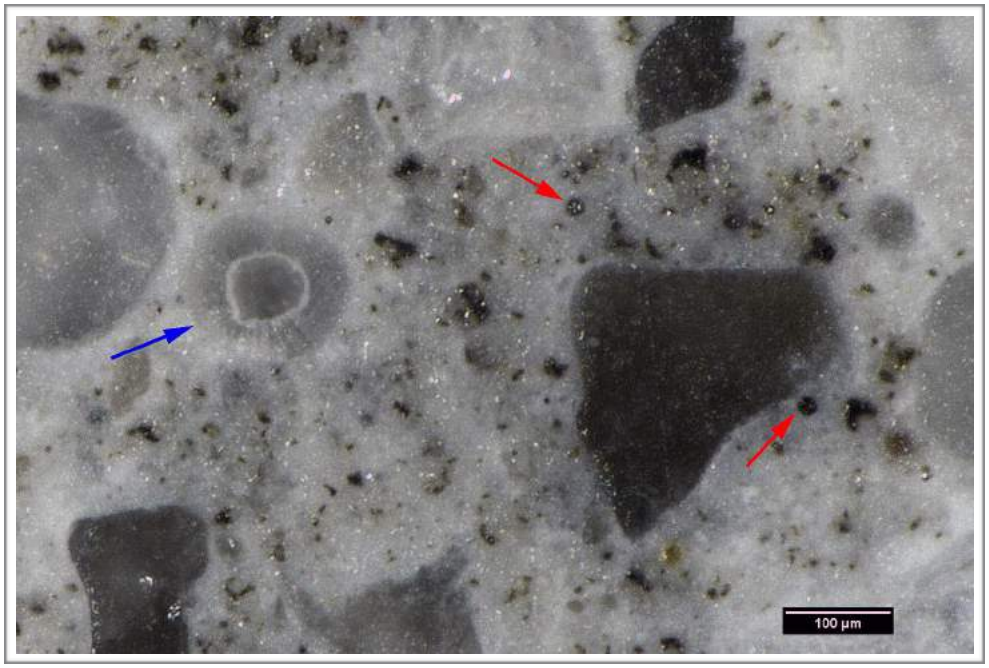

Figure C13. (a) Photograph of polished surface showing overview of paste at the top of the core. The scale is in millimeters. (b) Reflected light photomicrograph of polished surface showing detail of paste texture and luster. The red arrows indicate fly ash and the blue arrow indicates a void filled ettringite.

(a)

(b)

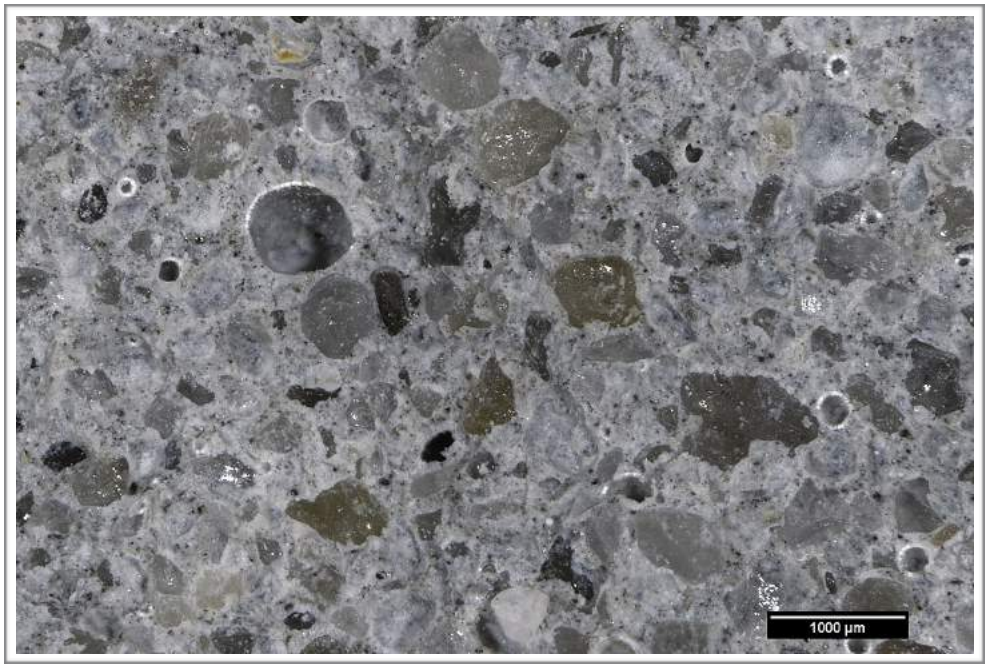

Figure C14. (a) Photograph and (b) reflected light photomicrograph of fresh fracture surface. The scale is in millimeters in (a).

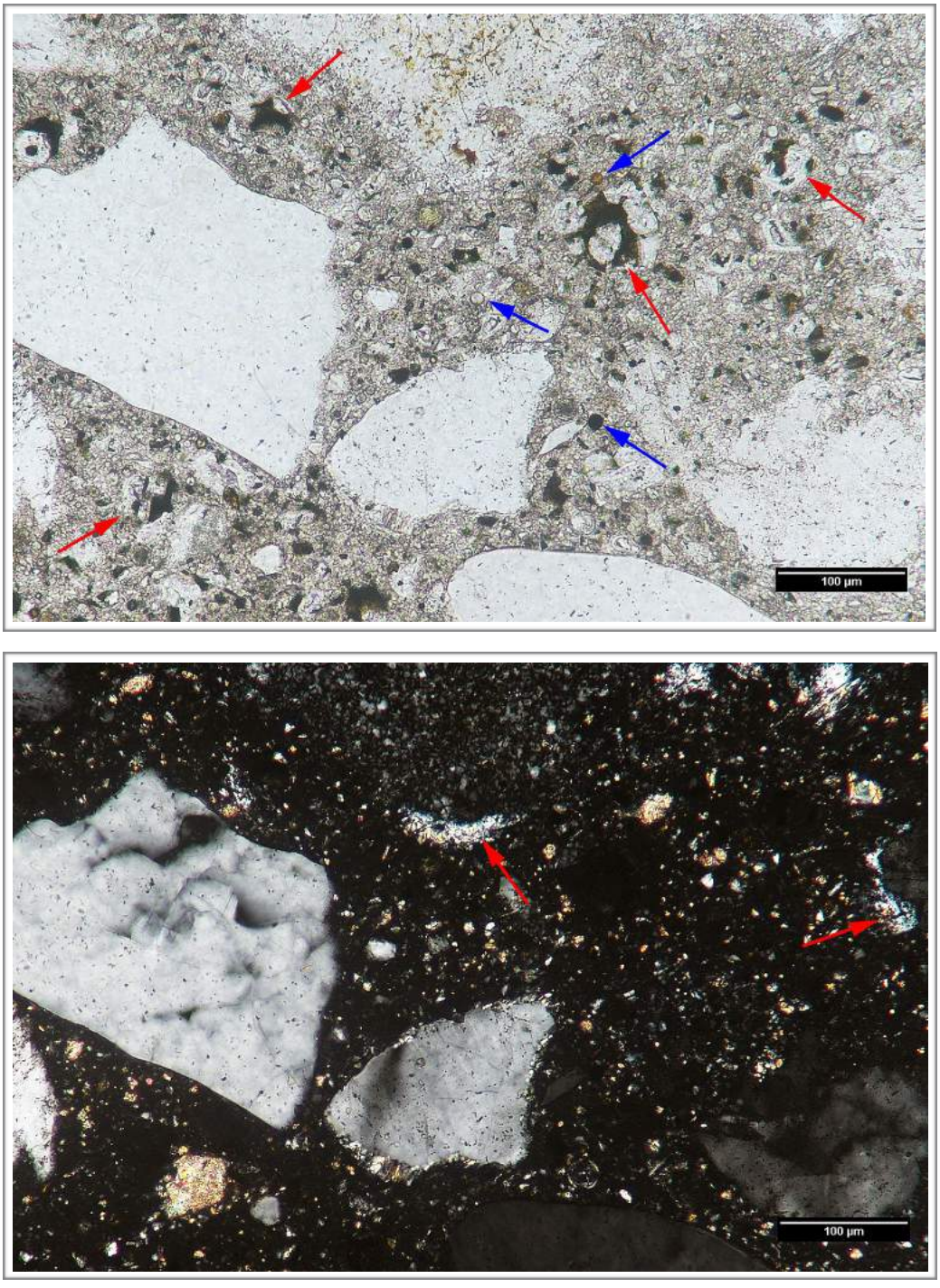

(a)

(b)

Figure C15. Transmitted light photomicrographs of thin section showing detail of paste in (a) plane-polarized and (b) cross-polarized light. The red and blue arrows in (a) indicate RRCG and fly ash, respectively. In (b) the red arrows indicate CH.

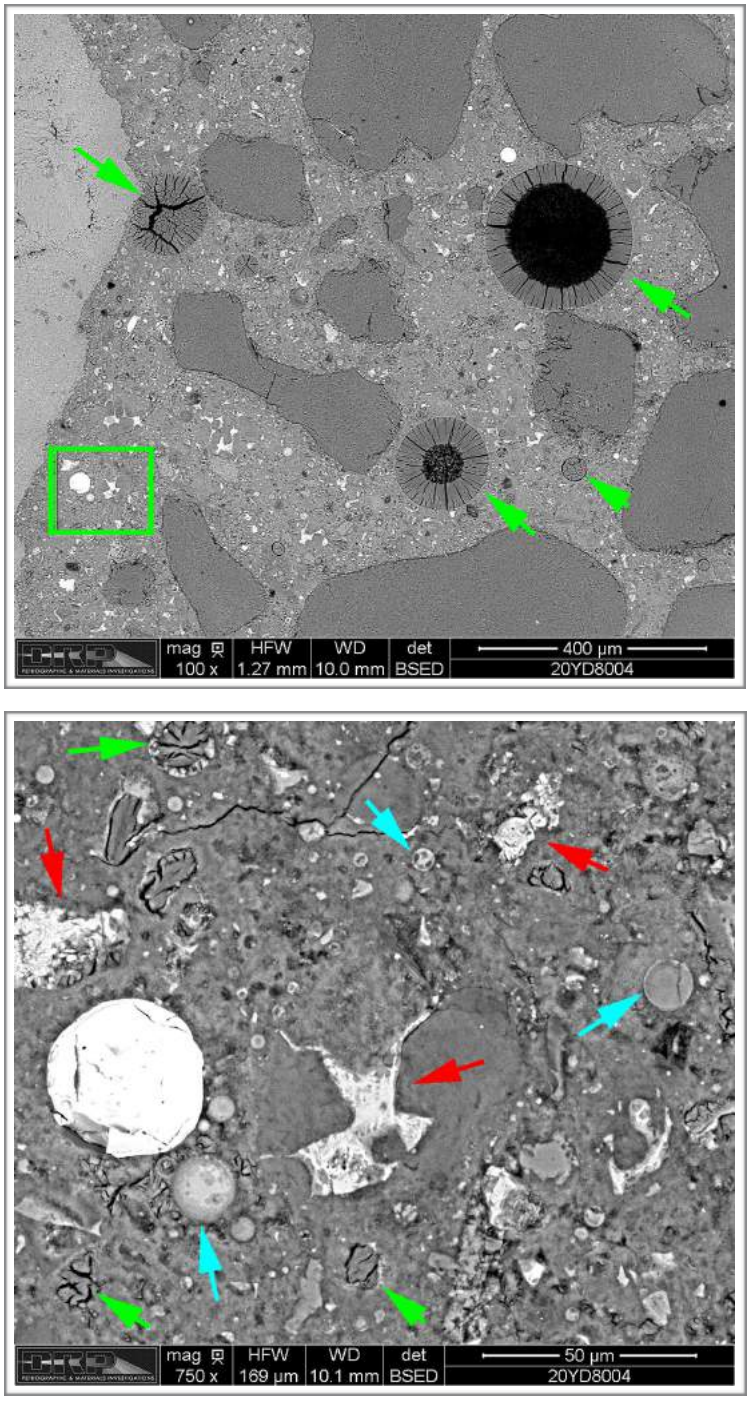

Figure C16. Backscatter electron (BSE) micrographs of polished surface showing (a) overview and (b) detail of paste. The green box in (a) shows the area of (b) and the green arrows in (a) indicate voids with ettringite. The red and blue arrows in (b) indicate RRCG and fly ash, respectively and the green arrows indicate deposits of ettringite.

(a)

(b)

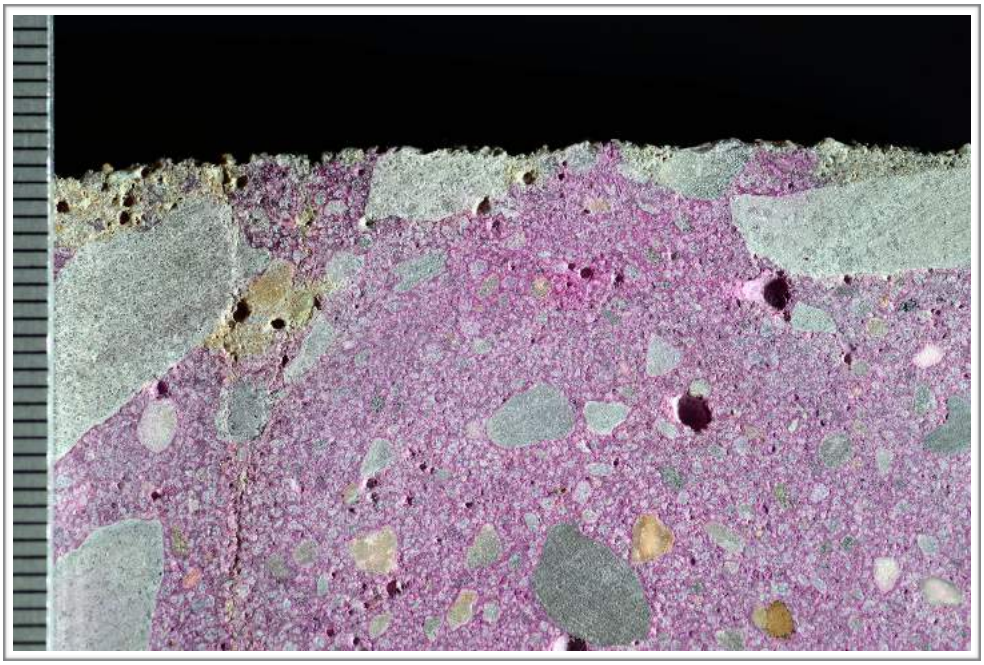

Figure C17. Photographs showing (a) overview of phenolphthalein stained surface and (b) detail of surface near the top of the core. Scale in millimeters in (b).

(a)

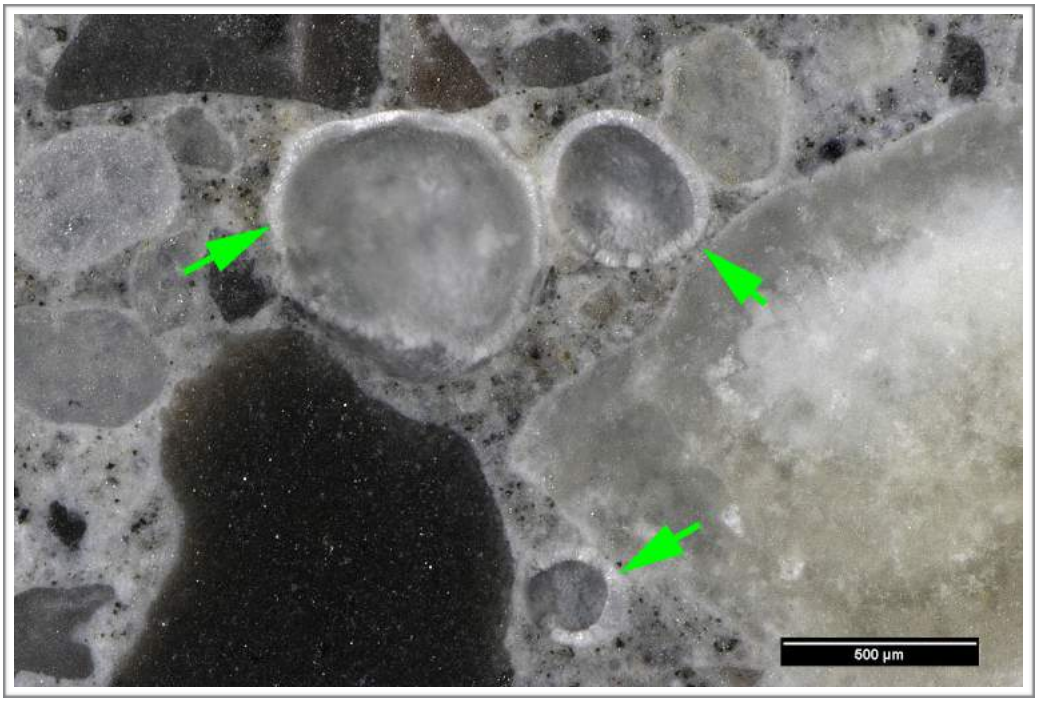

(b)

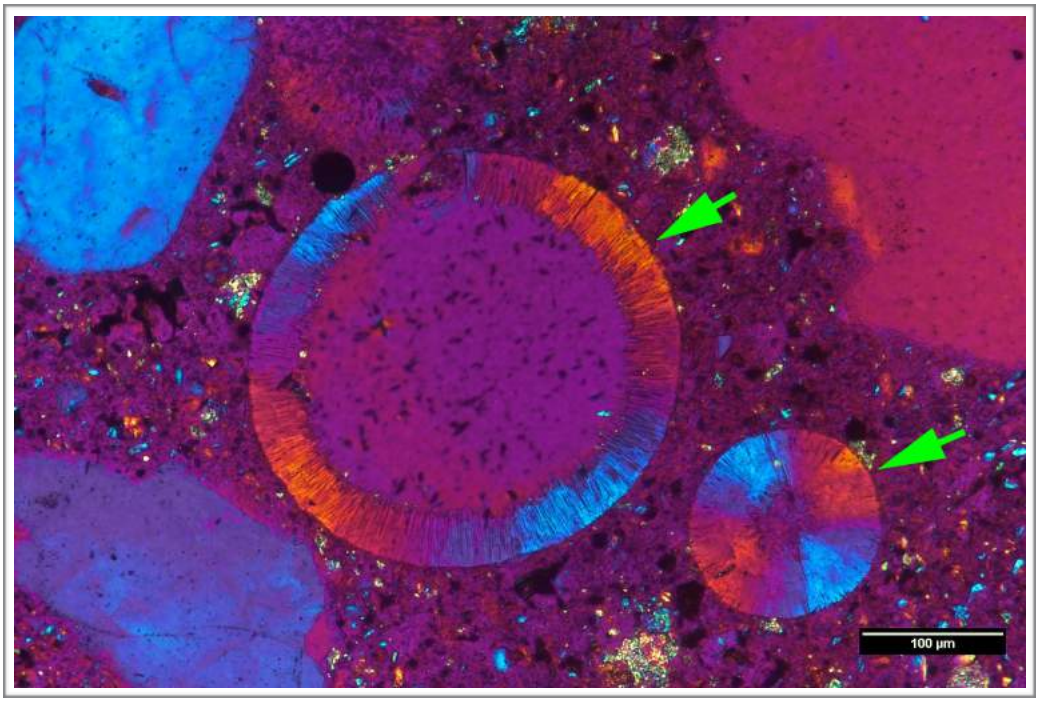

Figure C18. (a) Reflected light photomicrograph of the polished surface showing deposits of ettringite lining voids (green arrows). (b) Cross-polarized transmitted light photomicrograph of thin section with gypsum plate inserted showing voids lined with ettringite (green arrows).

(a)

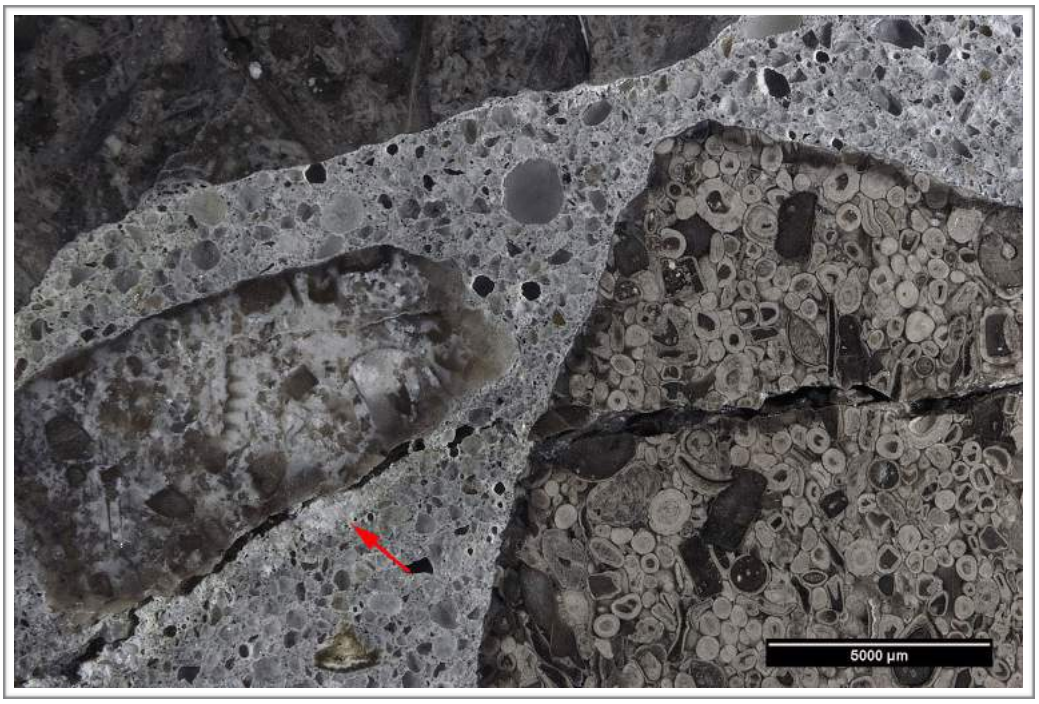

(b)

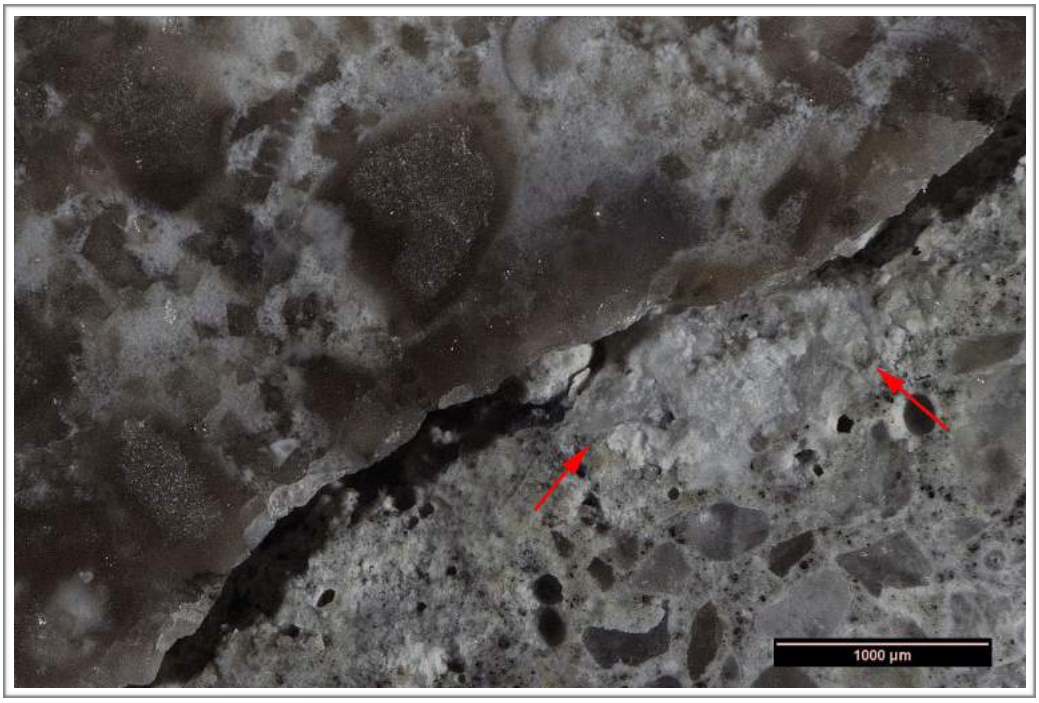

Figure C19. Reflected light photomicrographs of the polished surface showing (a) overview and (b) detail of gel deposit (red arrows) along the margin of an oolitic limestone particle about 90 mm (3 ½ in.) below the top surface. This deposit was scraped from the surface and analyzed by EDS.

(c)

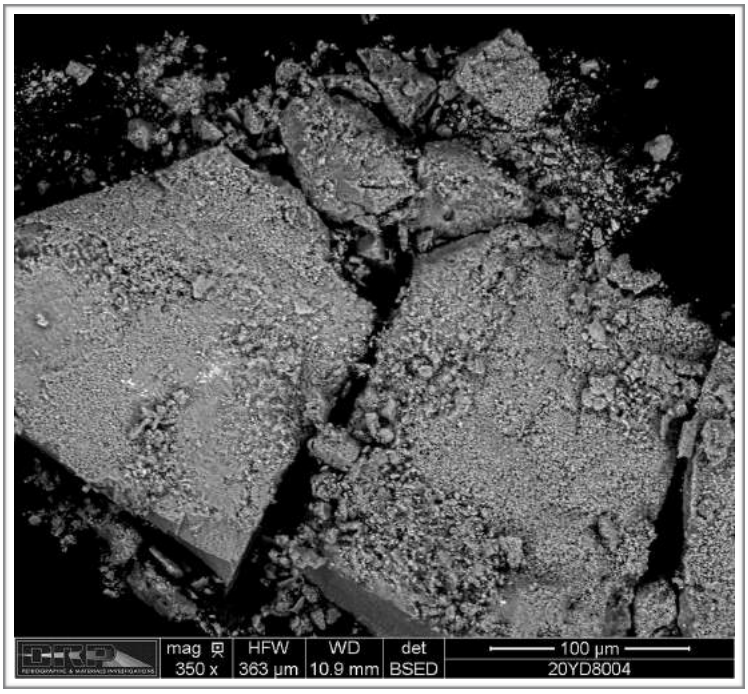

(d)

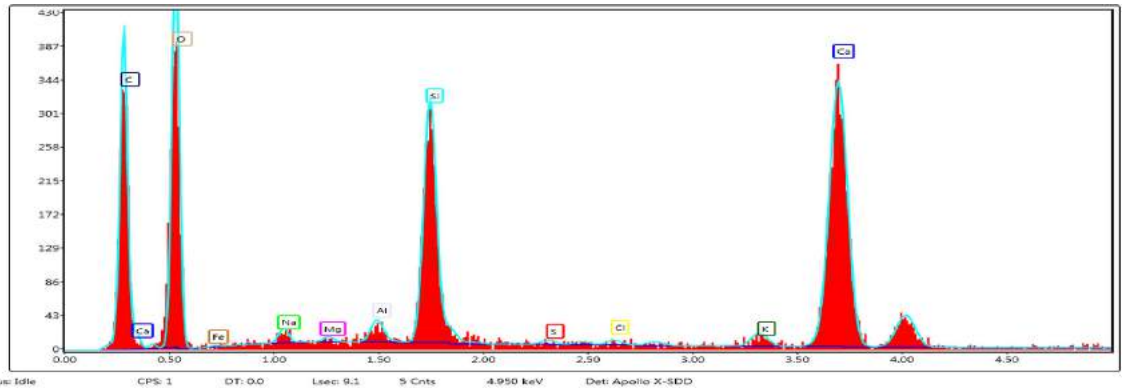

Figure C19 (cont'd). (c) BSE micrograph of gel deposit removed from polished surface of core and placed on carbon tape for EDS analysis. (d) EDS spectrum of deposit showing composition of the gel.

(a)

(b)

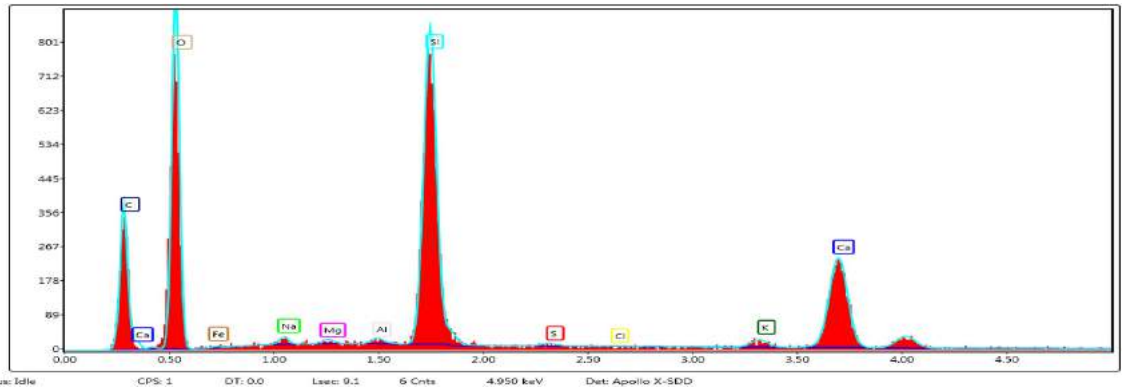

Figure C20. Reflected light photomicrograph of the polished surface showing gel deposit in a void about 130 mm (5 ⅛ in.) below the top surface. This deposit was scraped from the surface and analyzed by EDS; (b) indicates the EDS spectrum obtained from the deposit.

PROCEDURES

ASTM C856--Petrographic Analysis The petrographic work was done following ASTM C856 [**1**] with sample preparation done at **DRP** in the following manner. After writing the unique **DRP** sample number on each sample near the received label, the samples were measured and inspected visually and with a hand lens. The orientation of the saw cuts used to prepare the samples was then indicated on each sample with blue and red dots. The samples were then photographed in their as-received condition.

A slab representing a longitudinal cross section of each sample was cut from the central portion of the core using a Diamond Pacific® TR-24, a 24-inch diameter oil-lubricated saw. This produced three (3) longitudinal sections for each core. These sections were rinsed in an aqueous solution with a detergent to remove the cutting oil and oven dried overnight in a Gilson® Bench Top laboratory oven at ~ 40°C (~ 105°F) to remove remaining traces of the oil. After drying, each piece was labelled with the appropriate **DRP** sample number. One piece was set aside for phenolphthalein staining and the other was set aside for thin section preparation.

The central slab was then lapped and polished on a Diamond Pacific® RL-18 Flat Lap machine. This machine employs an 18-inch diameter cast iron plate onto which Diamond Pacific® Magnetic Nova Lap discs with progressively finer grits are fixed. The Nova Lap discs consist of a $^1/_{16}$ in. backing of solid rubber containing magnetized iron particles that is coated with a proprietary Nova resin-bond formula embedded with industrial diamonds of specific grit. The slab preparation involved the use of progressively finer wheels to a 3000 grit (~4 μm) final polish following procedures outlined in ASTM C457 [**2**]. An aqueous lubricant is used in the lapping and polishing process. The polished slab from each sample was examined visually and with a Nikon® SMZ-1500 stereomicroscope with 3-180x magnification capability following to the standard practice set forth in ASTM C856.

Phenolphthalein was applied to a freshly saw-cut surface from each sample to assess the extent of carbonation, along with thin section analysis. Phenolphthalein is an organic stain that colors materials with pH of greater than or equal to ~ 9.5 purple. Portland cement concrete generally has a pH of ~ 12.5. Carbonation lowers the pH of the paste below 9.5, so areas not stained by phenolphthalein are an indicator of carbonation. The depth of paste not stained by phenolphthalein was measured from each exposed surface.

Petrographic thin sections were prepared by cutting billets from the remaining longitudinal section. Outlines marking the area of the billets were drawn with a marker on the saw-cut surface after visual and microscopical examination of saw-cut and polished surfaces. The billets were labeled with the unique **DRP** number assigned to the sample and impregnated with epoxy. The impregnated billets

1 *Standard Practice for Petrographic Examination of Hardened Concrete.* Annual Book of ASTM Standards, Vol. 4.02., ASTM C856-14.

2 *Standard Test Method for Microscopical Determination of Parameters of the Air-Void System in Hardened Concrete*, Annual Book of ASTM Standards, Vol. 4.02, ASTM C457-12.

were then fixed to glass slides with epoxy. After the epoxy cured, the slide was trimmed and ground on a Buehler® Petro-Thin device to a thickness of ~ 30 µm (1.2 mil). The slide was then moved to a Buehler® Beta-Vector machine and polished to a final thickness of ~ 20 µm. The grinding and polishing of the thin sections were done in a non-aqueous environment. The thin sections were examined with a Nikon® E-Pol 600 petrographic microscope equipped to provide a 50-1000x magnification range following the standard practice set forth in ASTM C856.

ASTM C1723 Electron Microscopy A FEI™ Quanta 250 Environmental Scanning Electron Microscope (ESEM) was used to supplement the petrographic methods described above (see ASTM C1723 [**3**]). The Quanta 250 is capable of operation in three different vacuum modes: high vacuum (< 6 e^{-4} Pa) for conductive or conventionally prepared specimens; low vacuum (10-130 Pa) for non-conductive specimens without preparation; and ESEM™ mode (10-2600 Pa) for specimens such as hydrous materials (cement paste) that are incompatible with high vacuum. The instrument is equipped with several detectors for imaging: an Everhardt Thornley secondary electron detector (SED), a Large Field, Low vacuum SED, a high-sensitivity, low kV solid state backscatter electron detector (BSED), and gaseous SED and BSED for ESEM conditions.

The instrument uses a Tungsten hairpin filament mounted within a tetrode gun assembly and operates with an accelerating voltage of 200 V to 30 kV with beam currents up to 2 µA. The instrument has a magnification range from 6 to more than 1,000,000 x. The resolution of the instrument is as follows (measured as particle separation on a carbon substrate):

High vacuum mode: 3.0 nm at 30 kV and 8.0 nm at 3 kV for SED
4.0 nm at 30 kV for BSED

Low vacuum mode: 3.0 nm at 30 kV and 10.0 nm at 3 kV for SED
4.0 nm at 30 kV for BSED

Extended vacuum mode (ESEM): 3.0 nm at 30 kV for SED

The Quanta is also with an equipped with an EDAX® Apollo X Silicon Drift Detector for Energy Dispersive X-ray (EDX) analysis. The Apollo X is equipped with a 10 mm^2 window and has a resolution of 131 eV or better with peak to background ratios that are greater than 10,000:1. The detector is capable of handling input count rates up to 850,000 cps and throughput of more than 350,000 cps. The detector is capable of detecting all chemical elements down to Beryllium and is capable of quantitative analyses down to and including Boron. The EDX has a take-off angle of 35º at a 10 mm working distance.

---

3 *Standard Guide for Examination of Hardened Concrete Using Scanning Electron Microscopy,* Annual Book of ASTM Standards, Vol. 4.02, ASTM C1723-10.

Sections are prepared for the ESEM/EDX work in the following manner. After visual and microscopic examination of the polished surface used for stereomicroscopy, a coupon measuring ~ 50 mm x 50 mm (2 x 2 in.) in area and ~ 15 mm (⅝ in.) in thickness is cut out of one of the hemicylindrical sections from the core. The sample is then lapped and polished using rigid polishing wheels (Buehler Meta-Di Supreme™) embedded with the following sequence of progressively finer grits of industrial diamonds: 165 µm, 45 µm, 15 µm, 9 µm, 3 µm and 0.5 µm. A 0.05 µm diamond suspension and polishing cloth is used for the final polishing step. None of the abrasive wheels or suspensions contain silicon, aluminum or cesium.

For the present investigation, uncoated polished samples were examined in the low vacuum (~ 70 Pa) mode using an accelerating voltage of 15 kV and a spot size of 5, which gives a count rate of ~ 2,500 counts per second. Counting times of 10 seconds were used for the EDX analyses.

This public document is published at a total cost of $250
42 copies of this public document were published in this fi rst printing at a cost of $250. The total cost of all printings of this document including reprints is $250. This document was published by Louisiana Transportation Research Center to report and publish research fi ndings as required in R.S. 48:105. This material was duplicated in accordance with standards for printing by state agencies established pursuant to R.S. 43:31. Printing of this material was purchased in accordance with the provisions of Title 43 of the Louisiana Revised Statutes.